The Pennsylvania State University

The Graduate School

Department of Mechanical and Nuclear Engineering

IGNITION PROCESSES AND FLAME SPREADING IN A GRANULAR SOLID PROPELLANT BED

A Thesis in

Mechanical Engineering

by

Alexander E. Colletti

Submitted in Partial Fulfillment
of the Requirements
for the Degree of

Master of Science

May 2010

The thesis of Alexander E. Colletti was reviewed and approved* by the following:

Kenneth K. Kuo
Distinguished Professor of Mechanical Engineering
Thesis Advisor

Savas Yavuzkurt
Professor of Mechanical Engineering

Karen A. Thole
Professor of Mechanical Engineering
Head of the Department of Mechanical and Nuclear Engineering

*Signatures are on file in the Graduate School

Abstract

Understanding the detailed ignition, flame spreading, and combustion processes inside of a granular solid propellant bed is vital for accurate internal ballistic modeling and development of weapon systems. To characterize these items, a modular test chamber was designed, fabricated, and utilized to analyze ignition processes in axial, radial, and azimuthal directions. A percussion primer and black powder igniter jet were fired into a bed of an inert material which simulates the geometric properties of the live granular propellant to characterize its penetration. These particles were analyzed with energy dispersive X-ray spectroscopy (EDS) to confirm that the condensed phase species contain potassium species as predicted by equilibrium analyses. Three correlations were found which describe the region affected in the granular bed by condensed phase products of the igniter jet including: axial depth of penetration, maximum radial penetration, and the volume of the coated region. They are related by: the Reynolds number based on the jet diameter, the ratio of pressure in the igniter jet to the ambient, and the ratio of bed particle diameter to orifice diameter. Through the use of high-speed photography, photodetectors, and pressure transducers igniter jet penetration into the granular bed was examined in terms of its influence on flame spreading behavior. The igniter jet is shown to fully penetrate the bed, over approximately 1 ms, before any major granular bed combustion was measured through pressure time traces, high-speed photography, or photodetector signals. Tests performed with high-speed photodetectors, sensitive to either the visible and infrared spectrum, show that the relative spread between the hot gaseous front and the flame front can be determined utilizing this windowed test chamber. The axial fronts were separated by an average of 0.15 ms at 4000 to 6000 psia.

Table of Contents

List of Figures

List of Tables

Nomenclature

$d_{cond\ ,max}$	The maximum radial penetration of condensed phase deposition
d_{jet}	Jet/orifice diameter
d_{part}	Particle diameter
L	Axial depth of penetration of condensed phase products
$\dot{m}$	Mass flow rate
$\bar{P}$	Average pressure from first rise to blow-down to 500 pisa
P_{atm}	Back pressure of atmospheric
$Re_{d_{jet}}$	Reynolds number based on the orifice diameter and gas properties
U_0	Gas velocity at orifice
$V_{covered}$	The volume coated region by condensed phase products
V_{part}	The volume of an individual granular particle
x	Axial distance into the granular bed

Greek

γ	Ratio of specific heats
η	Packing density
μ_{jet}	Viscosity of the gas jet
ρ_{part}	Density of the particles in the propellant bed
ρ_{jet}	Density of the fluid at the orifice

Acknowledgements

The author would like to start by thanking his advisor Professor Kenneth K. Kuo whose support, direction, and leadership has made all of this work possible. His dedication to the field of combustion science and his students has been an inspiration.

The author also thanks Dr. Ralph Anthenien of the Army Research Office of the U.S. Army who sponsored this program under the grant W911NF-08-1-0176.

The help and friendship of all the members of the High Pressure Combustion Lab has been invaluable to me and greatly appreciated. I would like to thank Dr. Eric Boyer whose advice and help has been invaluable and countless. Thanks to Mr. Jon Essel for performing the SEM analyses for this project. I would also like to all of the members of the lab: Mr. Scott Blakeslee, Mr. Andrew Cortapassi, Mr. Matt Degges, Mr. Brian Evans, Mr. Ryan Houim, Mr. Jeff Krug, Mr. Heath Martin, Mr. Matt Sirignano, Mr. Trevor Wachs, and Prof. Baoqi Zhang.

Chapter 1

Introduction

Background

The use of solid propellants in many propulsion systems provides many advantages over liquid or gaseous propellants. Solid propellants are easy to store within the cartridge or vehicle and require no moving parts to operate. They contain chemically bound fuel and oxidizer so they require no other energy sources once burning begins. The propellant charge can be created in many shapes where the material and geometry of the propellant determine performance. [1]

The propellant can also be loaded as many discrete, regularly formed, particles of similar geometry (e.g.: spherical, cylindrical) into an enclosed chamber. Here there are many aspects that affect the performance of the burning propellant. Material, size, shape, packing density, and vessel geometry are a few. The burning rate of a spherical granular propellant provides regressive burning characteristics for the bed [2]. This is because as the solid propellant sphere burns from the outer surface to the inside the surface area for burning decreases.

Granular solid propellant beds are used as the main energetic charge in the ignition train (the sequence of energetic materials used) of many small and large arms. The combustion of granular bed materials is distinctly different from burning solid propellant grains. Since the granular material consists of many discrete particles, the very high surface area compared to a solid propellant grain allows for very fast burning. The interstitial spacing between them allows additional convective heat transfer. The process of convective burning is “a deflagration wave whose propagation rate is control by convective heat transfer via rapid, deep penetration of hot gases, instead of diffusional processes only. [3]” These combined effects allow the granular bed

to burn completely over several milliseconds, as opposed to a typical burn time of many seconds for a typical rocket motor burning similar fuel. The burning of the granular bed by this process allows for rapid chamber pressurization providing force which creates projectile motion. This is necessary to provide the required impulse to projectiles that do not burn propellant over their ballistic trajectories.

For the ignition train of interest, the main propellant is granular propellant bed which is the same as the one used in the U.S. Army 120mm mortar system. It consists of three main steps. First, a percussion primer is struck by a firing pin. This is an item which uses mechanical energy to initiate a small propellant charge. Essentially, it converts mechanical energy into chemical energy. It consists of a small metal cup which contains the chemicals for an explosive reaction and a crushable anvil. The mechanical energy is imparted to an anvil where friction between the metal and the propellant begins the reaction.

The hot gases from the primer are directed to a centrally-perforated black powder grain. Black powder is a mixture of sulfur, charcoal, and potassium nitrate (see Appendix D for details). The combined products transfer heat to the granular bed to initiate combustion. It is focused through one, or many, small ports which choke the flow and direct these hot combustion products into the granular bed. These products consist of both gaseous and condensed phase materials.

The black powder combustion is the least regular part of the ignition train. This is in part because black powder's chemical composition can be highly varying while still falling within military or other specifications. It is also extremely susceptible to moisture absorption, and manufacturing techniques vary significantly. However, compared with other propellants, black powder does excel at burning at atmospheric conditions (pressure and temperature). This makes it useful in the early stages of the ignition train when the system is not yet pressurized. [4]

The combined products of the primer and black powder are used to provide the initial pressurization and energy to ignite the granular material, in this case a double base propellant.

Double base propellants consist of a homogenous combination of nitrocellulose and nitroglycerin [1]. The ball propellant is heated convectively by the hot product gases which are the majority of the injector jet, by volume. The remainder of the jet consists of condensed phase products which come into direct contact with the individual granular propellant grains and provide an enhanced conductive heat transfer mechanism. Finally, the hot gases from the burning bed are forced to egress though chamber vent-holes where they provide energy to move the projectile. The round then exits the smooth-bore gun tube until it reaches its target. The first stages of the pyrotechnic ignition train are detailed in Figure 1.

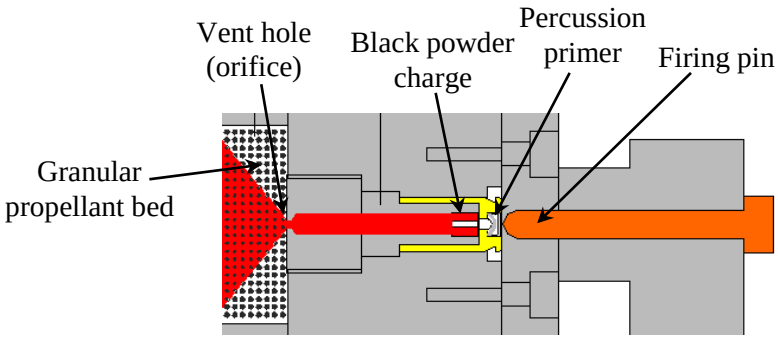

Figure 1: Typical components of the ignition train for granular propellants.

The granular material of interest is M48, a double base propellant. A characteristic of propellant is to burn with increasing intensity as pressure increases. In the case of the granular bed, the chamber volume is initially restricted by a pressure sensitive device and the burning rate increases until either the projectile starts to move or chamber vent-holes become unblocked.

Research Motivation

Understanding the detailed ignition, flame spreading, and combustion processes inside of a granular solid propellant bed is vital for accurate interior ballistic modeling and development of many weapon systems, including mortars and small- and medium- caliber gun systems. Modeling

of this complex system allows for a more thorough, and cost sensitive, design process to be followed. This is because the quality of a model is highly dependent on close agreement with the physical system in the early stages of the ignition train. There is therefore a need for highly accurate, detailed data on the ignition processes [2]. The system modeling also allows for the development of armaments which work with a high degree of consistency and therefore are safer and perform more accurately.

In the recent development of comprehensive predictive internal ballistics models at the Army and PSU, it was determined that certain fundamental information about the ignition and combustion behavior of granular propellant beds are be needed to enhance the basic understanding and to facilitate the predictive capability of the mortar codes. The codes have been required to use one-dimensional approximation for jet penetrations or assumptions for the two-phase flow heat transfer characteristics.

Since burning black powder results in two-phase (gaseous/condensed) product formation, its interaction with the granular bed is very complex. The convective heating of the granular particles is enhanced by the condensed phase product deposition onto the individual particles. It is, however, unknown what the degree of the condensed-phase deposition's affect on the bed ignition is. Information on the two-phase flow is currently lacking in detail from current modeling techniques [5].

The information gathered regarding igniter jet penetration and condensed phase product deposition could be useful as modeling correlations. Flame spreading rates determined experimentally would be useful for model validation.

Research Goals and Objectives

A high-pressure, windowed, test chamber equipped with pressure diagnostics was utilized for observation of the flame-spreading event. The goal of the research is to use this chamber to determine fundamental information about the ignition processes within the granular bed. The main objectives of the research were:

1. Characterize the igniter jet shape and penetration depth into the granular bed as a function of vent-hole geometry, strength of black powder charge, and bed geometry.
2. Determine the effect of the igniter jet on the flame spreading processes in the granular bed.
3. Measure the igniter jet influx time compared with the onset of granular bed combustion.
4. Find the relative rate of process of hot gas and flame fronts in the granular bed.

Chapter 2

Literature Review

In order to fully characterize the ignition process for a typical granular propellant bed each individual element must be studied separately. This is especially useful because the numerical simulations in question are developed piecewise. Additionally, there is a need for experimental models to have both validation and certain empirical correlations.

Characterization of the Primer

Despite their nearly ubiquitous use in many small and large arms, there has been little work on the characterization of primers for gun systems. Information regarding the jet strength, shape, and composition by phase (i.e. condensed vs. gaseous products) is minimal in the available literature. The Federal No. 150 large pistol primer, utilized in the 120-mm mortar system, will be used in this study.

Howard and Williams [6] characterized the two 120-mm primers for their ignition stimulus output. Exit jets were measured with high speed photography and where characterized by pressure and temperature of product gases. These measurements were used to develop and validate their computer models.

Horst and Conroy [7] investigated the No. 41 primer for a 5.56-mm round. They found that the affect of increased primer function time was to both increase initial granular bed pressurization and also to decrease flame spreading rates. Schmidt and Nusca [8] also looked into the 5.56-mm primer and found a correlation between condensed particle deposition and jet velocity. Chang and Williams [9] did work to capture and analyze these particles. It was determined in their investigation that there is minimal affect by the condensed phase particles on

solid propellant ignition but fine solid particles had a strong effect. Williams et al. [10] did further investigation on the No. 41 primer by recording pressure-time traces, examining jet shape into open air, and jet deposition onto an inert (Teflon) granular bed.

Characterization of the Igniter Jet

Any combination of elements that ignite the granular propellant bed are considered the igniter jet. For the system in consideration, it is the primer and black powder products. For this investigation, the products in the primer are considered in combination with the primer jet because that is its source of initiation energy for black powder burning.

Wildegger-Gaissmaier and Johnston [11] considered the igniter jet for the 127-mm gun system. In this system, the primer initiates a benite stick (composed of nitrocellulose, potassium nitrate, charcoal, and sulfur) which in turn starts the burning of the granular bed. Chamber pressure was used to characterize different placement and charge weights of the benite stick. Pressure will also be the primary mode of characterization of the burning igniter jet for this overall study.

The burning characteristics of black powder are highly unrepeatable. In the investigation by White and Sasse [4] it was found that the constituent parts of black powder are assembled though different processes from different manufactures. Additionally, black powder is especially susceptible to moisture absorption. Sasse [12] took samples created with the same manufacturing processes and compared physical grain structures and burning rates. A scanning electronic microscope (SEM) was used to analyze a compressed black powder pellet for voids. It was found that, even within the same lot, there was significant variation in open area within the grains. Water absorption by the black powder was found to retard the burning rate of black powder as it occupies the otherwise free volume in the grain.

Houim and Kuo [13] applied an ideal gas assumption, among others, to the two-phase igniter jet to create a numerical code studying black powder combustion in a flashtube. This is due to the volume ratio of condensed phase products of black powder products and the compressibility of the gas at the maximum typical pressure. This assumption will be used to calculate choked flow conditions for the igniter jet in this study.

Numerical Granular Bed Studies

There are many numerical studies of granular bed combustion in the literature. In studies surveyed there was often a need for experimental validation and even further physical understanding. This would increase the accuracy of the models created. This study seeks to resolve many of these issues.

Kuo et al. [14] did some of the earliest modeling work. This included mobile and fixed granular bed combustion codes relating to solid propellants with cracks and modeled a burning, mobile, granular bed including intergranular stresses and wall friction [15]. Bdzil et al. [16] reviewed a two-phase model to study the deflagration-to-detonation transition. It is described how detailed information about the ignition processes of granular particles is needed to create a model which is applicable over a wide range of conditions.

Nusca and Conroy [17] examined the Army's three dimensional modeling code (NGEN3) with specific application to gun propulsion. Their model found that small changes in design could make large changes in device efficiency. However, their model accuracy is highly dependent on experimental agreement during the early part of the model prediction. For a useful model, many model validating tests are required to ensure that the code functions properly.

A lumped parameter model with uniform ignition in a well mixed reactor was considered by Schmidt et al. [2]. They considered that the two phase jet is uniformly distributed into the

granular bed. Horst and Conroy [5] in their model considered the ignition of the bed as initiated by a predetermined mass injection profile. These assumptions can be refined with more detailed information on the igniter profile and interaction with the bed.

Experimental Granular Bed Studies

There have been limited studies done on granular bed combustion. Many of the articles found focused on only one type of measurement.

The basic physics of granular bed combustion relies on the understanding of convective burning. Asay et al. [3] examined the affect of bed porosity on a high gas jet penetration. It was found that high gas velocities (i.e. strong convective burning) were not possible in beds with low porosity. Also, optical systems for examining the bed combustion can suffer from problems of light blockage by unburned particles. Their analysis was therefore restricted to pressure-time traces and post-test bed analysis. The light blockage problem will be addressed in this study by attempting to create a planar combustion which will allow burning directly adjacent to the instrumented window.

Dijkhuizen et al. [18] considered a fluidized bed without burning to determine its heat and mass transfer characteristics. A particle image velocimetry (PIV) system was utilized to capture both velocity and temperature fields within the bed. Chukhanov et al. [19] also found heat and mass transfer rates for a non-reacting bed. This was compared against a combustible bed where it was determined that the variations in temperature within the bed had a substantial effect on mass transfer.

Many of the granular-propellant flame-spreading bed studies were done simultaneously with numerical studies for validation purposes. Baer et al. [20] did axial flame spreading studies on a compressed granular propellant bed contained in a Lexan tube for optical measurements.

Ignition was performed with a hot wire and high speed streak photography was recorded to measure particle speed to determine the deflagration to detonation transition (DDT) requirements and wave position. This information was used to validate the pressure dependent burn rate and the bed permeability in a multiphase, reactive flow model.

Another study of axial flame spreading was done by Chen et al. [21]. A 0.777" diameter cylindrical windowed chamber was used for high speed photography. It was also instrumented by pressure transducers and ionization probes to detect the arrival of the hot gas front. The data gathered was to validate model data on boundary conditions for the granular bed.

A cylindrical test chamber was created to test longitudinal flame spreading in low vulnerability (LOVA) propellants by Kooker et al. [22]. An igniter, with adjustable composition, was forced to be a planar wave by forcing it through a porous flow straighter before the granular bed. The chamber was sealed by a burst disk which failed at a repeatable pressure. The chamber was created to, and was successful to, validate a related flame spreading model.

Wildegger-Gaissmaier et al. [23] examined flamed spreading rates in LOVA by using fiber optic sensors. These sensors were able to sense flame front arrival but not intensity because as they were destroyed by the passage of hot gases. In a later study, Wildegger-Gaissmaier et al. [11] studied the ignition of LOVA granular propellants in a 127-mm gun. This set-up was equipped with a full window, fiber optic sensors, and pressure transducers. Igniter jets of various configurations were characterized by pressure-time traces and high speed video into both an empty and a propellant filled chamber.

To study the mechanisms of gun failure, Davis et al. [24] studied several different ignition train configurations in the same axial chamber. Their experiment showed that the igniter strength is strongly related to the pressure front acceleration in the bed and the induction period. Additionally, granular particle geometry was varied and it was found that higher surface area on the particles leads to an increased rate of mass consumption.

Davis et al. [24] also considered the affect of boundary conditions on granular bed combustion in a 30 caliber system. They found correlations for flame spreading rates to intergranular stress and particle wall friction. The results showed close agreement to their model. In another study, Kuo et al. [25] did experimental work with a variable gas pyrogen ignition system to vary igniter strengths. This allowed the igniter to be highly reproducible giving data useable for additional model validation.

A granular bed with an open boundary was examined by Ermolaev et al. [26] to look at the transition to explosion. Granular single-base (nitrocellulose) and double-base propellants were placed into a steel tube and ignited with a spark. High-speed photography and pressure-time traces were used for analysis. It was found that there is a strong influence by wall friction in the transition to explosion within these parameters.

Yang and Keairns [27] did a comprehensive review of data for single and multiple jets penetrating into fluidized beds. It was found that the single-phase jet may enter into the bed in gaseous bubbles. Scaling was used to find new correlations for depth of penetration which was dominated by a force balance of jet inertia and gravity forces in the bed. Strong Froude number dependency ($\frac{l}{d_o} = 26.9Fr^{0.322}\left(\frac{\rho}{\rho^s}\right)^{0.325} Re^{-0.124}$) was found, allowing for grouping all data for a single jet to within 40% of measured values. Blake et al. [28] also started with the conservation equations to find important parameters to describe the jet. Their research also emphasized the importance of the creation of gaseous bubbles in the jet relating to jet penetration. However, the ratio of the exit jet, d_o, to the particle diameter, d_{part} , is several orders of magnitude above the value for the system considered in this study. This effect had to do with the fluidization of the bed due to jet impingement which is less likely to be as strong of an effect when the ratio is on the order of unity.

None of the literature surveyed had data with simultaneous or comparative measurements of flame spreading and hot gas emissions nor were methods suggested. Thynell et al. [29] used rapid scanning FT-IR spectrometer system to look at burning propellant. It was determined that spectral emissions in the 5000-2400 cm^{-1} (the low- to mid-IR) wavenumber region corresponded to the burning surface itself and thus the flame front. The emissions in the visible region correspond to hot gas emissions. Therefore, visible light emissions can be used to detect the onset of a hot gas front and infrared emissions can be used to detect flame spreading. In this study, these two signals will be measured by photodetectors sensitive to two these two spectral ranges.

Chapter 3

Method of Approach

Chamber Design

The experimental test chamber was designed so that it could operate on the test stand already available at the High Pressure Combustion Lab (HPCL) where previous mortar experiments have been performed (Figure 2). The key features incorporated are:

- Reusable test chamber;
- Pressure taps for the igniter and granular bed sections;
- Modular granular bed test section to allow for investigation of axial, radial, or azimuthal flame spreading;
- Windowed access to the burning granular propellant bed which is transparent to both the visible and near-IR radiation.

In Appendix A, detailed schematics are given for the entire test chamber. Since the chamber is a pressurized test vessel it was designed with a minimum factor of safety of 4. Finite element simulation results are shown in Appendix B.

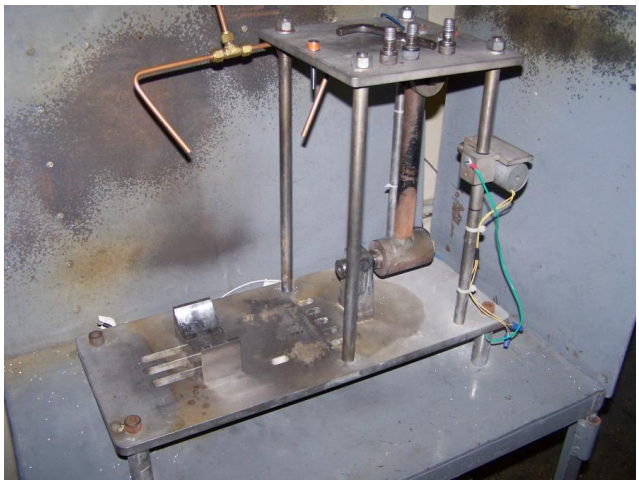

Figure 2: HPCL test stand for various mortar tests.

Head End

Common to all tests performed is the head end of the test section. This is shown in Figure 3. This part of the system is designed to house the percussion primer and black powder pellets (igniter products) and deliver their energy to the granular bed which will be located in the next section of the chamber. The flashtube tests can be run with just this section.

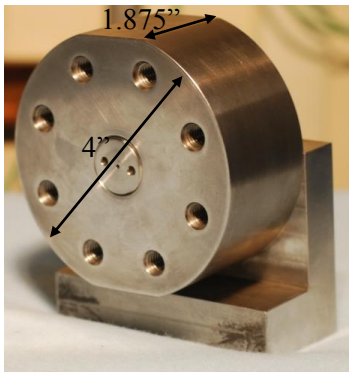

Figure 3: Head end of test set-up installed with L-bracket and flashtube section.

The percussion primer is the Federal No. 150 large pistol primer which begins the ignition train in the 120 mm mortar system (detailed in Figure 4). The same primer is also used in .45 ACP pistol cartridges. The brass gun cartridge is designed to expand and seal hot gases while

also being reusable. Therefore, this component is used directly to hold the primer in the head end. The cartridge sits over the black powder retainer which holds up to one black powder pellet. This simple part is modular and can be replaced to allow for different geometries or quantities of pellets to be used. From previous HPCL experience with the Army and the 120 mm mortar, the pressure developed from these components was expected to be 3000 to 4000 psia. However, due to backflow from the main section of the chamber, this section needed to be able to withstand the maximum chamber pressure. It was therefore designed for a maximum static pressure of 20,000 psia with a minimum factor of safety of 4. With this strength consideration, the need for hard steel which could resist deformation to seal the cartridge, and for corrosion resistance, a 17-4 PH stainless steel was chosen.

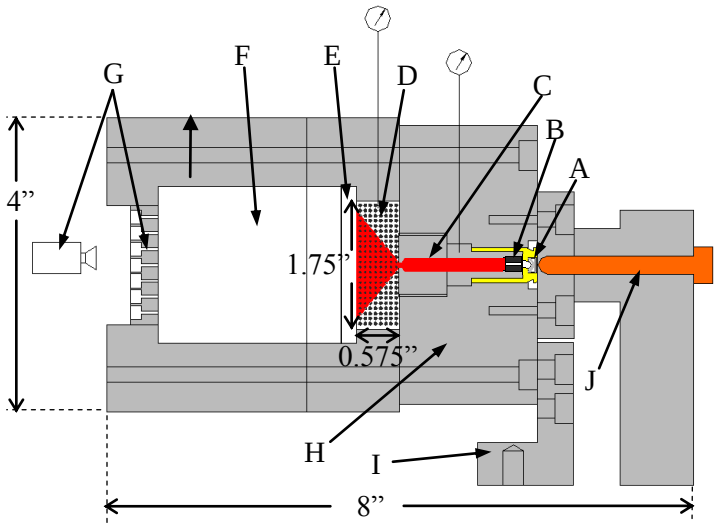

A	Percussion primer
B	Black powder pellet
C	Flashtube section
D	Granular bed
E	Sacrificial window
F	Quartz window
G	High-speed camera or photodetector array
H	Modular head-end piece
I	Test mounting stand
J	Firing pin

Figure 4: Schematic of igniter firing into granular bed.

The head end also has a pressure tap for measurement of the dynamic pressure in the flashtube. Alignment with the modular black powder retainer is ensured through a keyway in the black powder retainer and the head end (see Figure 5). Downstream of the transducer port is the modular flashtube transition section. It seals onto a corner with a crush seal o-ring and can be easily changed to accommodate different vent geometries. Various transition sections are shown in Figure 6 and connect to complete the flashtube section shown in Figure 5.

Figure 5: Half of the flashtube section installed with steel alignment pin.

Figure 6: Threaded sections with various orifices for the igniter jet.

The cartridge is held into place on one side by the black powder retainer and on the other side by the cartridge retainer (Figure 7). The latter also aligns the firing pin with the primer. The firing pin is made from two pieces for alignment purposes. One part sits next to the primer on a piston sealed o-ring. The friction of the seal acts to hold it in place before the test. It is struck on its flat surface by a second firing pin; that pin is struck directly by the pendulum hammer. This design is similar to a mortar ignition cartridge such as the M1020 (in the 120 mm mortar system) with a captive firing plug struck by a firing pin.

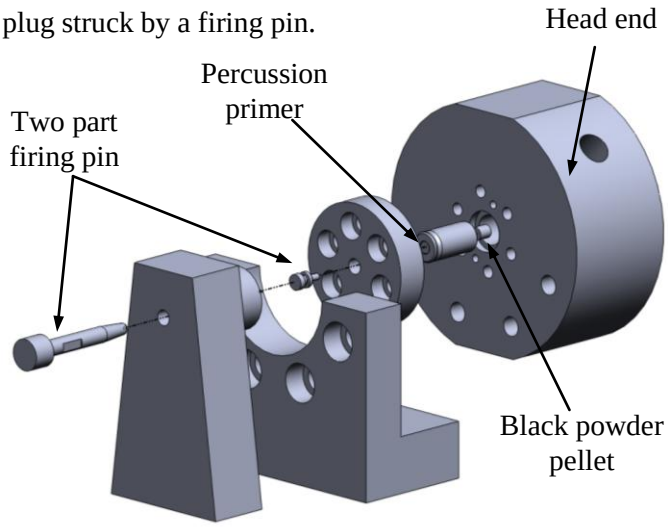

Figure 7: Head end of chamber showing the two part firing pin. The dashed line shows the alignment of the large firing pin with the smaller one and the latter with the percussion primer in the cartridge. The pendulum hammer strikes the pin on the left hand side.

Radial Configuration

The first configuration created was to investigate radial and azimuthal flame spreading and axial jet penetration into an inert bed. It is shown in Figure 8 and in Figure 9. The main chamber is created from the same 17-4 PH stainless steel as the head end to support the 15,000 psi of pressure expected to be seen from the burning granular bed (again the pressure is assumed from PSU mortar tests). The chamber is axisymmetric with four vent holes and four pressure taps.

Figure 8: Major components of radial configuration from left to right: head end, radial chamber, window holder.

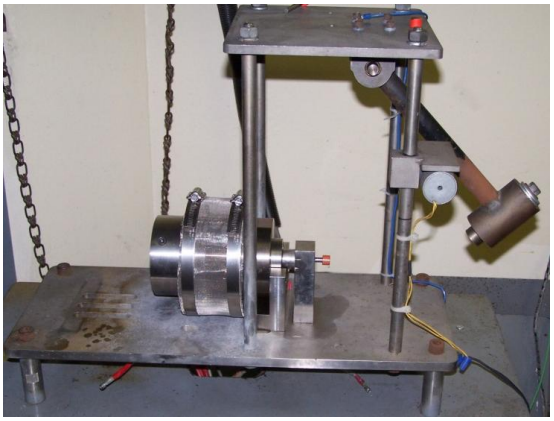

Figure 9: Photograph of radial configuration on test stand.

When assembled, the main chamber section and window support hold three windows in place. The first is a sacrificial window made of borosilicate glass. This member is not expected to hold the chamber pressure and is typically destroyed by the intense pressure and temperature of each test. The next two members are quartz; they are designed to hold the full chamber pressure and are reusable after each test. Both types of windows are transparent to the spectral emissions of interest.

The assembly of the chamber is shown schematically in Appendix A. After the head end is assembled the main test section is placed over it and the granular bed is added. The three windows are then put into place and the secured with the window retainer.

An array of photodetectors or high-speed camera sits directed at the windows in the configuration (shown previously in Figure 4). The spacing of the sensor ports for the

photodetectors was developed to allow a maximum amount of the physically larger IR photodetectors to view the event. A plastic spacer sits in this port to allow the visible light photodiode to be seated in the same position.

The window holder serves a secondary purpose; it creates a large open volume to allow for inert bed testing. This assembly can be completed by removing the radial test section and placing an inert granular bed placed into the free volume where the windows would be seated. A semi-permeable covering (in this case stiff paper) is placed over the viewing port to hold the inert bed in place but allow hot gases to exit. This is an ideal configuration because the gas path that must be taken to leave the chamber is downstream of the area of interest and does not affect the flow dynamics affecting condensed phase deposition.

An axial igniter jet is used to initiate radial flame spreading and it can be replaced with two radial jets this configuration can be used to observe azimuthal flame spreading. These flashtube sections were shown on page 16 in Figure 6. The azimuthal flame spreading section extends into the granular bed to initiate combustion directly in front of the sacrificial window.

Axial Configuration

The axial configuration also attaches to the head end. Again details are shown in Appendix A and it is pictured in Figure 10. It is designed to allow flame spreading for 4.575” inches in a 0.700” diameter cylinder. A window cutout is 3.330” of the length of the cylinder where flame spreading can be observed. The propellant is sealed into place inside of the cylinder by a steel burst disk. When the chamber reaches specified pressure, the burst disk will fail, in shear, allowing hot gases and particles to rapidly escape. Different pressures can be reached by varying the thickness of the burst disks or amount of propellant in the chamber.

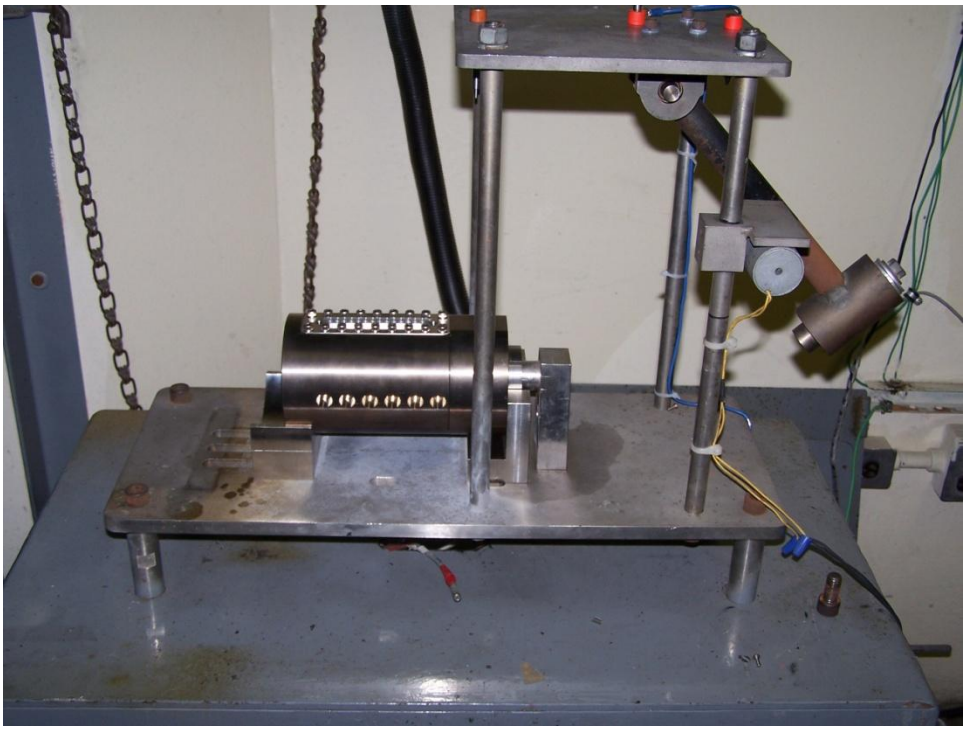

Figure 10: Photograph of axial configuration on test stand.

The shear disk is held in place so that uniform pressure inside of the chamber causes the disk to fail in a shearing mode. It is held in place by a vented bolt. The failing shear disk is shown in Figure 11. Along the axis of the cylinder, a 3.330” long window sits directly above the burning propellant. Similar to the radial set up, there is first a borosilicate sacrificial window followed by two quartz windows. Above these windows sits the detector array. It is designed so that each axial position can be monitored by both a visible light photodiode and infrared light photodetector. This is accomplished by setting the detectors and their apertures at an angle as shown in Appendix A.

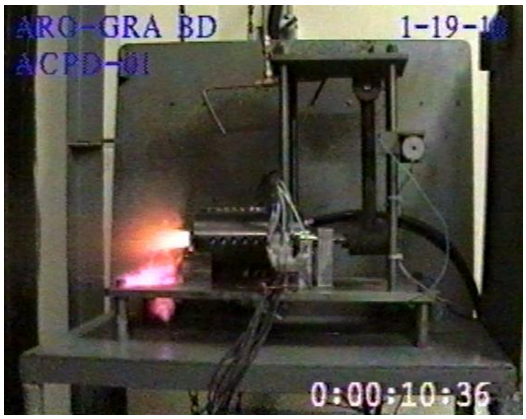

Figure 11: Video camera footage of axial chamber during test. Hot gasses can be seen venting after the ejection of the shear disk.

The flash tube section is designed to turn the flow 90° through four axi-symmetric vent holes, shown in Figure 12. This creates a planar gas-phase ignition wave in the granular bed so that pure axial flame spreading can be examined. It is extended past the head end of the chamber with a solid cylinder to fill some of the axial chamber. This allows the granular bed, and igniter jets, to begin directly below the window port inside the chamber.

Figure 12: Flashtube end section with four axi-symmetric, radial vent holes used in the axial configuration.

Diagnostics

All tests are instrumented with a minimum of both piezoelectric pressure transducers and a trigger signal from the test. The signals are measured on one of two data acquisition systems (DAQ), either a Nicolet Vision or a Nicolet MultiPro. The pressure transducers used are a PCB (111A23) capable of sampling pressure of up 20,000 psi at up to 100 kHz.

To create a common zero time among different tests, a 5-Volt TTL signal is generated when the pendulum hammer head strikes the firing pin. This reference signal is created by an ultra-low-current digital continuity circuit (circuit diagram in Appendix C) and allows measurement and comparison of ignition delays and flame spreading events. The circuit uses a NAND gate to transform the voltage change caused by the hammer striking the firing pin and completing a circuit to ground to a digital signal. However, mechanical friction in the system (between the hammer strike, the first firing, and the secondary primer striking the primer) keeps the repeatability from being as low as possible. The mechanical delay may change the time of the trigger signal by up to 0.5 ms. It was therefore mainly used as a common signal when it was necessary to operate a combination of multiple data acquisition systems and high-speed camera.

To measure the signal from both the visible light photodiodes (Perkin-Elmer VTP3310LA) and the infrared light photodetectors (EOS PBSE-010) a voltage divider circuit was created (circuit diagram in Appendix C). The signal was measured though a unity-gain op-amp buffer to prevent the high-impedance data acquisition system from influencing the measurement circuit. An adjustable voltage divider was also created so that the signal could be read differentially, thus nearer to the center of the DAQ's range. This allowed a smaller voltage range, and thus, higher resolution measurement to be taken.

A high-speed digital camera is also used to view the flame spreading event. It is a Photron FastCam PCI and can capture images at up to 2000 frames per second. This gives higher spatial resolution than the photodetectors but lower resolution in time.

To minimize signal distortion though from the flame-spreading event to the optical diagnostics, the window interfaces are filled with low viscosity mineral oil for every test. This has an index of refraction close to that of the quartz windows (near 1.45) and provides for a much better interface than air (index of refraction close to 1).

Determination of Product Species from Black Powder Combustion

NASA's Chemical Equilibrium with Applications (CEA2) code [29] was used to determine the combustion products of black powder. The combustion event inside the flashtube is neither constant pressure nor constant volume (the black powder does not burn with a neutral profile and the flow exits though a choked port). Both analyses for a combustion problem were considered to gain insight into the range of possible product species. Details of the analyses are shown in Appendix E.

The condensed phase products in black powder combustion are shown to be 14 and 19% of products on a molar basis. In both constant volume and constant pressure analyses, all of the condensed-phase products are potassium-containing species. Since black powder is the only place in the system where potassium exists before exiting the igniter jet firing, the presence of potassium can therefore be used as an indicator of the presence of condensed-phase products.

Species	*Mass Fraction*			
	Pressure = 1500 psi	Pressure = 2250 psi	Pressure = 3750 psi	Specific Volume = 0.265 g/cc
CO	0.18957	0.18606	0.18278	0.17467
CO_2	0.22791	0.21935	0.21248	0.16802
H_2	0.01514	0.01572	0.01613	0.01492
H_2O	0.10151	0.10515	0.10770	0.09194
H_2S	--	--	--	0.01665
KOH	0.06687	0.05873	0.05266	0.03465
N_2	0.18238	0.18445	0.18617	0.19037
S_2	0.01058	0.01331	0.01584	0.05073
S_2O	--	--	--	0.05073
KOH(*l*)	--	--	--	0.04446
K_2CO_3(*l*)	0.05698	0.07382	0.08787	0.03414
K_2S(*l*)	0.05394	0.04848	0.04338	--
K_2SO_4(*l*)	0.03143	0.02720	0.02369	--

Table 1: Major product species (> 1%) of black power combustion in a constant pressure reactor or constant volume reactor. Some species did not occur in both analyses.

Determination of Location of Condensed Phase Products from Black Powder Combustion

Since the condensed phase species of interest all contain potassium, a scanning electron microscope (SEM) with energy dispersive X-ray spectroscopy (EDS) is useful to perform an elemental analysis to identify potassium on samples. Unreacted propellants and particles were first analyzed. Then, specimens from a bed which was fired onto by an igniter jet will be analyzed to confirm the CEA results discussed above and also show that particles with condensed phase products can be visually indentified.

By replacing the live propellant bed with an inert bed of soda lime glass beads a post-test analysis of the igniter can be performed. The soda lime glass beads conformed to Mil Spec G-9954A and have a high degree of roundness and small size distribution, similar to the live granular propellant. The beads do not react with the jet and can be used to visually determine the location of condensed phase products. This is done by extracting the layers, layer-by-layer, with adhesive tape, photographing (Figure 13), and using software to analyze the particles. LABVIEW's NI Vision 8.6 software was used. The key steps of image analysis are shown in Figure 14.

Figure 13: Series of removed inert layers, the top left is closest to the orifice.

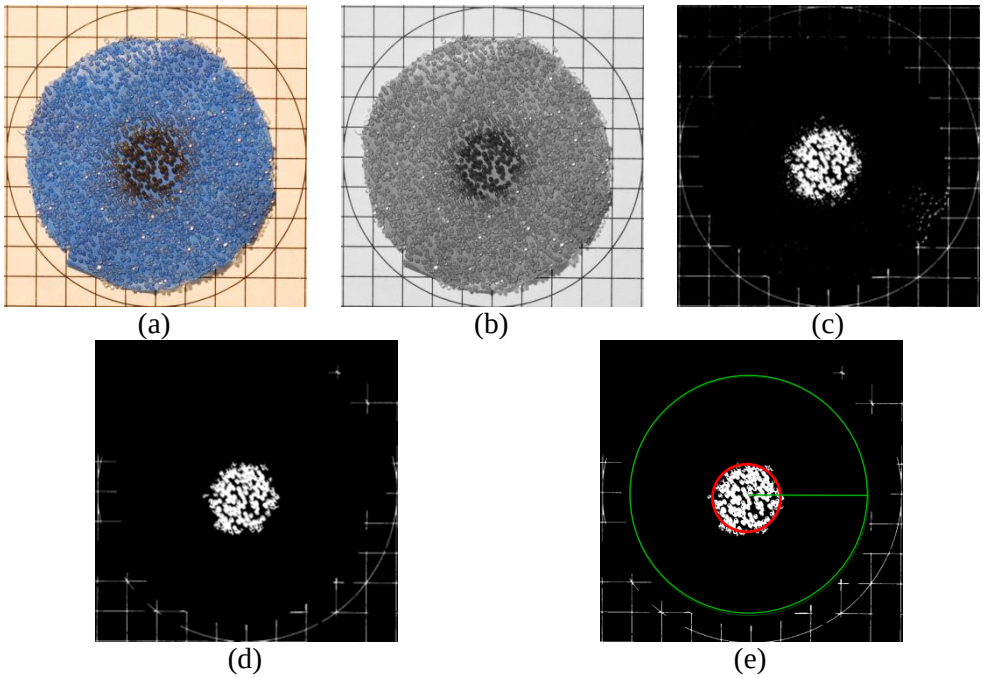

Figure 14: Images of a layer of inert particles after an igniter jet firing. a) Original image, b) image changed to grayscale, c) intensity threshold to remove light objects, d) small-scale artifacts are removed, e) circle finder is used to find the diameter coated domain.

This method makes several key assumptions. First, the jet acts axi-symmetrically. This is likely because the exit vent hole is round and gravity is unlikely to affect the high speed flow which only penetrates a short distance. Second, a binary system is created; particles are either covered with condensed phase products or not. Even a partially coated particle that is facing the camera with an uncoated portion will probably be identified by the software as a coated particle because of the transparent nature of the glass beads. Finally, for a live system, it is assumed that the penetration of the jet and the deposition of condensed phase particles precedes any granular propellant ignition.

Chapter 4

Results

Igniter Characterization

Pressure-time Curves

The first pyrotechnic component of the ignition train is a percussion primer. Details of the Federal No. 150 large pistol primer are given in Appendix D. Five pressure-time traces of the primer through an axial 0.065" vent hole are shown in Figure 15. The traces show a high degree of repeatability. The variation in time delay between various firings is attributed to the mechanical components of the system as the zero-time signal is created by the mechanical action of the hammer impacting the firing pin. The same set of traces is shown again in Figure 16 with the curves aligned by their first pressure rise. This time the similarity between each firing is more clearly seen.

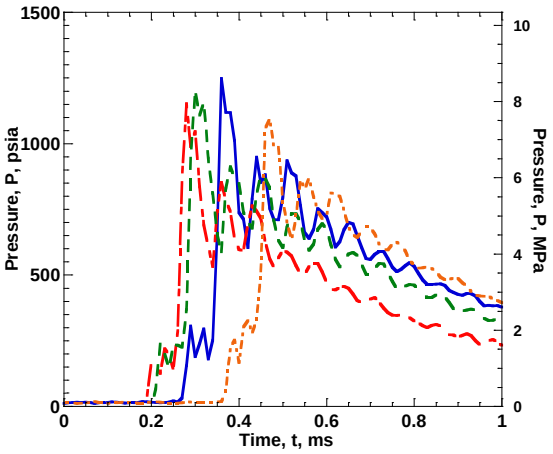

Figure 15: Pressure-time traces for 4 primer firings through a single, axial, 0.065," vent hole.

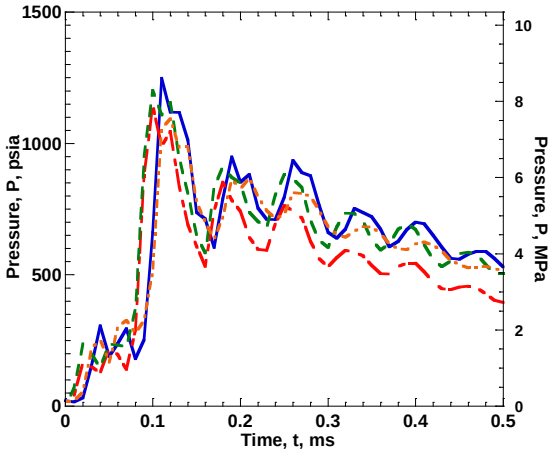

Figure 16: Pressure-time traces for 4 primer firings through a single, axial, 0.065," vent hole with the first rise aligned for comparison.

Shown in Figure 17 and in Figure 18 are two more sets of pressure-time traces for an axial jet. These show the burning of one black powder pellet (see details in Appendix D) initiated by the same primer as above. (In fact, all tests conducted in this investigation are initiated by the same type of percussion primer.) The characteristics of the primer's pressure-time history are absorbed into the overriding pressure of the black powder combustion. This shows that the black powder combustion event is very quickly initiated by the percussion primer. It is likely that the initial products from the primer, instead of the higher pressure or the bulk products, contribute to the black powder burning. This is likely because the products from the primer are a high percentage solid phase and black powder excels at burning at ambient conditions. The significant variation between individual pressure curves is due to the burning characteristics of the black powder only. Again, the misalignment of rise times is likely associated with a mechanical delay mechanism, but the curves still show around 500 psi of pressure variation. The curves also show significant differences in their peaks. Some show a sharp peak while others show a period of neutral burning. This jet configuration, through a single axial hole, is used to characterize jet penetration into an inert granular bed and initiate combustion radially.

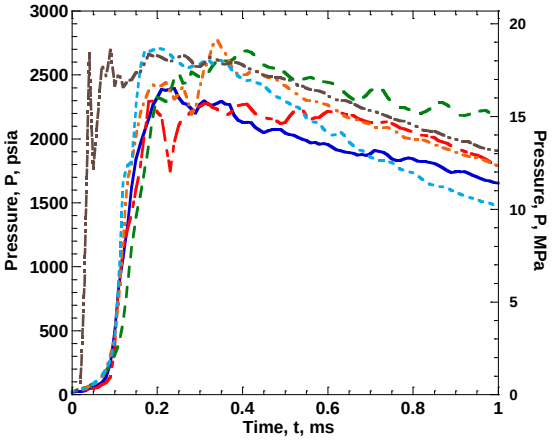

Figure 17: Pressure-time traces for 5 igniter jet firings through a single, axial, 0.065," vent hole.

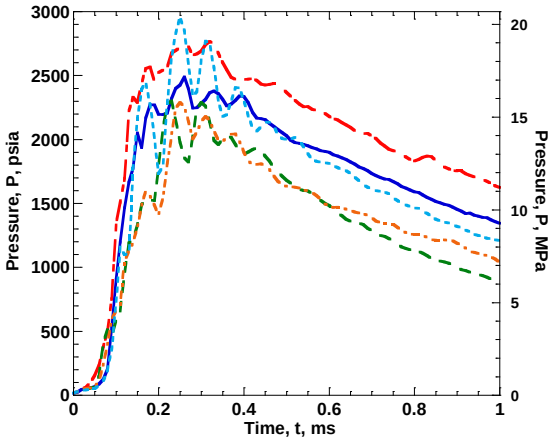

Figure 18: Pressure-time traces for 5 igniter jet firings through a single, axial, 0.073," vent hole.

The freely expanding axial igniter jet is shown in Figure 19. The resulting supersonic gas jet exiting the chamber is highly underexpanded.

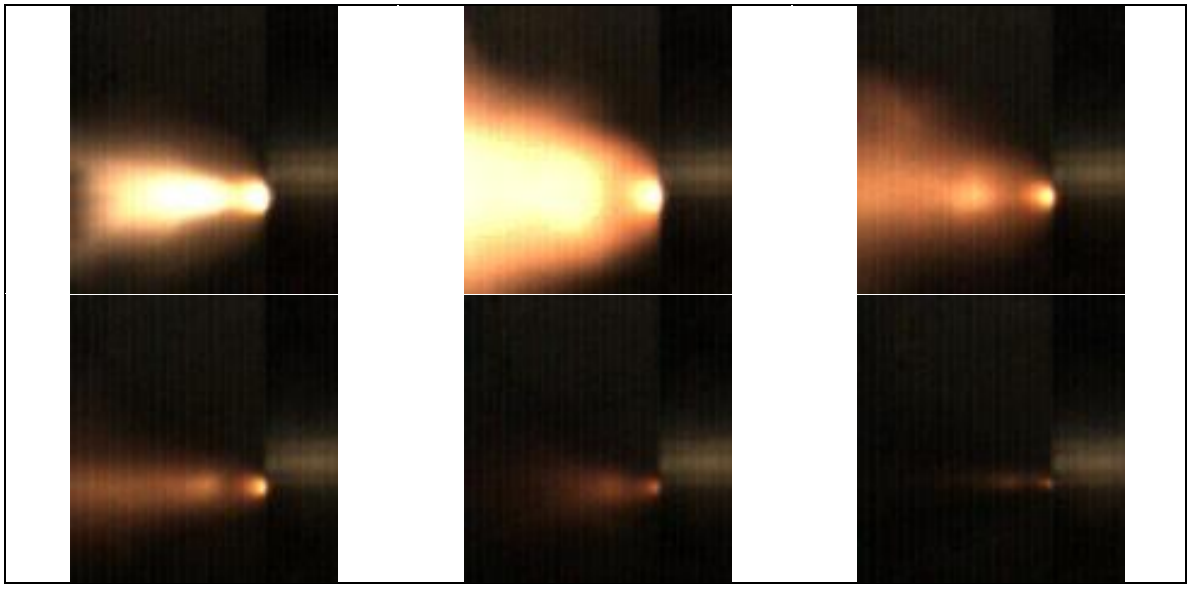

Figure 19: High speed photography (2000 fps) of a single black powder jet leaving a 0.065" axial orifice into quiescent air.

Finally, a single black powder pellet is burned and allowed to vent through 4 axi-symmetric, radial vent holes, 0.040" in diameter. The characteristic pressure-time traces are shown in Figure 20. This alternate jet configuration was used create a planar ignition wave in a

granular bed to examine axial flame spreading. The curves show much less repeatability than the axial cases. This is likely due to the more complex flow due to the turning of the jet.

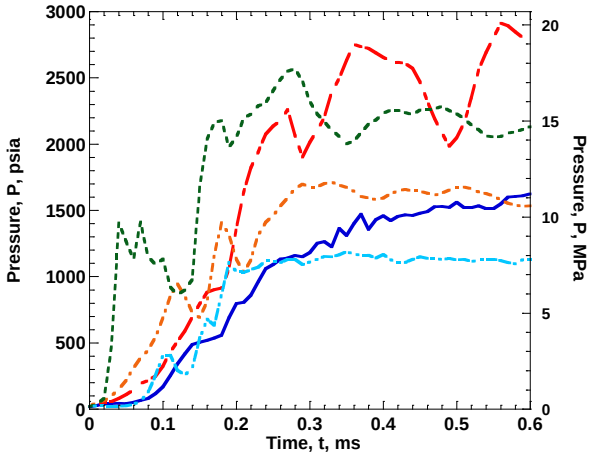

Figure 20: Pressure-time traces for 5 igniter jet firings through 4 radial 0.040" vent holes.

Scanning Electron Microscopy with Energy Dispersive Spectroscopy

Since potassium is not present in any of granular bed materials before the igniter is fired, an elemental analysis provides useful information about the location of the condensed phase product deposition from the black powder. A total of 5 cases were analyzed on a Scanning Electron Microscopy with Energy Dispersive Spectroscopy (SEM-EDS): 1) an unburned black powder pellet, 2) M48 ball propellant 3) an inert glass bead, and 4) inert glass beads recovered from after an igniter firing. Two types of recovered beads were tested, with and without visible products (shown in Figure 21). The resulting EDS analyses are shown in Figure 22.

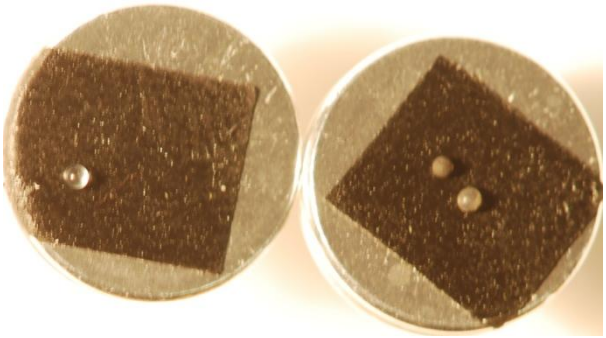

Figure 21: Glass beads after an igniter firing mounted for SEM analysis. The particles on the right hand side are covered with condensed phase igniter products.

The analysis for the control samples (i.e. unburned) shows a high concentration of potassium on the black powder specimen and no potassium on the propellant or inert particle. From the post firing inert propellant bed, the particles that show visible products from the igniter firing have high concentrations of potassium relative to their concentration of oxygen. The particles without visible products show no potassium. Some of the inert beads showed high concentrations of carbon. This was most likely due to the carbon mounting tape that the samples were on and the magnification of the analysis which brought the mounting tape into focus and not high concentrations of carbon the samples themselves.

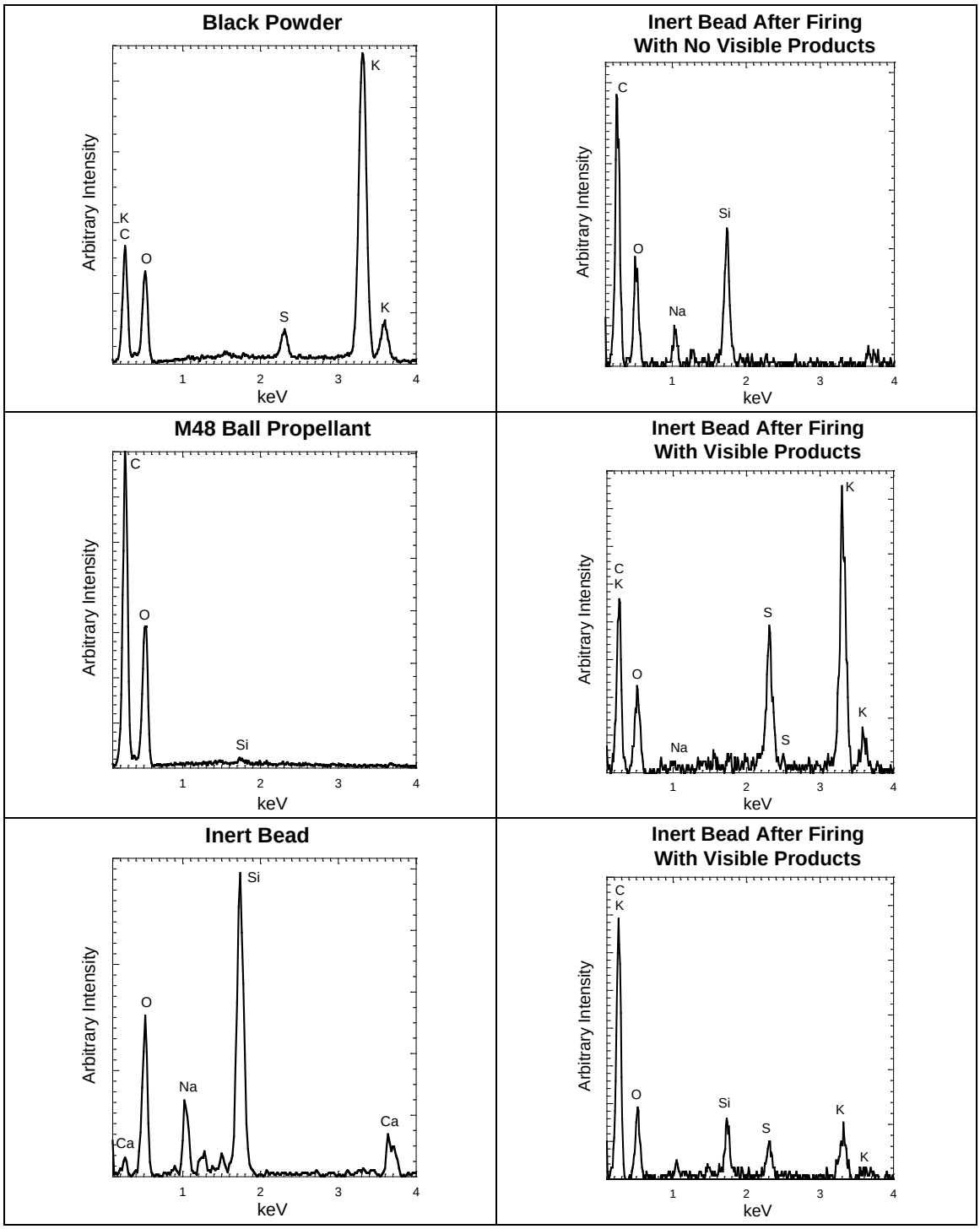

Figure 22: Left hand side: Energy spectra from various propellants used in the ignition train of the system. Right hand side: Energy spectra from inert beads recovered after an igniter firing.

This analysis of the inert propellant shows that the dark condensed-phase products contain the potassium species that are only present in the black powder pellet. These are expected to be condensed phase product species of black powder combustion (see page 22). SEM pictures showing the coating of the particles is shown in Figure 23. The particle coated with condensed phase product appears to be completely, but not uniformly covered.

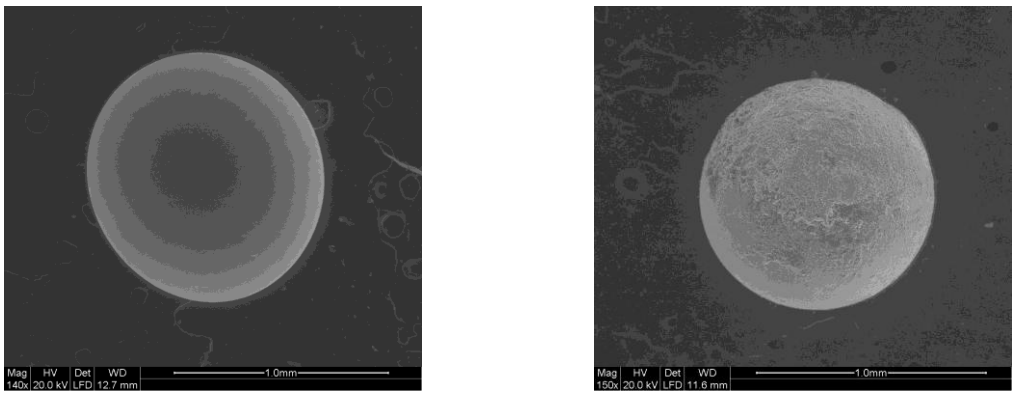

Figure 23: SEM images of two inert propellant particles at 150x magnification. Left) no visible condensed phase products, right) a particle which is completely coated with condensed phase products.

Inert Bed Firings

Axial igniter jets, whose characteristics were varied by orifice diameter and amount of black powder charge, were fired into an inert bed of glass beads. The following factors were systematically varied during testing: particle diameter, orifice diameter, and propellant mass. The various conditions for testing and results are shown in Appendix G.

For comparison, a primer jet was fired into an inert propellant bed. The depth of penetration was defined by the depth to the first layer of the granular bed where there were no visible condensed phase products. The jet profiles are shown in Figure 24. The flow initially expands from the orifice and then decreases in radius as it continues axially.

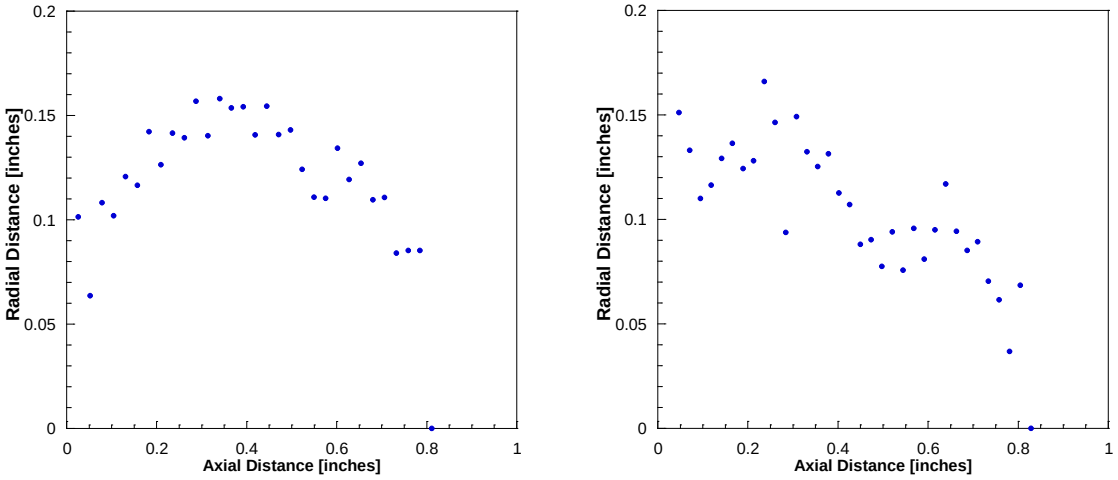

Figure 24: Two profiles of condensed phase percussion primer jets into an inert granular bed. The left hand side is a 0.065" orifice and the right hand side is a 0.055" orifice both into an inert bed with average particle diameter of 0.051."

Two typical examples of the form of the condensed phase product's jet boundary shape in the granular bed are shown in Figure 25 (a summary of profiles is given in Appendix G.). The condensed-phase jet shape does not have the same sharp angles as a supersonic gas jet. It shows a very steep turning angle at the exit where the jet diameter is the largest. Then the jet has a relatively flat profile before turning to a blunted point. This shape is likely due to a combination of effects: the supersonic nature of the gaseous part of the jet, momentum of the condensed phase products bouncing off of the granular particles, and momentum loss due to condensed phase deposition onto the granular particles.

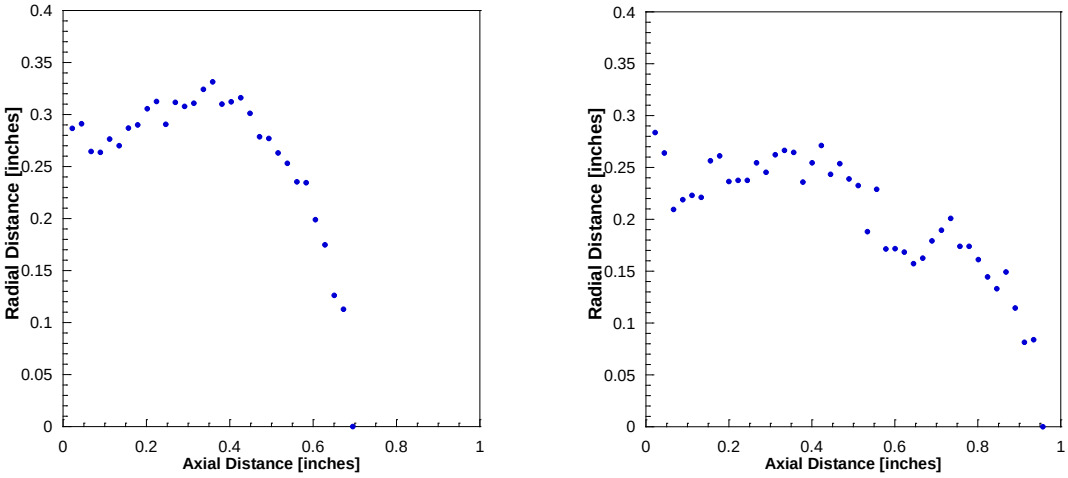

Figure 25: Two typical jet profiles of condensed phase products into an inert granular bed.

A correlation for the depth of penetration of the condensed-phase products into the bed was found in the form:

$$\frac{L}{d_{jet}} = 9360.9\left(Re_{d_{jet}}\right)^{-1.99}\left(\frac{\bar{P}}{P_{atm}}\right)^{1.86}\left(\frac{d_{part}}{d_{jet}}\right)^{-0.55}$$

The first term is the Reynolds number based on the jet properties at the orifice defined as $Re_{d_o} = \frac{\rho_{jet}\, U_o\, d_{jet}}{\mu_{jet}}$. The flow is assumed to be an ideal gas with gas properties taken from Appendix E. The average measured pressure was determined by integrating the pressure from the first recorded rise to subsequent decay down to 500 psia. The correlation is shown in Figure 26. Perfect correlation would be represented by the line y = x. The error bounds shown are at $\pm$30% consistent with the literature. The x error bars are at $\pm$ one layer of inert propellant. The outliers are likely due to the inconsistency of black powder combustion and the complex flow dynamics which are not completely described by the non-dimensional parameters given.

This correlation gives three important relationships. As the Reynolds number based on jet diameter increases the condensed phase deposition on adjacent particles increases which lowers the jet ability to penetrate further into the bed. An increased average pressure is analogous to an increased driving force for jet penetration and results in higher depth of penetration. Finally, as

the particle diameter decreases the degree of diversion of penetrating products from the axial direction decreases which also increases the depth of penetration.

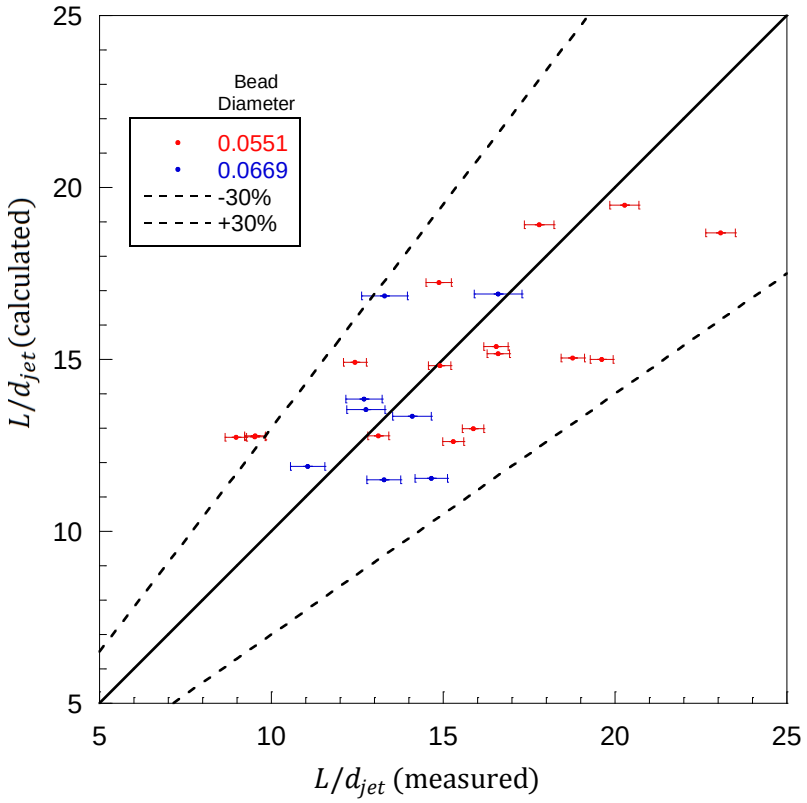

Figure 26: Plot of correlation for depth of penetration of condensed phase products into granular bed.

The condensed phase jet's boundary was used to create a correlation of the ratio of volume coated region to the volume of a single inert particle. The correlation was found in the same terms as the L/d_{jet} correlation:

$$\frac{V_{covered}}{V_{part}} = 195800\left(Re_{d_{jet}}\right)^{-1.94}\left(\frac{\bar{P}}{P_{atm}}\right)^{2.18}\left(\frac{d_{part}}{d_{jet}}\right)^{-1.28}$$

This is plotted in Figure 27. The error bounds for the volume measurement are due to error in measuring the radius of condensed phase deposition before integration to find the volume. Again as the Reynolds number increases the condensed phase deposition to adjacent particles increases which decreases the outer boundary of the volume affected by the jet. The average pressure again

acts as a driving force to increase the volume covered. Finally, as the particle diameter decreases the specific particle surface area increases. This increases the number of coated particles which increases the volume affected.

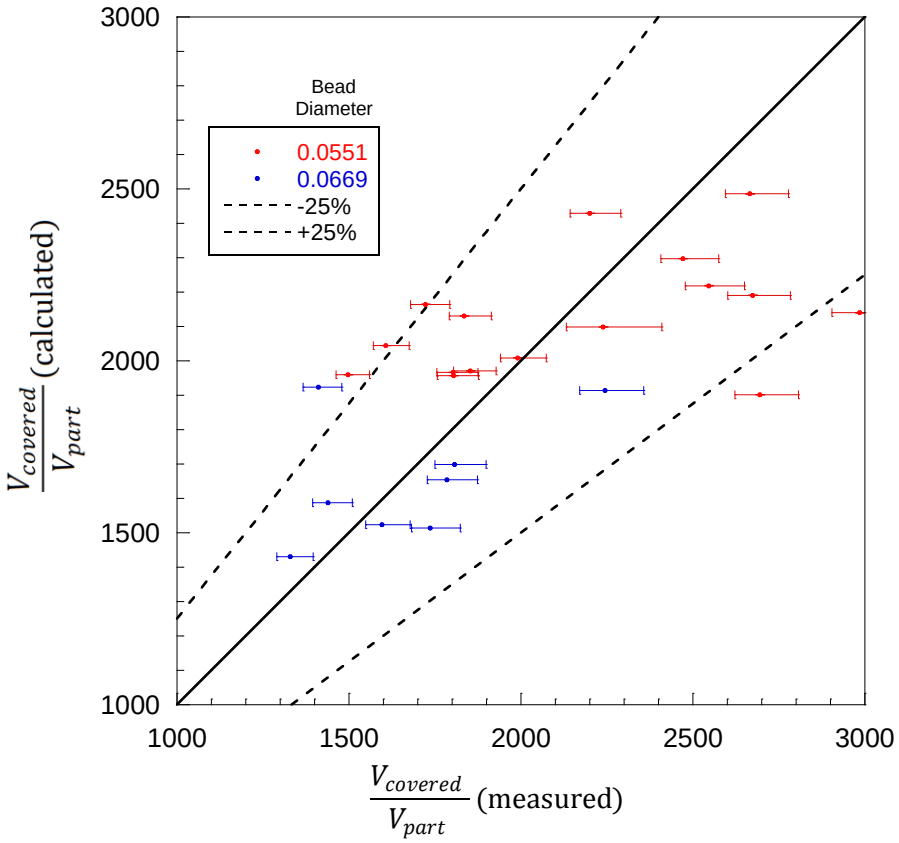

Figure 27: Plot of correlation for outer boundary of the volume affected by the jet.

Finally, a correlation was created to find the maximum radial spread of condensed phase products from the jet. Again the same non-dimensional parameters were used.

$$\frac{d_{cond\,,max}}{d_{jet}} = 1218.\left(Re_{d_{jet}}\right)^{-0.44}\left(\frac{\bar{P}}{P_{atm}}\right)^{0.37}\left(\frac{d_{part}}{d_{jet}}\right)^{0.74}$$

This is plotted in Figure 28. The same relationship holds for the Reynolds number as for the previous correlations. As the average pressure increases, the degree of underexpansion of the jet increases and thus the radial penetration increases. As the average diameter of the particles in the bed increases the tortuosity of the jet penetration increases and the radial penetration increases.

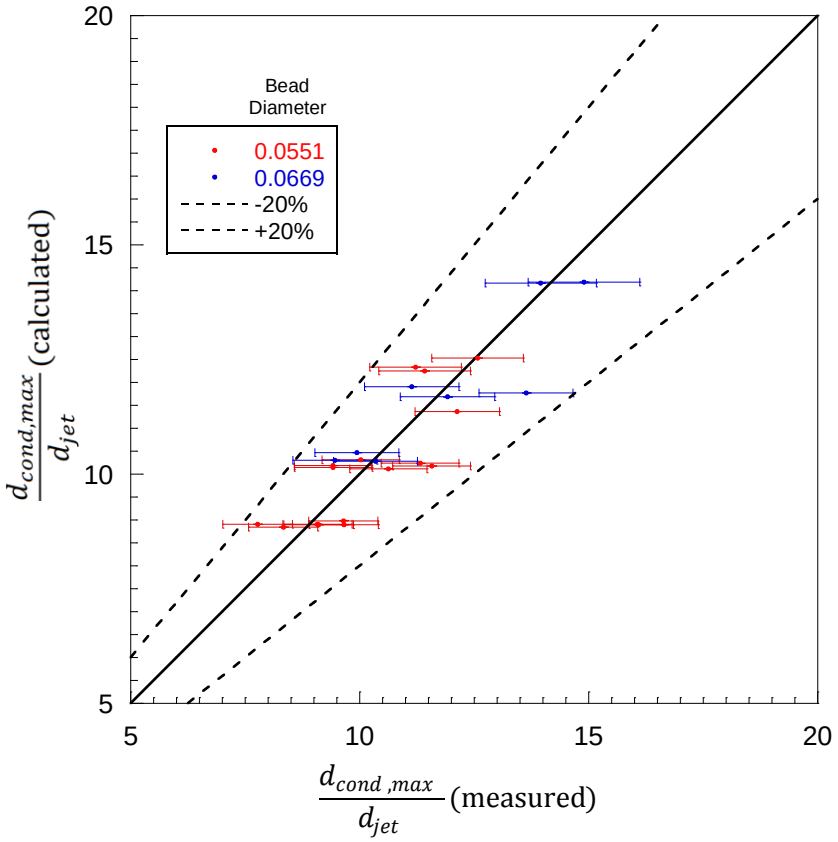

Figure 28: Plot of the ratio of maximum radial penetration of condensed phase deposition to jet diameter.

Azimuthal Flame Spreading

The radial test chamber is used in the azimuthal configuration for jet penetration and flame spreading study by using a flash tube section having two radial jets, shown in Figure 29. The igniter was fired into an inert propellant bed resulting in the pressure-time traces and high-speed camera images, shown in Figure 29 and in Figure 30.

In this test, the bed does not react with the igniter jet and therefore the camera results only correspond to the visible products of the discharging igniter jet from the combustion of a single black powder pellet. There is negligible chamber pressure increase shown because there are no reactions inside of the chamber and its volume is very large compared with the flashtube

volume. The three images that are shown cover a span of 1.0 ms and correspond to the majority of the time duration shown on the pressure-time trace. The times listed below the images are referenced to first discernible pressure rise at t = 0 on the pressure-time plot. The two jets are shown to penetrate the bed from the center to the wall of the chamber with nearly the same geometry and spread angles. As shown in the second image, the hot gas spread a short distance azimuthally before finally quenching in the third image. These high-speed images show a characteristic horseshoe-shaped dark region between the initial bright circular region immediately downstream of the vent hole and the fan-shaped outer bright region, shown most clearly at t = t_1 + 0.5 ms. This shape corresponds to condensed phase products deposited on the sacrificial window and is also visible on live granular propellant bed tests discussed later where it continues to be an artifact of the obscured window.

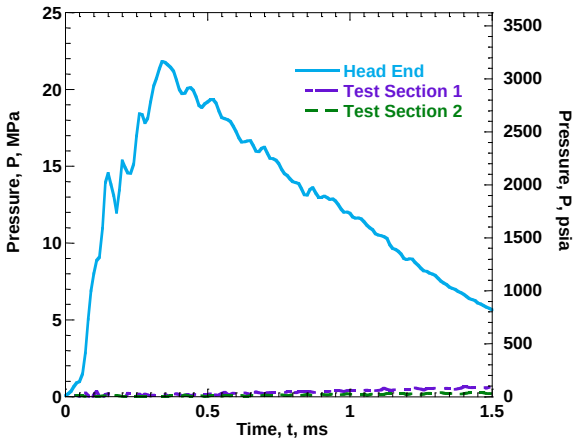

Figure 29: Left) Pressure-time traces, right) flash tube end section.

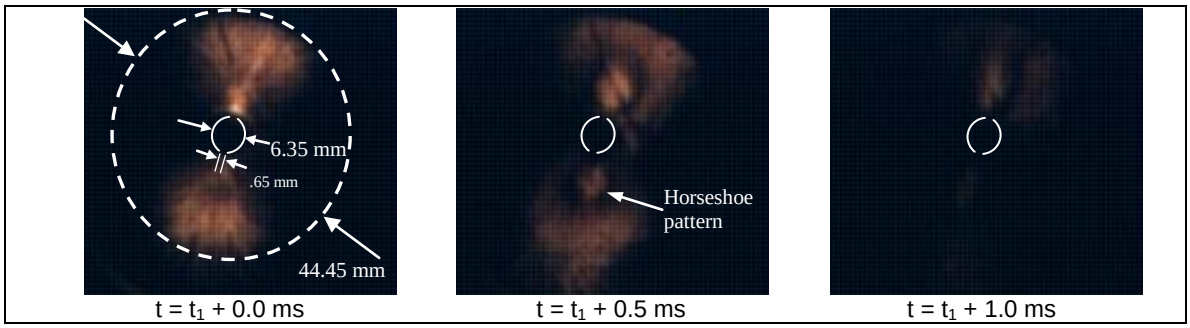

Figure 30: High-speed movie images (filmed at 2000 frames per second with a Photron Fastcam, times were measured from the onset of visible light) of igniter jet penetrating into granular bed in windowed test rig. The dashed circle represents the inner radius of the test rig and the smaller circle is the flash tube.

To study the igniter jet penetration into the live granular bed and to limit the pressurization rate in the test rig, two layers of live propellant particles were substituted for the inert propellants in the region next to the window. For this mixed granular bed, the results are shown in Figure 31.

Figure 30Figure 31 shows the high-speed movie of the igniter jet. t_1 is referenced because the pressure-time trace is not synchronized with the images shown. At $t = t_1$, the image shows the first signs of igniter jet penetration. The subsequent images are at intervals of 0.5 ms. In this test, the pressure in the granular bed stayed nearly constant since there was a minimal amount of propellant burned in the early event followed by the discharge of the gas and particles out of the granular bed when the rupture disks burst. From these images, one can see that the flame spread only to the downstream regions of the two vent holes with limited burning in the azimuthal direction. There are pockets of localized flame spreading in the periphery of the igniter jet. At $t = t_1 + 2.5$ ms, the flame starts to quench and extinguish as hot gas escapes from the radial vent ports. Post test visual analysis of the granular bed showed localized burning in the periphery of the igniter jets while the rest of the bed was minimally affected by the event. The incomplete flame spreading and combustion is explained by the low chamber pressure during the test (compared to the igniter pressure).

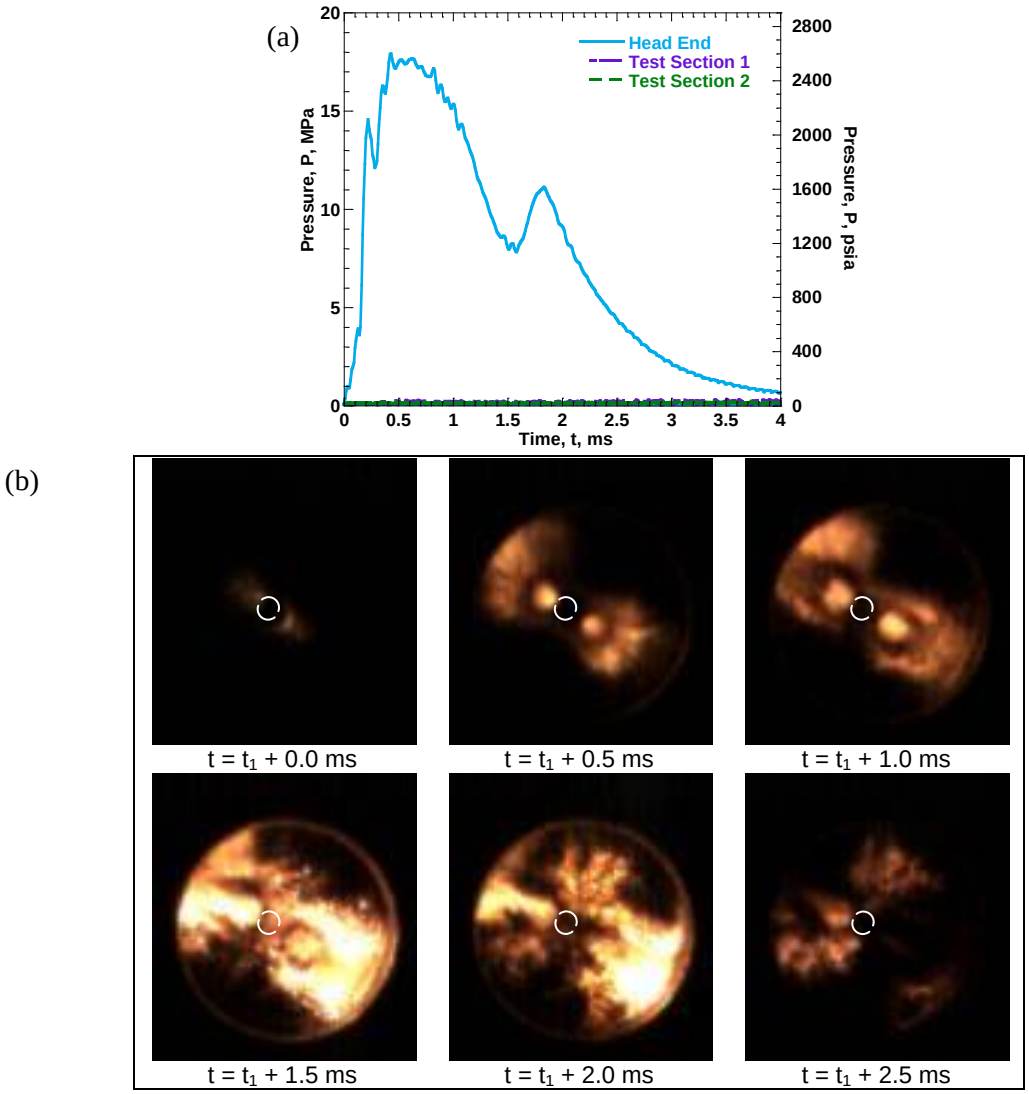

Figure 31: a) Pressure-time trace and b) high-speed movie images of granular bed with approximately two layers of live propellant next to window.

In order to achieve higher chamber pressure, a thin metal strip was added to the paper rupture disks with a single hole punched through the metal strip in the center of one of the four vent ports. By restricting the flow through the vent ports, chamber pressure in the granular bed peaked at over 6000 psia. The pressure-time trace and a set of high-speed camera images of the burning granular bed are displayed in Figure 32. In this case, the igniter jet has a chance to reach the edge of the test rig before the abrupt flame spreading and combustion of the granular

propellants. At t = t_1 + 1.5 ms some granular propellants were ignited at the periphery of the luminous regions. As time continues, the flame spreads to granular propellants in the chamber wall region. Between t = t_1 + 2.5 and t_1 + 3.0 ms, the flame spread rapidly from the wall region to the center portion of the granular bed. After t = t_1 + 3.0 ms, the whole window revealed intense radiation in the chamber, indicating severe burning of the propellant.

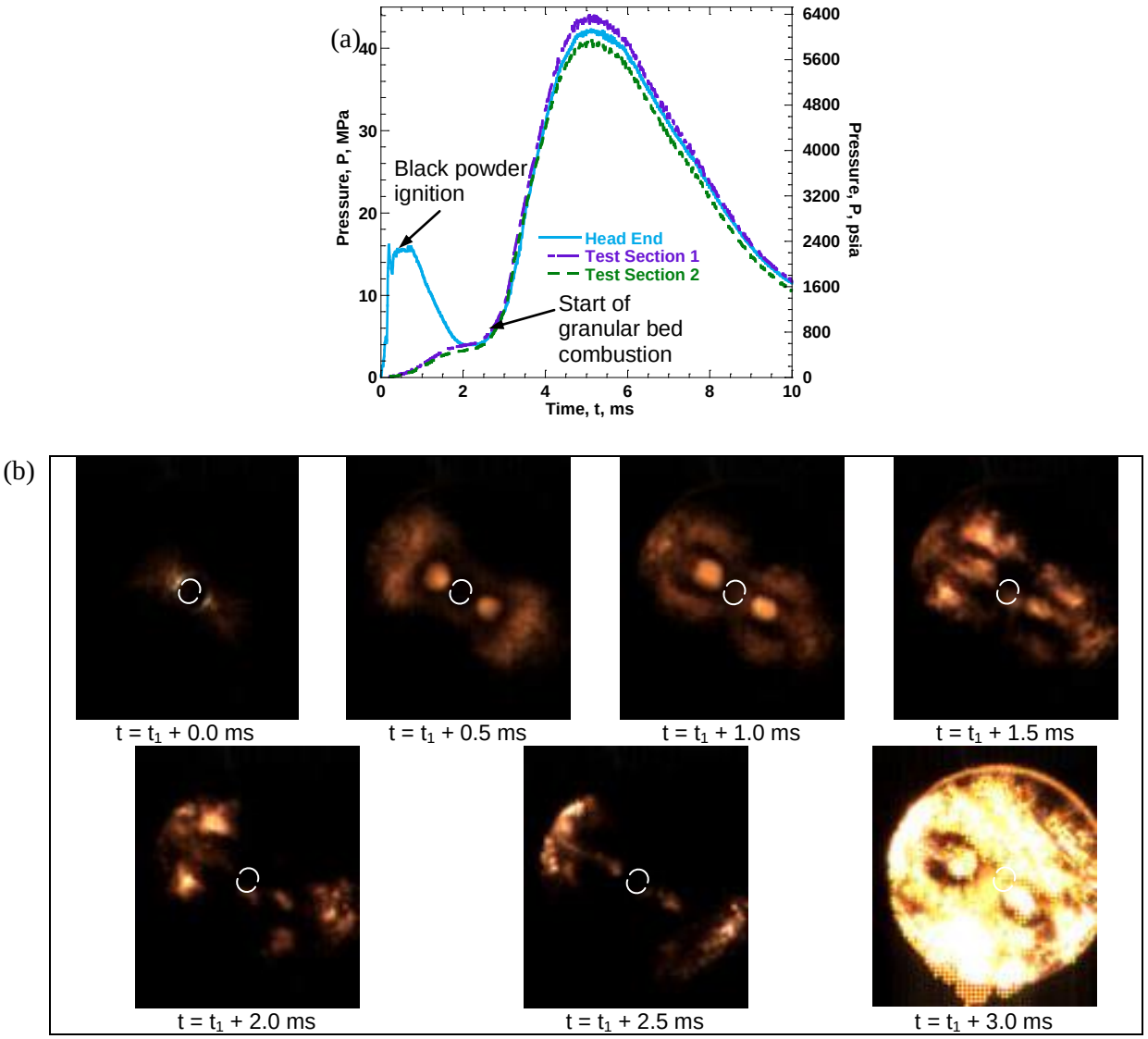

Figure 32: a) Pressure-time trace and b) high-speed movie images of granular bed with several layers of live propellant next to window.

Although the peak chamber pressure was reached at t_1 + 5.0 ms (Figure 32), the burning

continued until about 15 ms as recorded by visible light emissions (these images are not shown in Figure 32). The chamber pressure decay is due to the venting of propellant products from the radial vent port of the test rig. This higher pressure test allows much more of the granular propellants to burn than during the low-pressure test which results in a longer burn time despite the increased pressure.

Figure 33 shows pressure-time traces from another test with the same propellant loading as the test shown in Figure 32. These pressure-time traces are nearly identical to those in Figure 32 and both show an initial pressurization spike in the flash tube due to the combustion of black powder. This test was instrumented with high-speed visible light photodetectors instead of the high-speed movie camera. The recorded visible light intensity-time traces and array positions of these detectors are shown in Figure 34 and Figure 35. The light signal between 1 to 1.9 ms is largely due to the discharge of igniter jets. The onset of flame spreading occurs between 2.0 and 2.5 ms as can be seen from the superimposed plot of the main chamber pressure rise and the photodetector signal rise in Figure 35b.

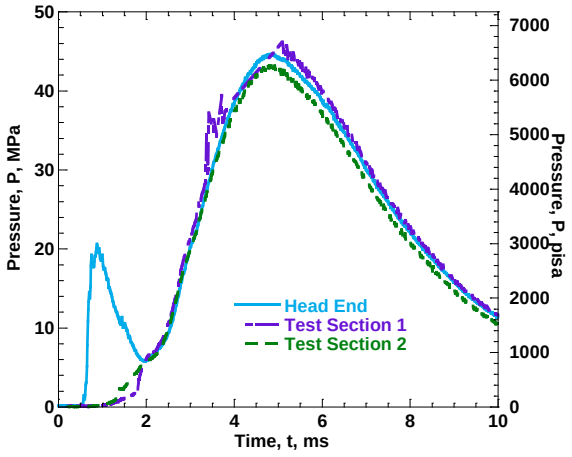

Figure 33: Pressure-time traces corresponding to photodetector signals shown in Figure 34 and Figure 35.

(a)

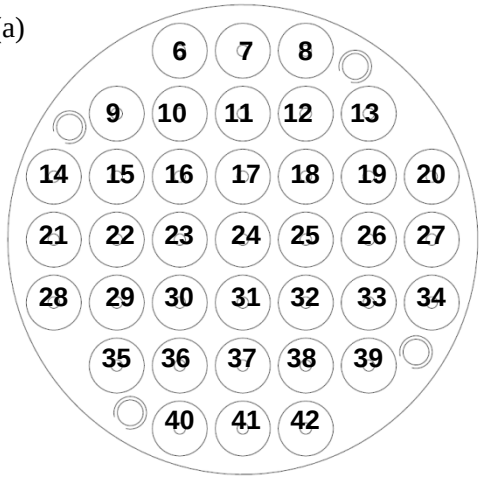

Numbering scheme for photodetector/photodiode array on the radial chamber. (1-5 represent pressure transducer locations)

(b)

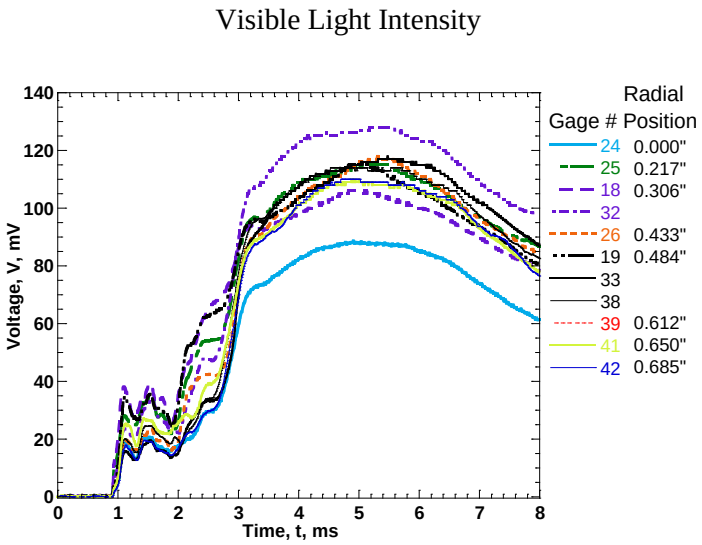

Figure 34: Test of black powder initiating M48 and propellant simulant in radial test configuration. a) Sensor configuration, b) Signal from visible light photodetectors by radial distance from center of chamber.

(a) Visible Light Intensity

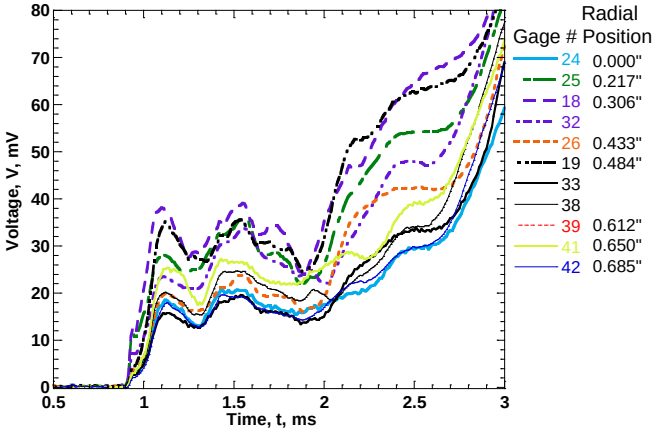

(b) Pressure and Visible Light Intensity

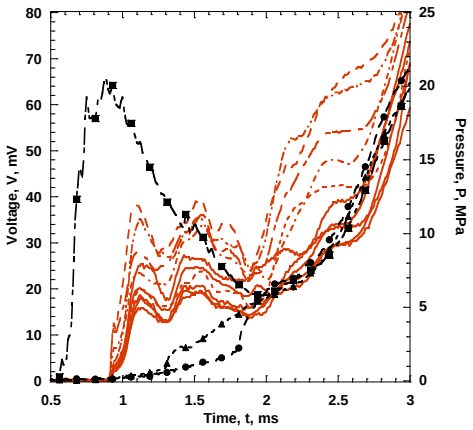

Figure 35: a) Visible light signal showing the early stages of the event, b) Superimposed plot of pressure-time data (black) and light intensity-time (red) curves.

Axial Flame Spreading

High-Speed Camera Results

To get a qualitative assessment of flame spreading, the axial chamber configuration was run with a partial granular propellant bed loading and a high speed camera. The overall propellant loading for this test was: the percussion primer, one centrally perforated black powder pellet, and 3.0 grams of M48 ball propellant. The rest of the free volume was filled with the same inert propellant used for igniter jet firings to keep the packing density similar to a volume completely filled with live propellant. The pressure-time traces are shown on the left of Figure 36. The depressurization indicates that the shear disk ruptured at about 2.0 ms. Later tests instrumented with photodetectors would implement a break-wire to confirm this depressurization time.

Four frames of a high-speed (2000 fps) movie were captured (right hand side of Figure 36). Since the live granular propellant only takes up a small fraction of the chamber and the inert propellant is very hard and unlikely to compress much, the light emissions seen do not correspond to the burning surfaces. Instead they show the hot gasses are produced on the right hand side (upstream) and move through the interstitial spacing between inert granules in the first three images. This indicates that the visible light photodetectors will still receive a signal even if the hot gas front is not in close proximity to a burning surface. The final image is after the shear disk failure and shows the rapid depressurization of the hot gases from the chamber.

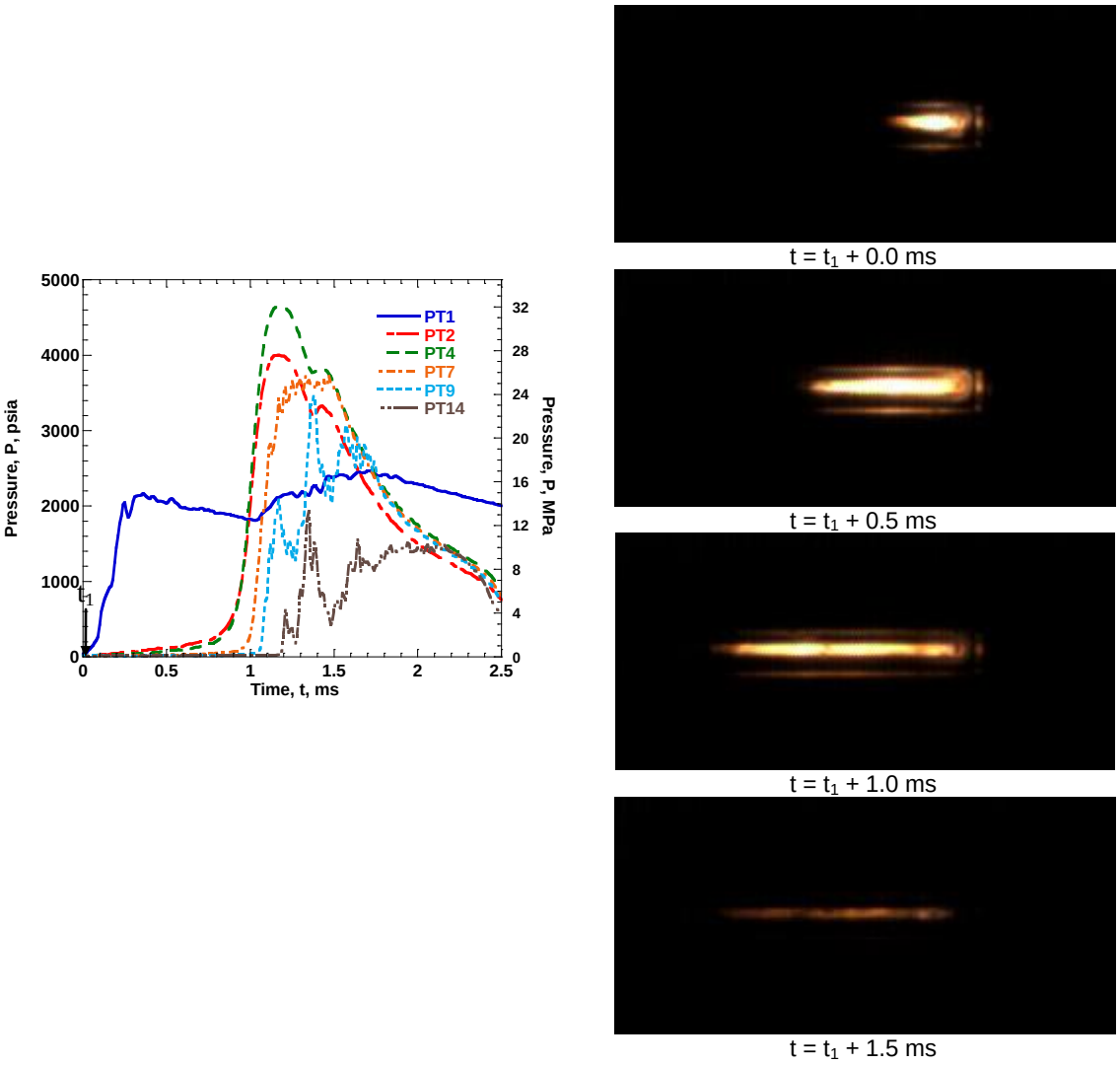

Figure 36: Left) Pressure time traces, and Right) high-speed camera images of burning granular propellant in axial chamber. Flow is from right to left.

Comparison of Burning Surface and Hot Gas Fronts

The same propellant configuration as the previous test (3.0 grams granular propellant upstream) with the high-speed camera was instead run with a photodetector array. The overall pressure-time and intensity time plots are shown in Figure 37. Details of the photodetector rises and corresponding pressure-time traces are shown in Figure 38.

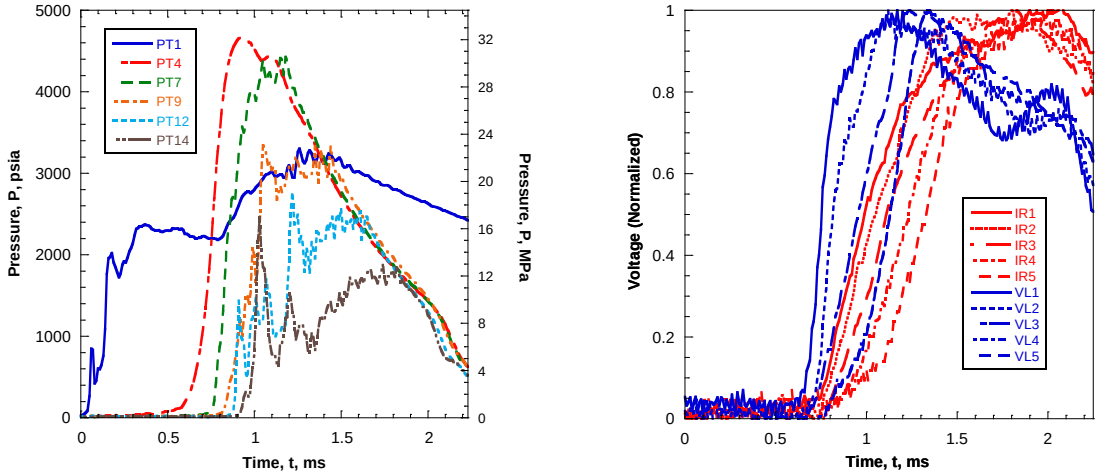

Figure 37: Axial chamber with 3.0 g of live granular propellant and remainder inert. Left: Pressure-time plot. Right: Intensity-time plot for both visible and infrared light photodetectors.

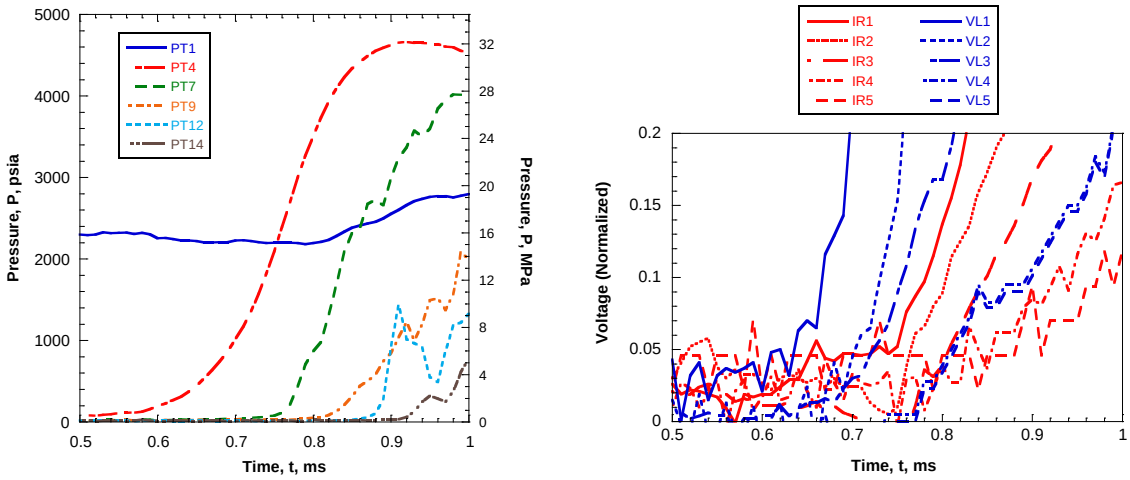

Figure 38: Detailed pressure and photodetector plots showing flame front passage in front of PT4.

The live propellant is placed upstream, in front of stations 1, 2, and PT 4. The flame front trails the hot gas front by 0.12 ms at stations 1 and 2 as determined by the time when each signal passes 20% of its peak value. Photodetectors at stations 4 and 5 show some discretization noise as they were recorded on a different DAQ with lower bit resolution. In 4 different tests, with peak pressures between 4000 and 6000 psia, the hot gas and flame front showed an average separation of 0.15 ms. These tests only go to 25% of the design value for the pressure of the system; higher propellant loadings can be achieved which will place the live propellant in front of the other

photodetector stations providing more flamespreading data and increased maximum chamber pressure.

The first rise of photodetectors at station 1 is again after the action of the igniter jet. However, in this set-up, the photodetectors do not have line-of-sight to the igniter jet. This again points to the igniter jet penetrating the bead before intense burning begins.

Chapter 5

Conclusions

The fundamental ignition processes of a granular propellant bed were studied. The first stage of ignition consists of a percussion primer and black powder primer jet impinging onto a granular propellant bed. The condensed phase products of this jet were characterized for composition and penetration into the granular bed. The interaction of the igniter jet with the propellant bed was qualified to determine the onset of the flame spreading event relative to the hot jet injection in the propellant bed. Finally, once ignited, the relative progression of hot gas and burning surface fronts were measured as a function of pressure and igniter jet strength.

Igniter Jet

CEA calculations for a constant pressure and constant volume reactor determine that the condensed phase species in black powder combustion are between 20 and 30% of the jet by mass. The most likely species contained in the jet are KOH, K_2CO_3, K_2S, and K_2SO_4. The presence of these elements (except H) was confirmed via EDS on samples with condensed phase products.

Multiple layer analysis of an inert granular bed, fired onto by an igniter jet, allowed for the development of three correlations which describe the condensed phase penetration of the igniter jet. These correlations resolve the parameters of interest to within 30% and are based on measured parameters of the system.

$$\frac{L}{d_{jet}} = 9360.9\left(Re_{d_{jet}}\right)^{-1.99}\left(\frac{\bar{P}}{P_{atm}}\right)^{1.86}\left(\frac{d_{part}}{d_{jet}}\right)^{-0.55}$$

$$\frac{V_{covered}}{V_{part}} = 195800\left(Re_{d_{jet}}\right)^{-1.94}\left(\frac{\bar{P}}{P_{atm}}\right)^{2.18}\left(\frac{d_{part}}{d_{jet}}\right)^{-1.28}$$

$$\frac{d_{cond\,,max}}{d_{jet}} = 1218.\left(Re_{d_{jet}}\right)^{-0.44}\left(\frac{\bar{P}}{P_{atm}}\right)^{0.37}\left(\frac{d_{part}}{d_{jet}}\right)^{0.74}$$

Propellant Bed Ignition

Many different measurements taken independently confirm that the igniter jet fully penetrates the granular bed over 0.7 to 1.0 ms, depending on jet and bed configuration, before ignition begins to take place. This is shown most notably by the azimuthal flame spreading tests where a weak visible light photodetector signal arrives 0.3 ms is detected after the first pressure signal in the igniter jet section. This is followed by a decline in both pressure and light intensity and subsequently followed simultaneously by much stronger signals after an additional 1 ms. These later signals relate to the burning propellant bed. The same phenomenon is also seen in the high-speed movie results which show the discretized events of the igniter penetrating and subsequent flame spreading events. In the axial chamber, the igniter jet is not visible through the window port but the pressure-time traces show a pressure signal 0.5 to 0.7 ms before downstream pressure starts to rise. This is confirmed by the visible light and infrared light photodetector signals which arrive after the start of blow-down of the igniter jet.

Hot Gas and Flame Spreading Front Progression

The axial configuration shows that the simultaneous measurement of pressure, visible light, and infrared light signals can be measured from a burning granular propellant bed. At chamber pressures ranging from 4000 – 6000 psia the hot gas and burning surface fronts were separated by approximately 0.15 ms. Further tests at up to 20,000 psia can be conducted to find a functional relationship between these fronts and flow parameters.

References

[1] Sutton, George P., and Oscar Biblarz. Rocket Propulsion Elements. Seventh. New York: John Wiley & Sons, Inc., 2001.

[2] Schmidt, John R., Michael J. Nusca, and Albert W. Horst. "Mortar Interior Ballistics: Sensitivity Studies Using IBHVG2 and Progress Toward a Multi-Dimensional Representation." JANNAF, 2007.

[3] Asay, B. W., S. F. Son, and J. B. Bdzil. "The role of gas permeation in convective burning." Int. J. Multiphase Flow 22.5 (1996): 923-952.

[4] White, Kevin J., and Ronald A. Sasse. "Relationship of Combustion Characteristics and Physical Properties of Black Powder." Ballistic Research Laboratory, 1982: ADA122264.

[5] Horst, Albert W., and Paul J. Conroy. "Flamespreading Processes in a Small-Caliber Gun." JANNAF, 2007.

[6] Howard, Stephen L., and Anthony W. Williams. "Characterization of Two 120-mm Primers - the M129 and M125." Army Research Laboratory, 2007: ARL-TR-4346.

[7] Horst, Albert W., and Paul J. Conroy. "Flamespreading in a Small-Caliber Gun." Army Research Laboratory, 2007: ARl-TR-4181.

[8] Schmidt, John R., and Michael J. Nusca. "Flamespreading Progress in the Development of a Multiphase Turbulent Model of the Gas/Particle Flow in a Small-Caliber Ammunition Primer." Army Research Laboratory, 2006: ARL-TR-3860.

[9] Chang, Lang-Mann, and Anthony W. Williams. "Characterization of Particle Output From a Percussion Primer." Army Research Laboratory, 2006: ARL-TR-3860.

[10] Williams, Anthony W., Andrew L. Brant, Pamela J. Kaste, and Joseph W. Colburn. "Experimental Studies of the No. 41 Primer and Ignition of the 5.56-mm Ammunition." Army Research Laboratory, 2006: ARL-TR-3922.

[11] Wildegger-Gaissmaier, Anna E., and Ian R. Johnston. "Ignition of a Granular Propellant Bed." Combustion and Flame 106 (1996): 219-230.

[12] Sasse, Ronald A. "The influence of physical properties on black powder combustion." Ballistic Research Laboratory, 1981: ARLBL-TR-02308.

[13] Houim, Ryan W., and Kenneth K. Kuo. "Understanding Interior Ballistic Processes in a Flash Tube." JAM, 2009.

[14] Kuo, Kenneth and Kumar, Mridul. "Dynamic Burning Effects in the Combustion of Solid Propellants with Cracks, and the Use of Granular Bed Combustion Models." Naval Weapons Center, Dec. 1980.

[15] Kuo, Kenneth. "Combustion Process in Granular Beds of Solid Propellants." ARO-14963.6-E, May 1981.

[16] Bdzil, J. B., R. Menikoff, S. F. Son, A. K. Kapila, and D. S. Stewart. "Two-phase modeling of deflagration-to-detonation transition in granular materials: A critical examination of modeling issues." Physics of Fluids 11.2 (1999): 378-402.

[17] Nusca, Michael J., and Paul J. Conroy. "Multiphase CFD Simulations of Solid Propellant Combustion in Gun Systems." Army Research Laboratory.

[18] Dijkhuizen, W., G. A. Bokkers, N. G. Deen, M. van Sint Annaland, and J. A. M. Kuipers. "Extension of PIV for Measuring Granular Temperature Field in Dense Fluidized Beds." AIChE Journal 53.1 (2007): 108-118.

[19] Chukhanov, Z. F. "Heat and Mass Transfer Between Gas and Granular Material." Int. J. Heat Mass Transfer 6 (1963): 691-701.

[20] Baer, Melvin R., Robert J. Gross, Jace W. Nunziato, and Eugene A. Igel. "An Experimental and Theoretical Study of Deflagration-to-Detonation Transition (DDT) in the Granular Explosive, CP." Combustion and Flame 65 (1986): 15-30.

[21] Chen, D. Y., V. Yang, and K. K. Kuo. "Boundary Condition Specification for Mobile Granular Propellant Bed Combustion Processes." AIAA 19.11 (1981): 1429-1437.

[22] Kooker, Douglas E., Lang-Mann Chang, and Stephen L. Howard. "Flamespreading in Granular Solid Propellant: Design of an Experiment." Army Research Laboratory, 1993: ARL-MR-80.

[23] Wildegger-Gaissmaier, A. E., I. R. Johnston, and G. Teague. "Flame Spreading in a LOVA Charge: An Experimental Study." Propellants, Explosives, Pyrotechnics 20 (1995): 139-143.

[24] Davis, T. R., and K. K. Kuo. "Experimental Study of the Combustion Processes in Granular Propellant Beds." J. Spacecraft 16.4 (1979): 203-209.

[25] Kuo, K. K., J. H. Koo, T. R. Davis, and G. R. Coates. "Transient combustion in mobile gas-permeable propellants." Acta Astronautica 3 (1976): 573-591.

[26] Ermolaev, B. S., V. A. Foteenkov, B. A. Khasainov, A. A. Sulimov, and S. E. Malinin. "Critical conditions for the passage from combustions into explosion in granular explosive materials." UDC 662.215 (1991): 590-597.

[27] Yang, Wen-Ching, and Dale L. Keairns. "Estimating Jet Penetration Depth of Multiple Vertical Grid Jets." Industrial and Engineering Chemistry Fundamentals 18, No. 4 (1979): 317-319.

[28] Blake, T. R., H. Webb, and P. B. Sunderland. "The Nondimensionalization of Equations Describing Fluidization with Application to the Correlation of Jet Penetration Height." Chemical Engineering Science 45, no. 2 (1990): 365-371.

[29] Thynell, S. T., I. T. Huang, C. S. Kuo, W. H. Hsieh, and K. K. Kuo. "Approach to Measurements of Flame Spreading Over Solid Propellants." J. Propulsion 8.4 (1991): 914-917.

[30] Gordon, S., and B. J. McBride. "Computer Program for Calculation of Complex Chemical Equilibrium Compositions and Applications I. Analysis." NASA Reference Publication 1311. 1994.

Appendix A

Chamber Schematics

Parts List

Part Name	*Part No.*	*Used In:*	*Quantity*	*Material*
Axial Chamber	101	Axial	1	17-4 PH Hardened Stainless
End Support	102	Axial	1	303 Stainless
Linear Photodetector Array	103	Axial	1	6061-T6 Aluminum
Plug	104	Axial	1	303 Stainless
T-Transition	105	Axial	1	303 Stainless
Shear Disk Retainer	106	Axial	3	17-4 PH Hardened Stainless
Window Holder	107	Axial	1	303 Stainless
BP Retainer	301	Both	1	303 Stainless
Cartridge Retainer	302	Both	1	303 Stainless
Head End	303	Both	1	17-4 PH Hardened Stainless
PCB Plug	304	Both	16	316 Stainless
Spanner Wrench	305	Both	2	Steel
Firing Pin Assembly	306	Both	1	303 Stainless
Mounting Bracket	307	Both	1	303 Stainless
Photodetector Array	201	Radial	1	PVC
Radial Window Holder	202	Radial	1	303 Stainless
Radial Chamber	203	Radial	1	17-4 PH Hardened Stainless
Retainer Ring 1	204	Radial	2	6061-T6 Aluminum
Retainer Ring 2	205	Radial	2	6061-T6 Aluminum
Transition	206	Radial	1	303 Stainless
Window Spacer	207	Radial	1	303 Stainless
Photodetector Holder	208	Radial	2	303 Stainless

Radial Configuration

CAD models

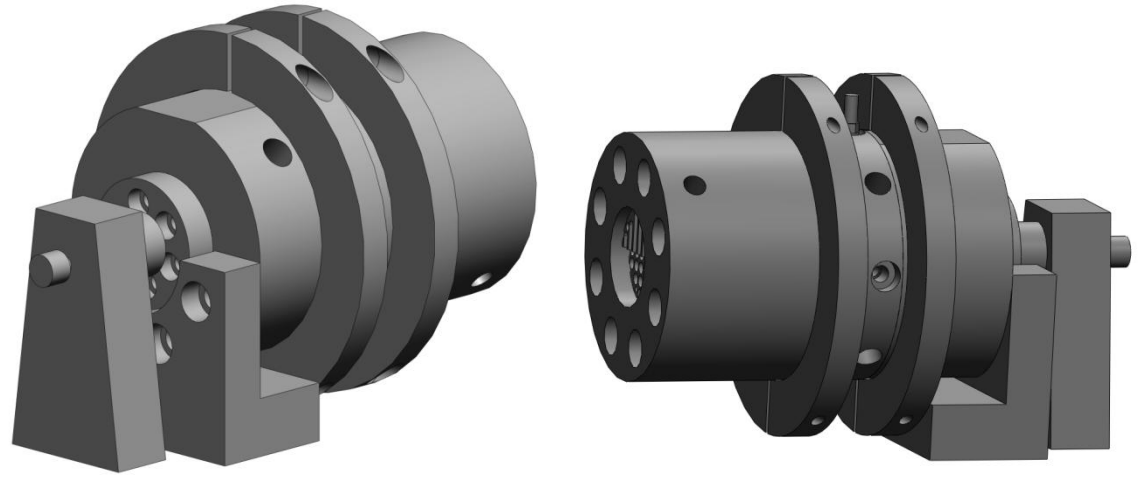

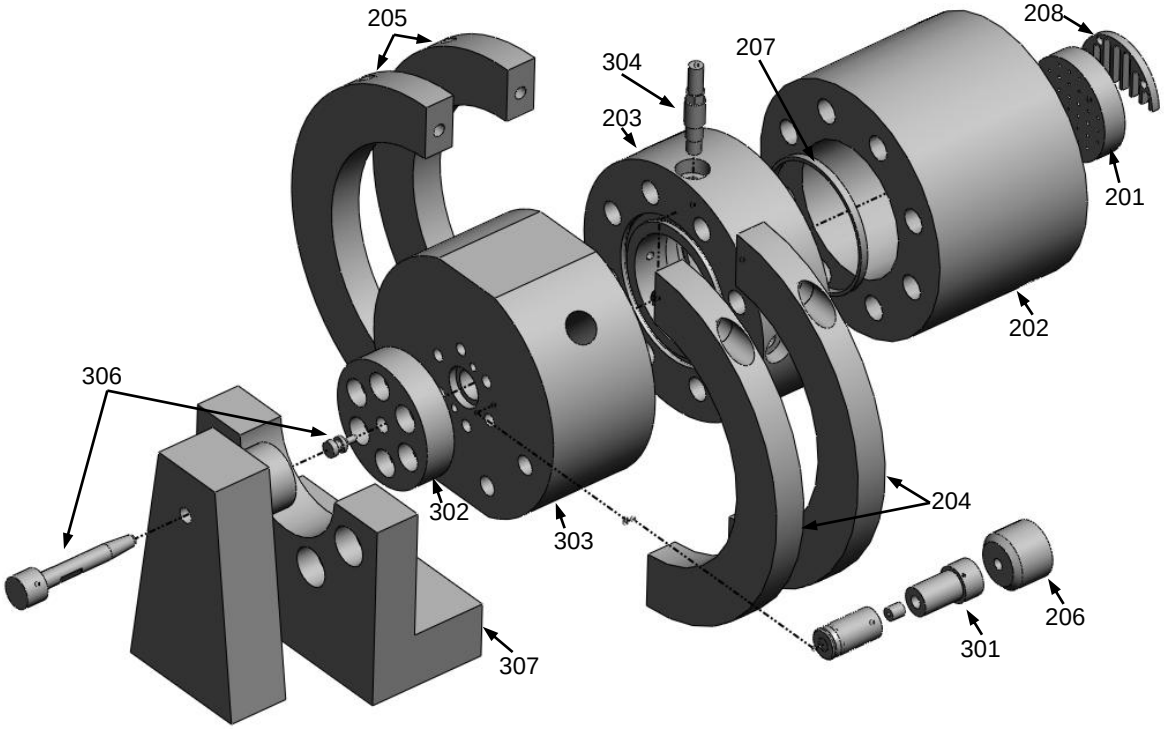

Drawings

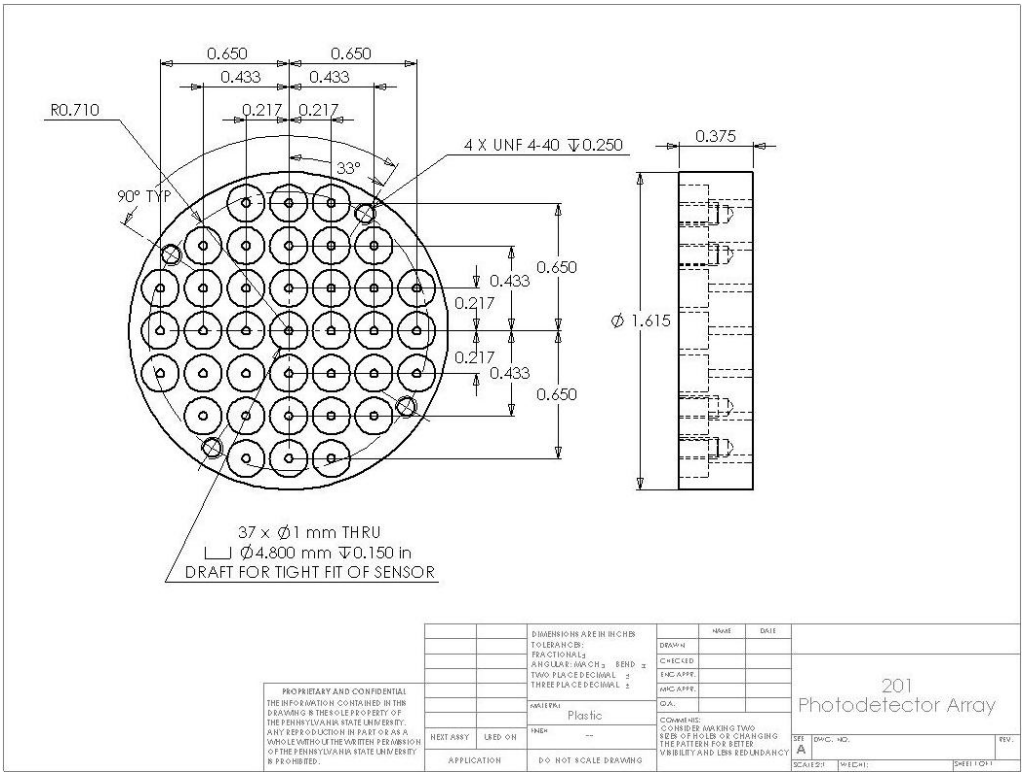
0.650
0.650
0.433
0.433
0.217
0.217
R0.710
33°
90° TYP
4 X UNF 4-40 ↧0.250
0.375
0.650
0.433
0.217
0.217
0.433
0.650
Ø 1.615
37 x Ø1 mm THRU
⌴ Ø4.800 mm ↧0.150 in
DRAFT FOR TIGHT FIT OF SENSOR
DIMENSIONS ARE IN INCHES
TOLERANCES:
FRACTIONAL ±
ANGULAR: MACH ± BEND ±
TWO PLACE DECIMAL ±
THREE PLACE DECIMAL ±
MATERIAL
Plastic
NEXT ASSY
USED ON
FINISH

APPLICATION
DO NOT SCALE DRAWING
NAME
DATE
DRAWN
CHECKED
ENG APPR.
MFG APPR.
Q.A.
COMMENTS:
CONSIDER MAKING TWO
SETS OF HOLES OR CHANGING
THE PATTERN FOR BETTER
VISIBILITY AND LESS REDUNDANCY
PROPRIETARY AND CONFIDENTIAL
THE INFORMATION CONTAINED IN THIS
DRAWING IS THE SOLE PROPERTY OF
THE PENNSYLVANIA STATE UNIVERSITY.
ANY REPRODUCTION IN PART OR AS A
WHOLE WITHOUT THE WRITTEN PERMISSION
OF THE PENNSYLVANIA STATE UNIVERSITY
IS PROHIBITED.
201
Photodetector Array
SIZE
A
DWG. NO.
REV.
SCALE:1:1
WEIGHT:
SHEET 1 OF 1

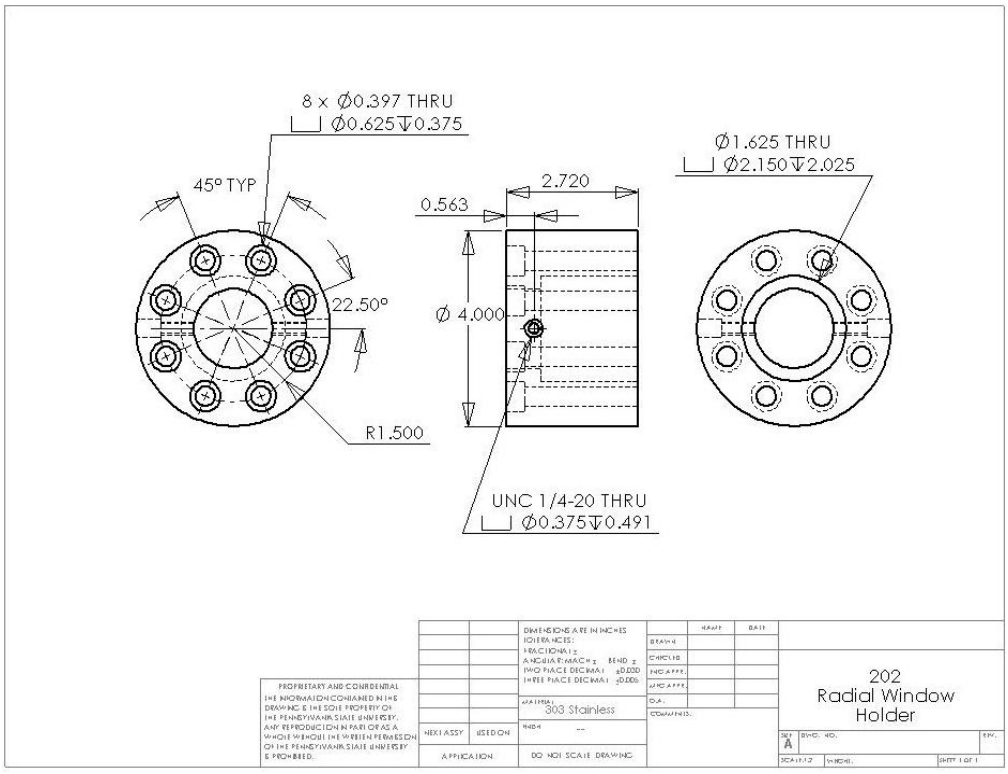
8 x Ø0.397 THRU
⌴ Ø0.625↧0.375
45° TYP
22.50°
R1.500
2.720
0.563
Ø 4.000
Ø1.625 THRU
⌴ Ø2.150↧2.025
UNC 1/4-20 THRU
⌴ Ø0.375↧0.491
DIMENSIONS ARE IN INCHES
TOLERANCES:
FRACTIONAL ±
ANGULAR: MACH ± BEND ±
TWO PLACE DECIMAL ±0.030
THREE PLACE DECIMAL ±0.005
MATERIAL
303 Stainless
NEXT ASSY
USED ON
FINISH

APPLICATION
DO NOT SCALE DRAWING
NAME
DATE
DRAWN
CHECKED
ENG APPR.
MFG APPR.
Q.A.
COMMENTS:
PROPRIETARY AND CONFIDENTIAL
THE INFORMATION CONTAINED IN THIS
DRAWING IS THE SOLE PROPERTY OF
THE PENNSYLVANIA STATE UNIVERSITY.
ANY REPRODUCTION IN PART OR AS A
WHOLE WITHOUT THE WRITTEN PERMISSION
OF THE PENNSYLVANIA STATE UNIVERSITY
IS PROHIBITED.
202
Radial Window
Holder
SIZE
A
DWG. NO.
REV.
SCALE:1:2
WEIGHT:
SHEET 1 OF 1

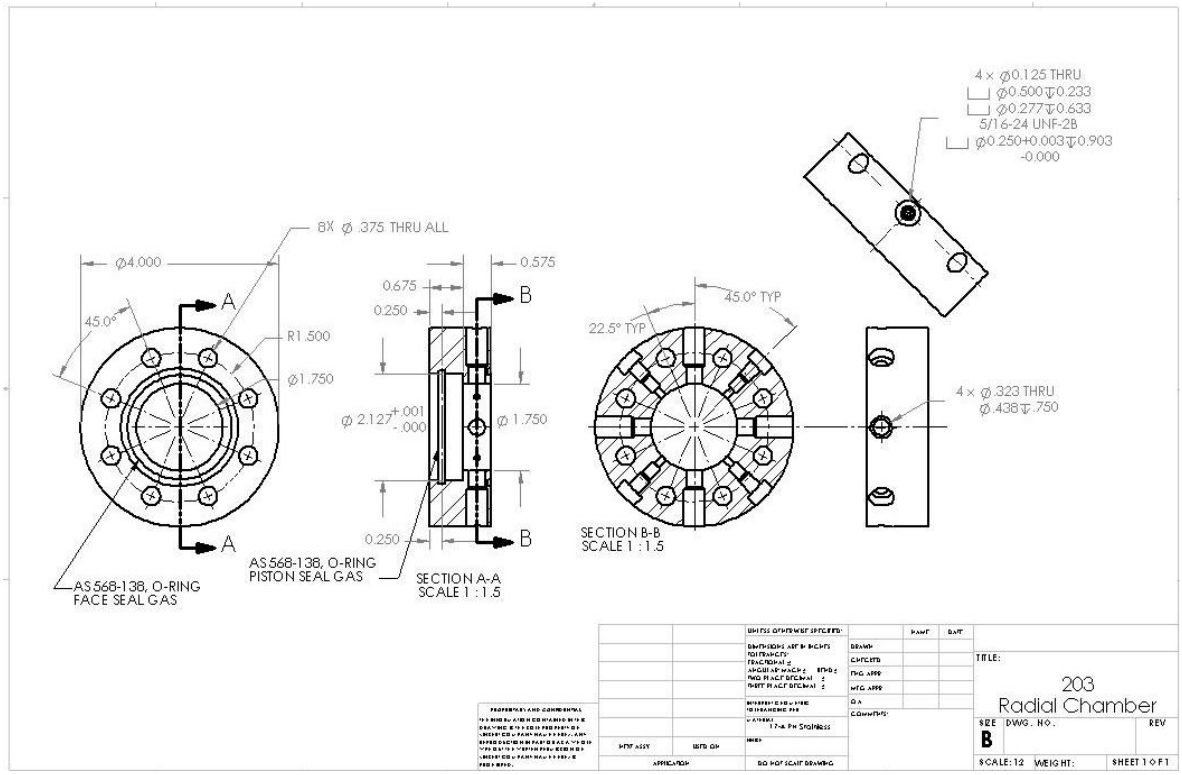
4 × ⌀0.125 THRU
⌴ ⌀0.500↧0.233
⌴ ⌀0.277↧0.633
5/16-24 UNF-2B
⌴ ⌀0.250+0.003-0.000↧0.903
8X ⌀ .375 THRU ALL
⌀4.000
45.0°
R1.500
⌀1.750
A
A
0.675
0.250
0.575
B
B
⌀ 2.127 +.001 -.000
⌀ 1.750
0.250
AS568-138, O-RING
FACE SEAL GAS
AS568-138, O-RING
PISTON SEAL GAS
SECTION A-A
SCALE 1 : 1.5
22.5° TYP
45.0° TYP
SECTION B-B
SCALE 1 : 1.5
4 × ⌀ .323 THRU
⌀ .438↧.750
UNLESS OTHERWISE SPECIFIED:
DIMENSIONS ARE IN INCHES
TOLERANCES:
FRACTIONAL ±
ANGULAR: MACH ± BEND ±
TWO PLACE DECIMAL ±
THREE PLACE DECIMAL ±
NAME
DATE
DRAWN
CHECKED
ENG APPR.
MFG APPR.
Q.A.
COMMENTS:
MATERIAL
17-4 PH Stainless
FINISH
NEXT ASSY
USED ON
APPLICATION
DO NOT SCALE DRAWING
PROPRIETARY AND CONFIDENTIAL
TITLE:
203
Radial Chamber
SIZE
B
DWG. NO.
REV
SCALE: 1:2
WEIGHT:
SHEET 1 OF 1

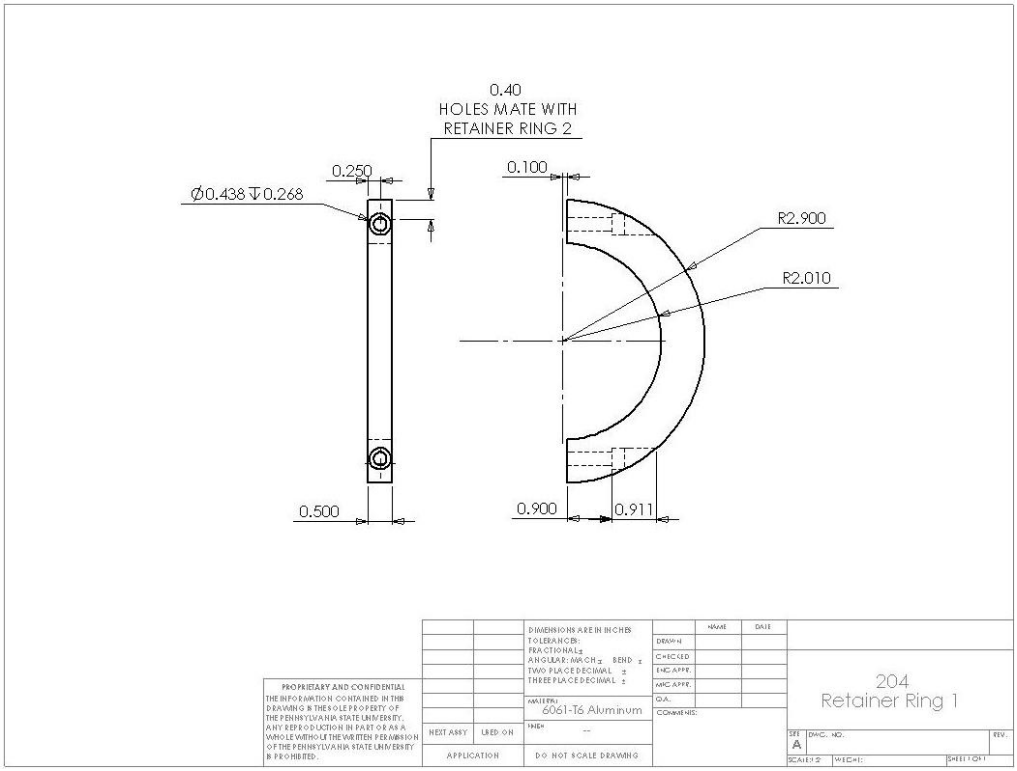
0.40
HOLES MATE WITH
RETAINER RING 2
0.250
⌀0.438↧0.268
0.100
R2.900
R2.010
0.500
0.900
0.911
PROPRIETARY AND CONFIDENTIAL
THE INFORMATION CONTAINED IN THIS DRAWING IS THE SOLE PROPERTY OF THE PENNSYLVANIA STATE UNIVERSITY. ANY REPRODUCTION IN PART OR AS A WHOLE WITHOUT THE WRITTEN PERMISSION OF THE PENNSYLVANIA STATE UNIVERSITY IS PROHIBITED.
DIMENSIONS ARE IN INCHES
TOLERANCES:
FRACTIONAL ±
ANGULAR: MACH ± BEND ±
TWO PLACE DECIMAL ±
THREE PLACE DECIMAL ±
NAME
DATE
DRAWN
CHECKED
ENG APPR.
MFG APPR.
Q.A.
COMMENTS:
MATERIAL
6061-T6 Aluminum
FINISH
--
NEXT ASSY
USED ON
APPLICATION
DO NOT SCALE DRAWING
204
Retainer Ring 1
SIZE
A
DWG. NO.
REV
SCALE: 2
WEIGHT:
SHEET 1 OF 1

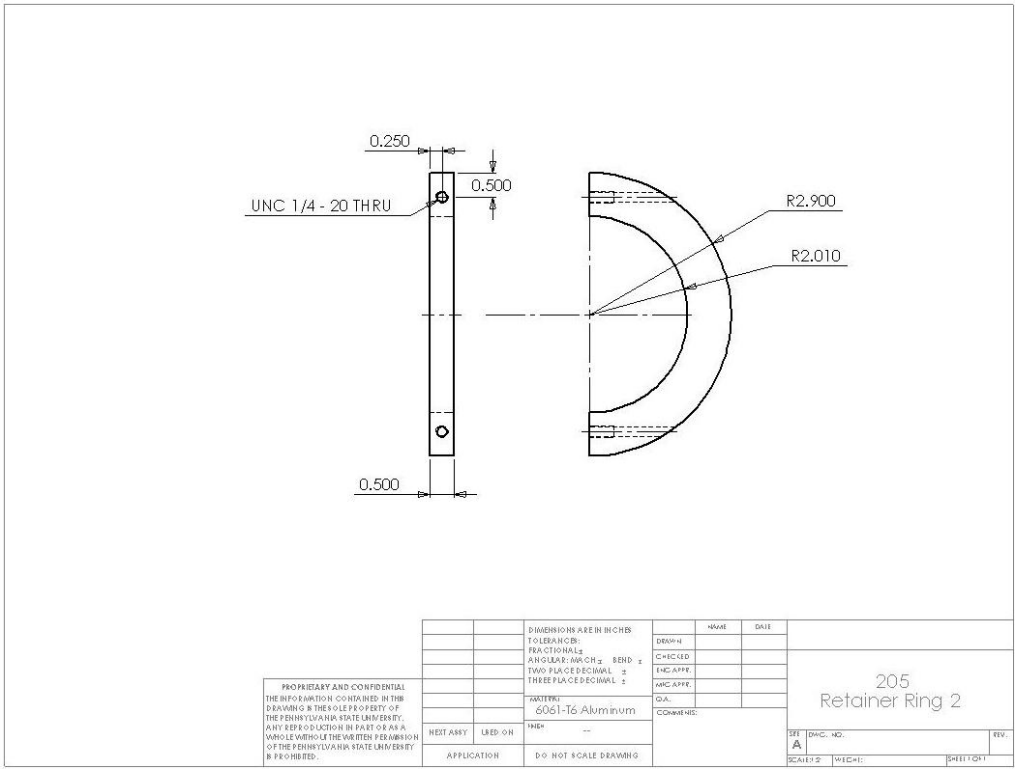
0.250
0.500
UNC 1/4 - 20 THRU
R2.900
R2.010
0.500
DIMENSIONS ARE IN INCHES
TOLERANCES:
FRACTIONAL ±
ANGULAR: MACH ± BEND ±
TWO PLACE DECIMAL ±
THREE PLACE DECIMAL ±
MATERIAL
6061-T6 Aluminum
FINISH
--
DO NOT SCALE DRAWING
NAME
DATE
DRAWN
CHECKED
ENG APPR.
MFG APPR.
Q.A.
COMMENTS:
205
Retainer Ring 2
SIZE A
DWG. NO.
REV.
SCALE: 2/1
WEIGHT:
SHEET 1 OF 1
PROPRIETARY AND CONFIDENTIAL
THE INFORMATION CONTAINED IN THIS DRAWING IS THE SOLE PROPERTY OF THE PENNSYLVANIA STATE UNIVERSITY. ANY REPRODUCTION IN PART OR AS A WHOLE WITHOUT THE WRITTEN PERMISSION OF THE PENNSYLVANIA STATE UNIVERSITY IS PROHIBITED.
NEXT ASSY
USED ON
APPLICATION

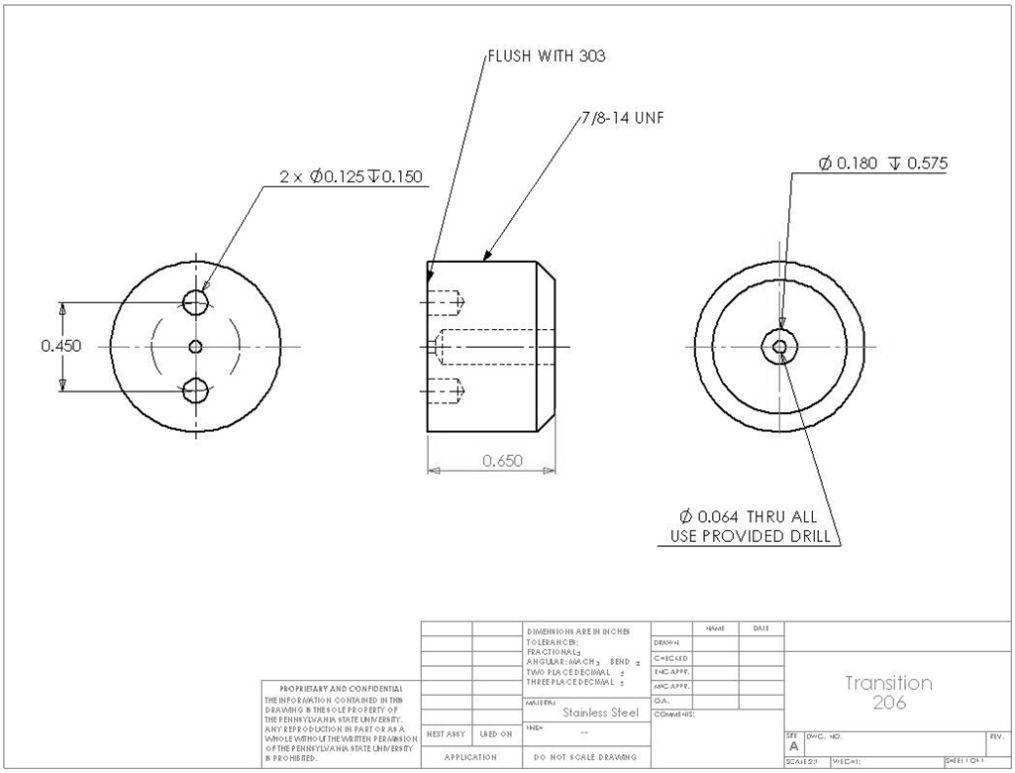
FLUSH WITH 303
7/8-14 UNF
2 x Ø0.125 ↧0.150
Ø 0.180 ↧ 0.575
0.450
0.650
Ø 0.064 THRU ALL
USE PROVIDED DRILL
DIMENSIONS ARE IN INCHES
TOLERANCES:
FRACTIONAL ±
ANGULAR: MACH ± BEND ±
TWO PLACE DECIMAL ±
THREE PLACE DECIMAL ±
MATERIAL
Stainless Steel
FINISH
--
DO NOT SCALE DRAWING
NAME
DATE
DRAWN
CHECKED
ENG APPR.
MFG APPR.
Q.A.
COMMENTS:
Transition
206
SIZE A
DWG. NO.
REV.
SCALE: 2/1
WEIGHT:
SHEET 1 OF 1
PROPRIETARY AND CONFIDENTIAL
THE INFORMATION CONTAINED IN THIS DRAWING IS THE SOLE PROPERTY OF THE PENNSYLVANIA STATE UNIVERSITY. ANY REPRODUCTION IN PART OR AS A WHOLE WITHOUT THE WRITTEN PERMISSION OF THE PENNSYLVANIA STATE UNIVERSITY IS PROHIBITED.
NEXT ASSY
USED ON
APPLICATION

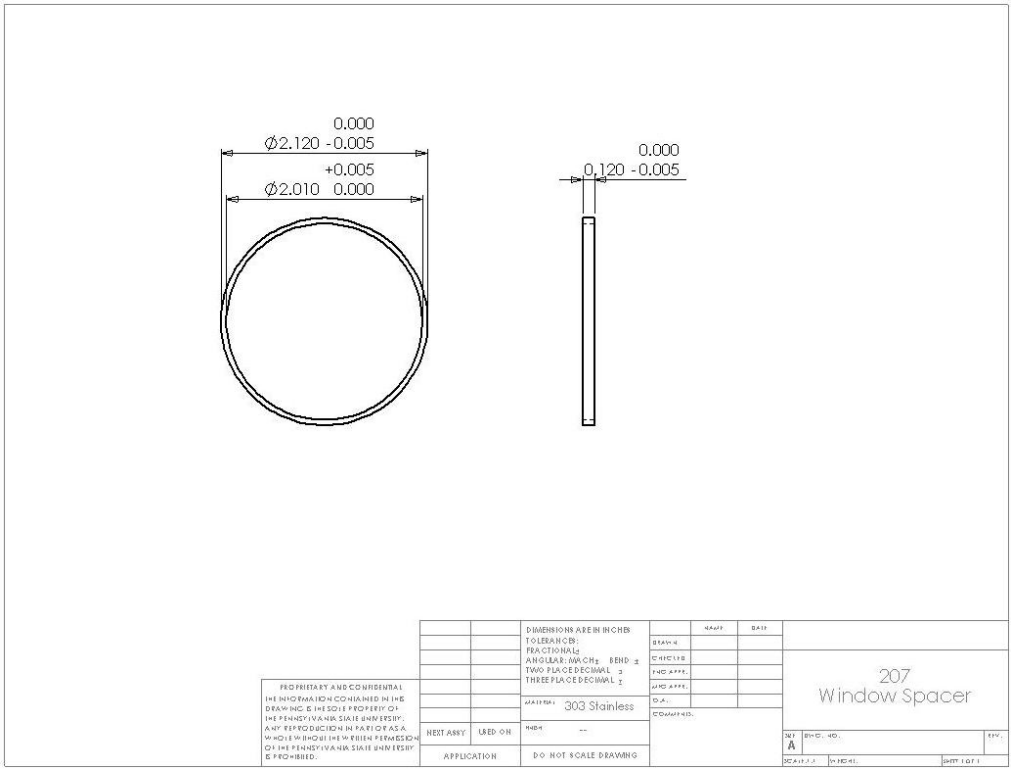
0.000
Ø2.120 -0.005
+0.005
Ø2.010 0.000
0.000
0.120 -0.005
DIMENSIONS ARE IN INCHES
TOLERANCES:
FRACTIONAL ±
ANGULAR: MACH ± BEND ±
TWO PLACE DECIMAL ±
THREE PLACE DECIMAL ±
MATERIAL 303 Stainless
FINISH --
DO NOT SCALE DRAWING
NAME
DATE
DRAWN
CHECKED
ENG APPR.
MFG APPR.
Q.A.
COMMENTS:
207
Window Spacer
SIZE A
DWG. NO.
REV.
SCALE: 3/2
WEIGHT:
SHEET 1 OF 1
PROPRIETARY AND CONFIDENTIAL
THE INFORMATION CONTAINED IN THE DRAWING IS THE SOLE PROPERTY OF THE PENNSYLVANIA STATE UNIVERSITY. ANY REPRODUCTION IN PART OR AS A WHOLE WITHOUT THE WRITTEN PERMISSION OF THE PENNSYLVANIA STATE UNIVERSITY IS PROHIBITED.
NEXT ASSY
USED ON
APPLICATION

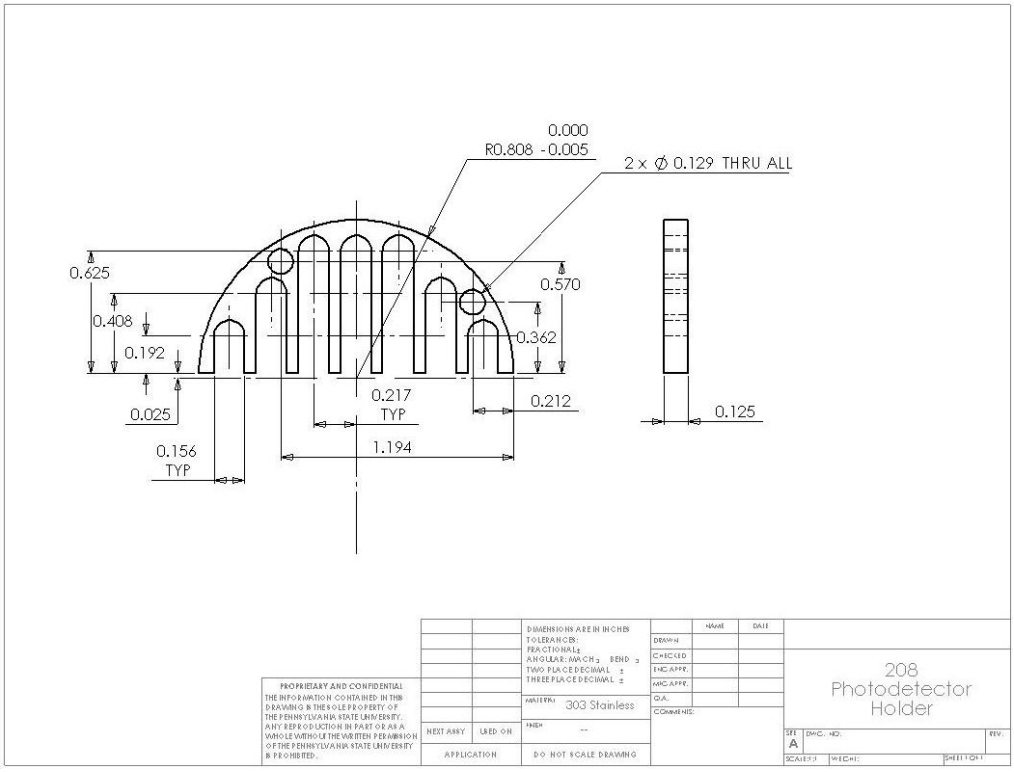
0.000
R0.808 -0.005
2 x Ø 0.129 THRU ALL
0.625
0.408
0.192
0.025
0.156
TYP
0.570
0.362
0.217
TYP
0.212
1.194
0.125
DIMENSIONS ARE IN INCHES
TOLERANCES:
FRACTIONAL ±
ANGULAR: MACH ± BEND ±
TWO PLACE DECIMAL ±
THREE PLACE DECIMAL ±
MATERIAL 303 Stainless
FINISH --
DO NOT SCALE DRAWING
NAME
DATE
DRAWN
CHECKED
ENG APPR.
MFG APPR.
Q.A.
COMMENTS:
208
Photodetector
Holder
SIZE A
DWG. NO.
REV.
SCALE: 3/2
WEIGHT:
SHEET 1 OF 1
PROPRIETARY AND CONFIDENTIAL
THE INFORMATION CONTAINED IN THIS DRAWING IS THE SOLE PROPERTY OF THE PENNSYLVANIA STATE UNIVERSITY. ANY REPRODUCTION IN PART OR AS A WHOLE WITHOUT THE WRITTEN PERMISSION OF THE PENNSYLVANIA STATE UNIVERSITY IS PROHIBITED.
NEXT ASSY
USED ON
APPLICATION

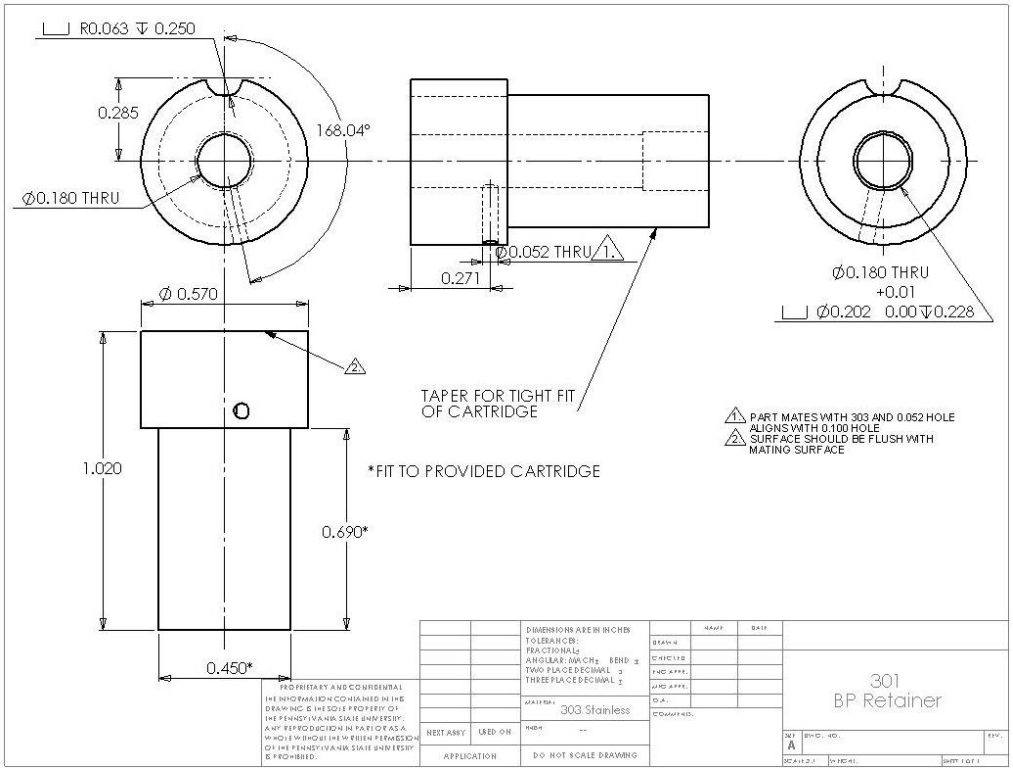
R0.063 ↧ 0.250
0.285
168.04°
Ø0.180 THRU
Ø0.052 THRU 1.
0.271
Ø0.180 THRU
+0.01
Ø0.202 0.00↧0.228
Ø 0.570
2.
TAPER FOR TIGHT FIT
OF CARTRIDGE
1. PART MATES WITH 303 AND 0.052 HOLE ALIGNS WITH 0.100 HOLE
2. SURFACE SHOULD BE FLUSH WITH MATING SURFACE
1.020
*FIT TO PROVIDED CARTRIDGE
0.690*
0.450*
PROPRIETARY AND CONFIDENTIAL
DIMENSIONS ARE IN INCHES
TOLERANCES:
FRACTIONAL
ANGULAR: MACH BEND
TWO PLACE DECIMAL
THREE PLACE DECIMAL
MATERIAL 303 Stainless
NEXT ASSY
USED ON
APPLICATION
DO NOT SCALE DRAWING
NAME
DATE
DRAWN
CHECKED
ENG APPR.
MFG APPR.
Q.A.
COMMENTS:
301
BP Retainer
SIZE A
DWG. NO.
REV.
SCALE:
WEIGHT:
SHEET 1 OF 1

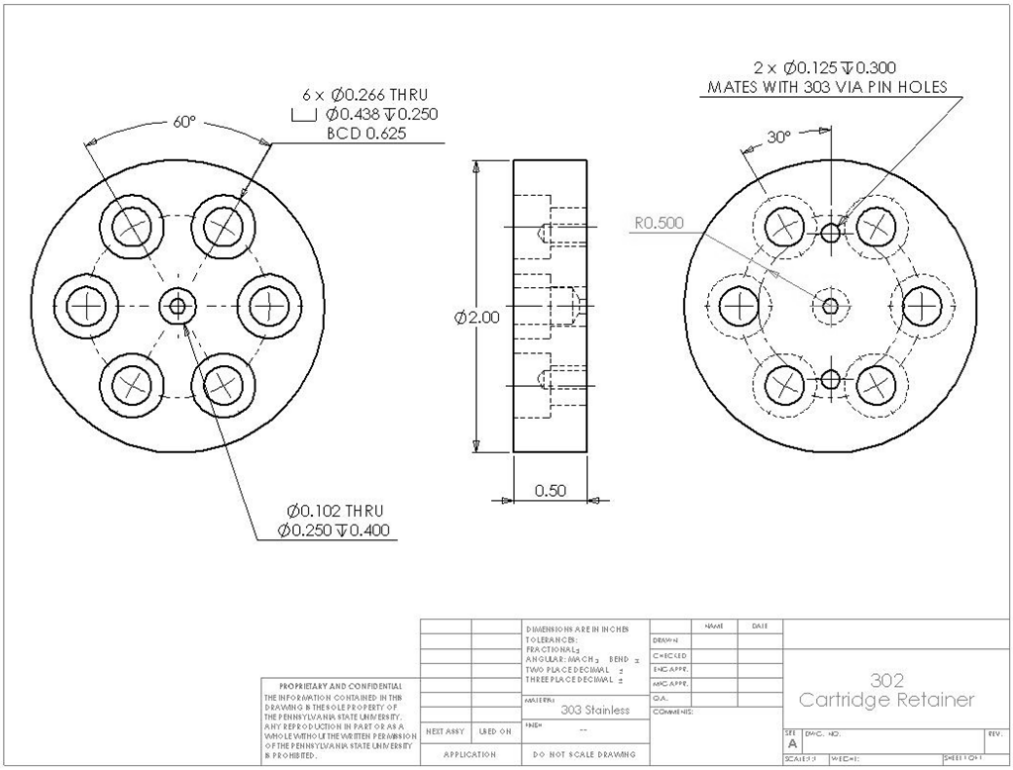
6 x Ø0.266 THRU
Ø0.438 ↧0.250
BCD 0.625
60°
2 x Ø0.125 ↧0.300
MATES WITH 303 VIA PIN HOLES
30°
R0.500
Ø2.00
0.50
Ø0.102 THRU
Ø0.250 ↧0.400
PROPRIETARY AND CONFIDENTIAL
DIMENSIONS ARE IN INCHES
TOLERANCES:
FRACTIONAL
ANGULAR: MACH BEND
TWO PLACE DECIMAL
THREE PLACE DECIMAL
MATERIAL 303 Stainless
NEXT ASSY
USED ON
APPLICATION
DO NOT SCALE DRAWING
NAME
DATE
DRAWN
CHECKED
ENG APPR.
MFG APPR.
Q.A.
COMMENTS:
302
Cartridge Retainer
SIZE A
DWG. NO.
REV.
SCALE:
WEIGHT:
SHEET 1 OF 1

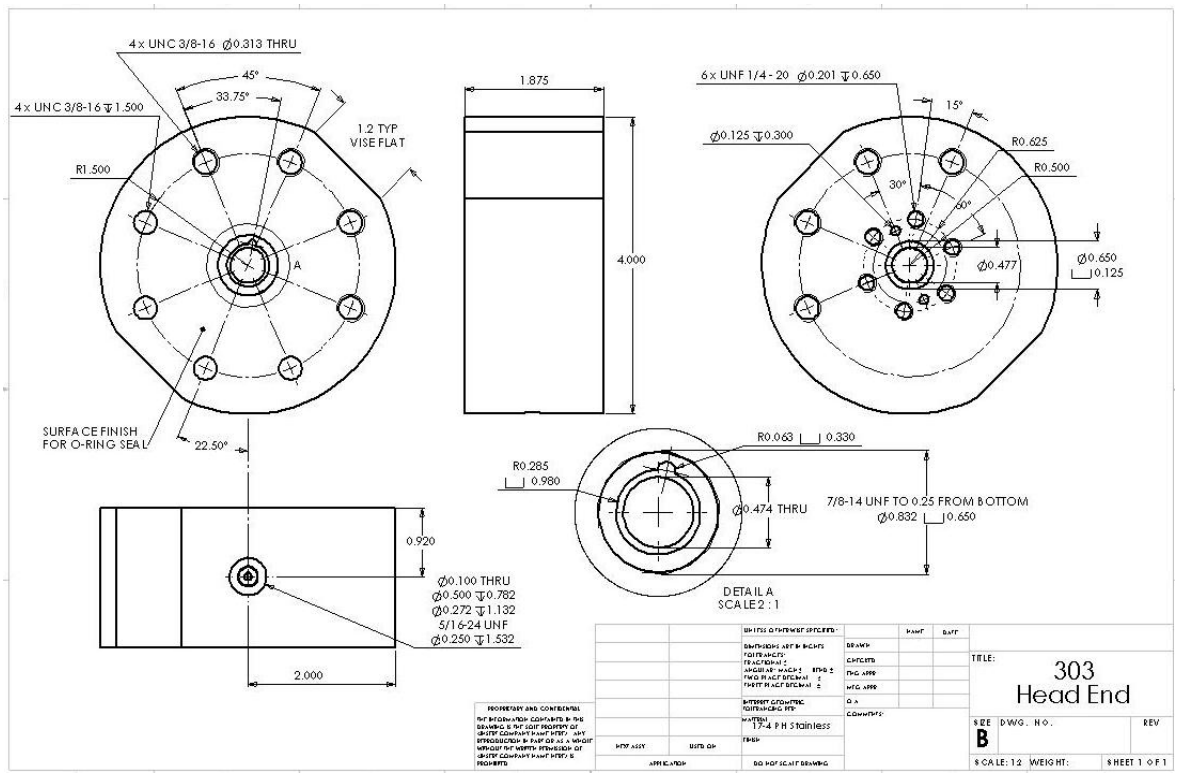
4 x UNC 3/8-16 Ø0.313 THRU
45°
33.75°
4 x UNC 3/8-16 ↧1.500
1.2 TYP
VISE FLAT
R1.500
1.875
4.000
6 x UNF 1/4 - 20 Ø0.201 ↧0.650
15°
Ø0.125 ↧0.300
R0.625
R0.500
30°
60°
Ø0.650
0.125
Ø0.477
SURFACE FINISH
FOR O-RING SEAL
22.50°
R0.063
0.330
R0.285
0.980
Ø0.474 THRU
7/8-14 UNF TO 0.25 FROM BOTTOM
Ø0.832
0.650
0.920
Ø0.100 THRU
Ø0.500 ↧0.782
Ø0.272 ↧1.132
5/16-24 UNF
Ø0.250 ↧1.532
2.000
DETAIL A
SCALE 2 : 1
UNLESS OTHERWISE SPECIFIED:
DIMENSIONS ARE IN INCHES
TOLERANCES:
FRACTIONAL ±
ANGULAR: MACH ± BEND ±
TWO PLACE DECIMAL ±
THREE PLACE DECIMAL ±
INTERPRET GEOMETRIC TOLERANCING PER:
MATERIAL
17-4 PH Stainless
FINISH
NEXT ASSY
USED ON
APPLICATION
DO NOT SCALE DRAWING
NAME
DATE
DRAWN
CHECKED
ENG APPR.
MFG APPR.
Q.A.
COMMENTS:
PROPRIETARY AND CONFIDENTIAL
THE INFORMATION CONTAINED IN THIS DRAWING IS THE SOLE PROPERTY OF <INSTITUTE COMPANY NAME HERE>. ANY REPRODUCTION IN PART OR AS A WHOLE WITHOUT THE WRITTEN PERMISSION OF <INSTITUTE COMPANY NAME HERE> IS PROHIBITED.
TITLE:
303
Head End
SIZE
B
DWG. NO.
REV
SCALE: 1:2
WEIGHT:
SHEET 1 OF 1

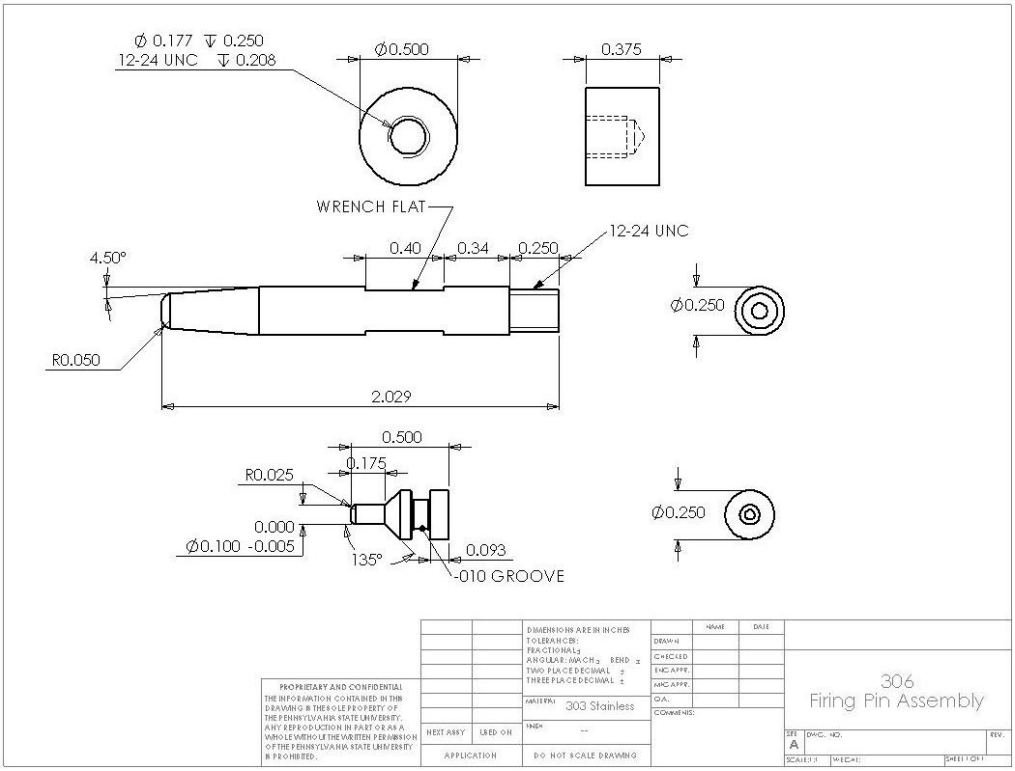
Ø 0.177 ↧ 0.250
12-24 UNC ↧ 0.208
Ø0.500
0.375
WRENCH FLAT
12-24 UNC
0.40
0.34
0.250
4.50°
Ø0.250
R0.050
2.029
0.500
0.175
R0.025
0.000
Ø0.100 -0.005
135°
0.093
-010 GROOVE
Ø0.250
DIMENSIONS ARE IN INCHES
TOLERANCES:
FRACTIONAL ±
ANGULAR: MACH ± BEND ±
TWO PLACE DECIMAL ±
THREE PLACE DECIMAL ±
MATERIAL
303 Stainless
FINISH
--
NEXT ASSY
USED ON
APPLICATION
DO NOT SCALE DRAWING
NAME
DATE
DRAWN
CHECKED
ENG APPR.
MFG APPR.
Q.A.
COMMENTS:
PROPRIETARY AND CONFIDENTIAL
THE INFORMATION CONTAINED IN THIS DRAWING IS THE SOLE PROPERTY OF THE PENNSYLVANIA STATE UNIVERSITY. ANY REPRODUCTION IN PART OR AS A WHOLE WITHOUT THE WRITTEN PERMISSION OF THE PENNSYLVANIA STATE UNIVERSITY IS PROHIBITED.
306
Firing Pin Assembly
SIZE
A
DWG. NO.
REV.
SCALE: 1:1
WEIGHT:
SHEET 1 OF 1

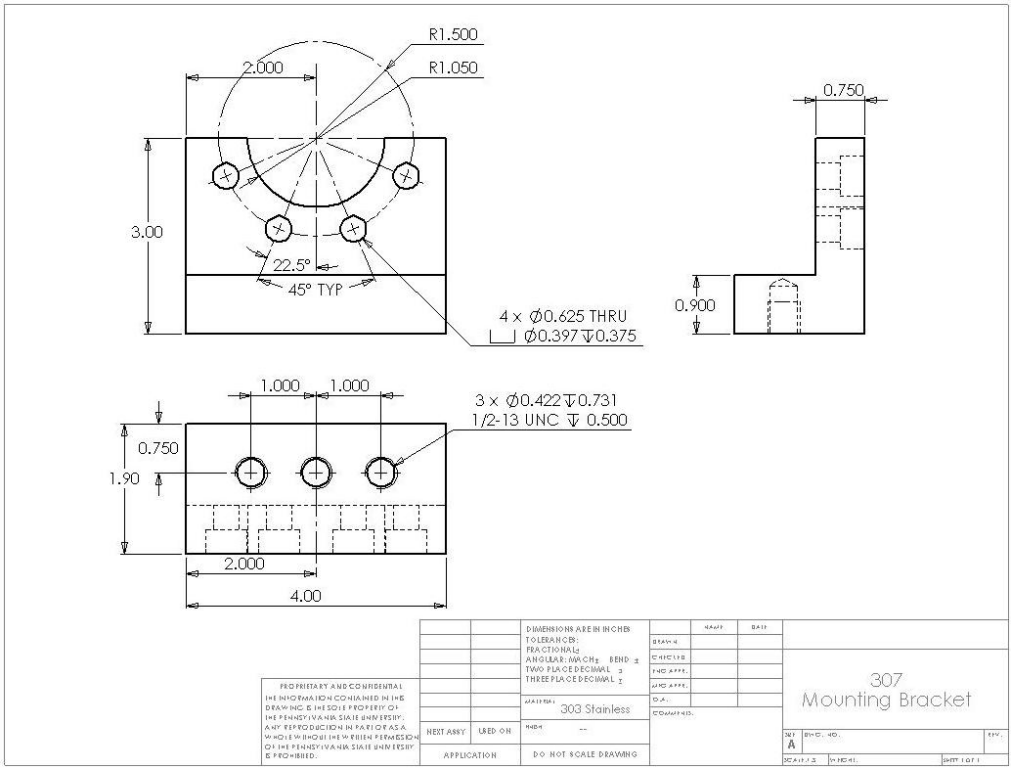
R1.500
R1.050
2.000
3.00
22.5°
45° TYP
4 x ⌀0.625 THRU
⌴ ⌀0.397 ↧0.375
0.750
0.900
1.000
1.000
3 x ⌀0.422 ↧0.731
1/2-13 UNC ↧ 0.500
0.750
1.90
2.000
4.00
DIMENSIONS ARE IN INCHES
TOLERANCES:
FRACTIONAL
ANGULAR: MACH ± BEND ±
TWO PLACE DECIMAL ±
THREE PLACE DECIMAL ±
MATERIAL
303 Stainless
FINISH
--
DO NOT SCALE DRAWING
NAME
DATE
DRAWN
CHECKED
ENG APPR.
MFG APPR.
Q.A.
COMMENTS:
307
Mounting Bracket
SIZE
A
DWG. NO.
REV
SCALE: 1:2
WEIGHT:
SHEET 1 OF 1
NEXT ASSY
USED ON
APPLICATION
PROPRIETARY AND CONFIDENTIAL
THE INFORMATION CONTAINED IN THE DRAWING IS THE SOLE PROPERTY OF THE PENNSYLVANIA STATE UNIVERSITY. ANY REPRODUCTION IN PART OR AS A WHOLE WITHOUT THE WRITTEN PERMISSION OF THE PENNSYLVANIA STATE UNIVERSITY IS PROHIBITED.

Axial Configuration

CAD Models

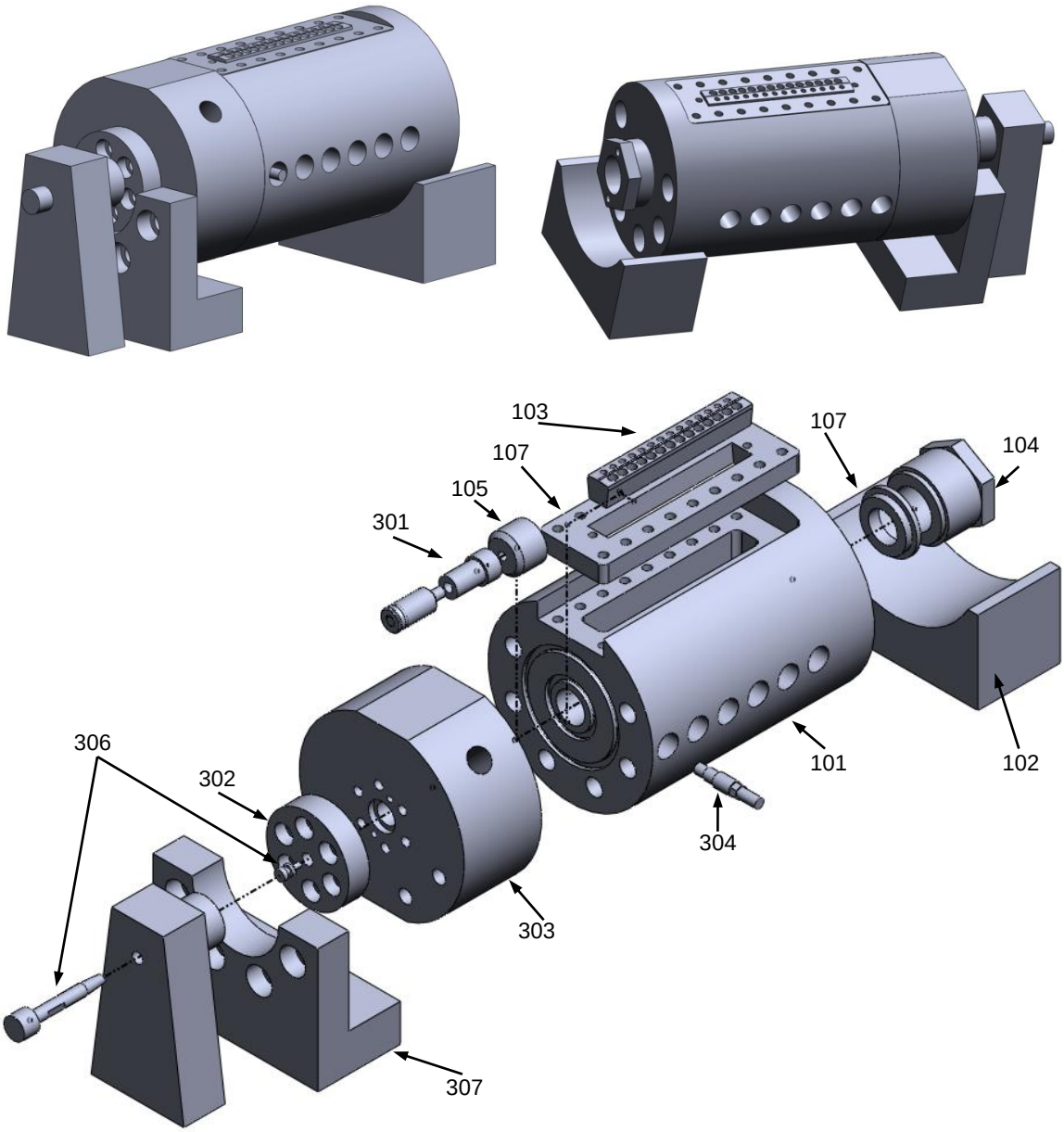

Drawings

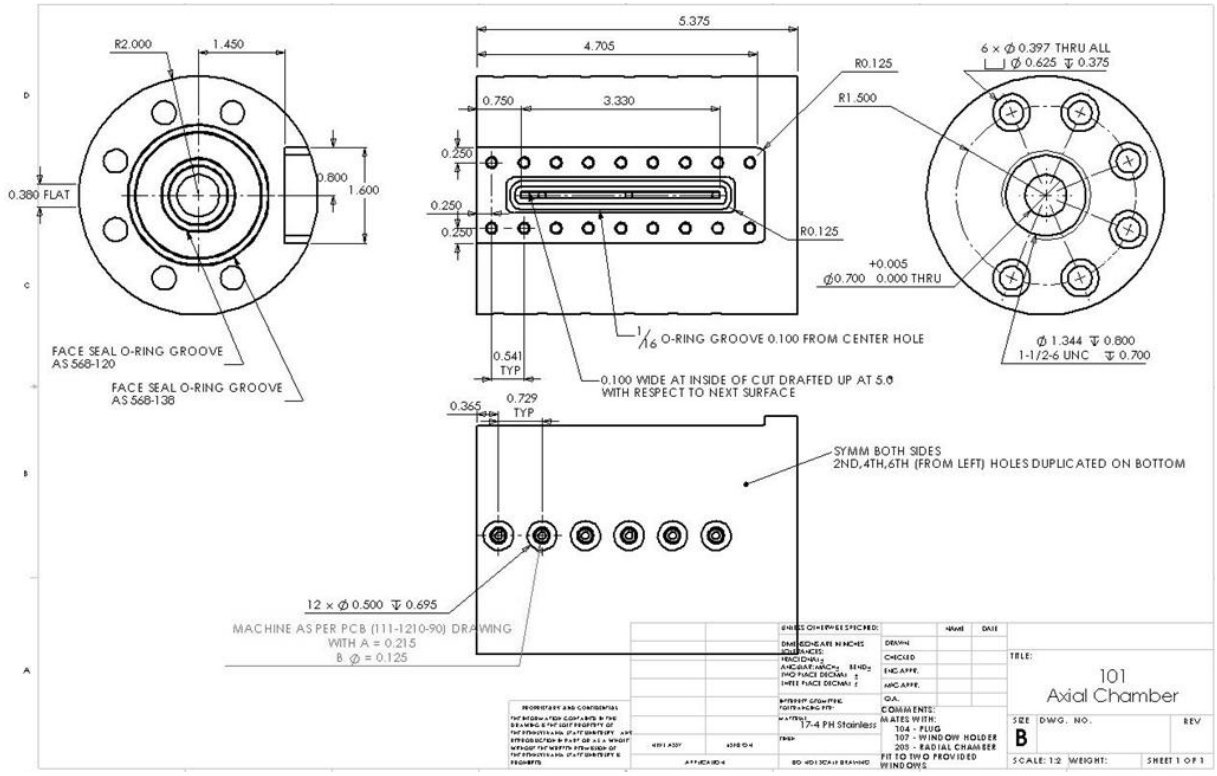
5.375
4.705
R2.000
1.450
0.750
3.330
R0.125
R1.500
6 × Ø 0.397 THRU ALL
⌴ Ø 0.625 ↧ 0.375
0.250
0.250
0.250
0.800
1.600
0.380 FLAT
R0.125
+0.005
Ø0.700 0.000 THRU
FACE SEAL O-RING GROOVE
AS 568-120
FACE SEAL O-RING GROOVE
AS 568-138
1/16 O-RING GROOVE 0.100 FROM CENTER HOLE
Ø 1.344 ↧ 0.800
1-1/2-6 UNC ↧ 0.700
0.541
TYP
0.100 WIDE AT INSIDE OF CUT DRAFTED UP AT 5.0
WITH RESPECT TO NEXT SURFACE
0.365
0.729
TYP
SYMM BOTH SIDES
2ND,4TH,6TH (FROM LEFT) HOLES DUPLICATED ON BOTTOM
12 × Ø 0.500 ↧ 0.695
MACHINE AS PER PCB (111-1210-90) DRAWING
WITH A = 0.215
B Ø = 0.125
17-4 PH Stainless
COMMENTS:
MATES WITH:
104 - PLUG
107 - WINDOW HOLDER
205 - RADIAL CHAMBER
FIT TO TWO PROVIDED
WINDOWS
TITLE:
101
Axial Chamber
SIZE
B
DWG. NO.
REV
SCALE: 1:2
WEIGHT:
SHEET 1 OF 1

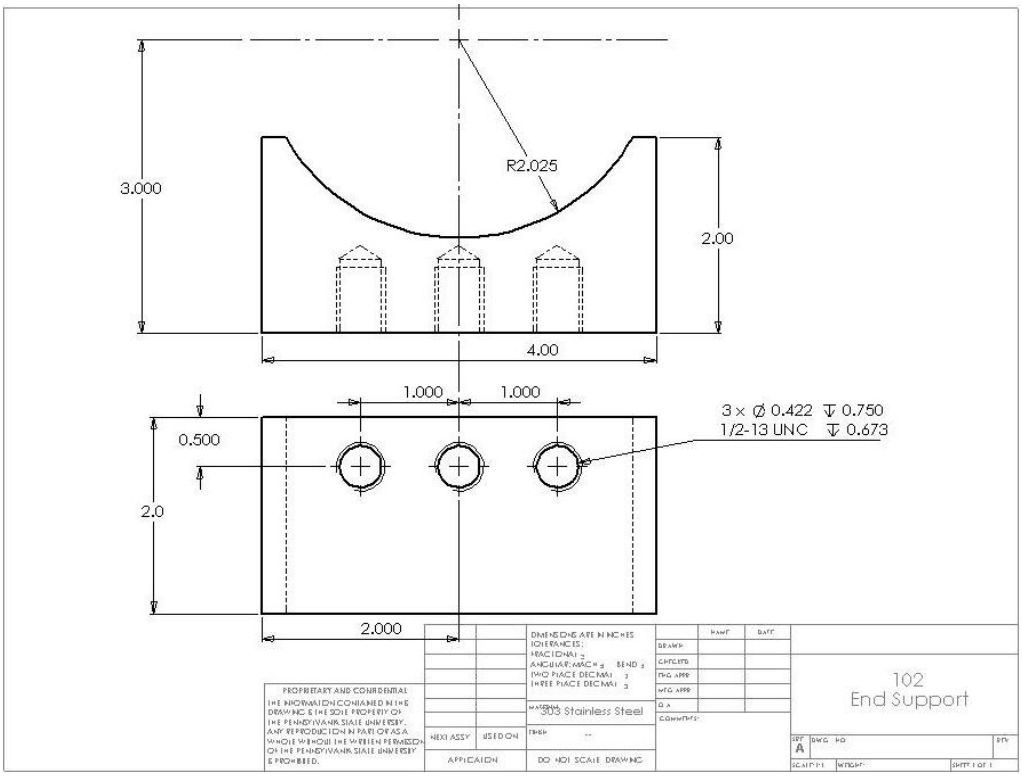
R2.025
3.000
2.00
4.00
1.000
1.000
3 × Ø 0.422 ↧ 0.750
1/2-13 UNC ↧ 0.673
0.500
2.0
2.000
DIMENSIONS ARE IN INCHES
TOLERANCES:
FRACTIONAL ±
ANGULAR: MACH ± BEND ±
TWO PLACE DECIMAL ±
THREE PLACE DECIMAL ±
MATERIAL
303 Stainless Steel
FINISH
--
NAME
DATE
DRAWN
CHECKED
ENG APPR.
MFG APPR.
Q.A.
COMMENTS:
NEXT ASSY
USED ON
APPLICATION
DO NOT SCALE DRAWING
PROPRIETARY AND CONFIDENTIAL
THE INFORMATION CONTAINED IN THE
DRAWING IS THE SOLE PROPERTY OF
THE PENNSYLVANIA STATE UNIVERSITY.
ANY REPRODUCTION IN PART OR AS A
WHOLE WITHOUT THE WRITTEN PERMISSION
OF THE PENNSYLVANIA STATE UNIVERSITY
IS PROHIBITED.
102
End Support
SIZE
A
DWG. NO.
REV
SCALE: 1:1
WEIGHT:
SHEET 1 OF 1

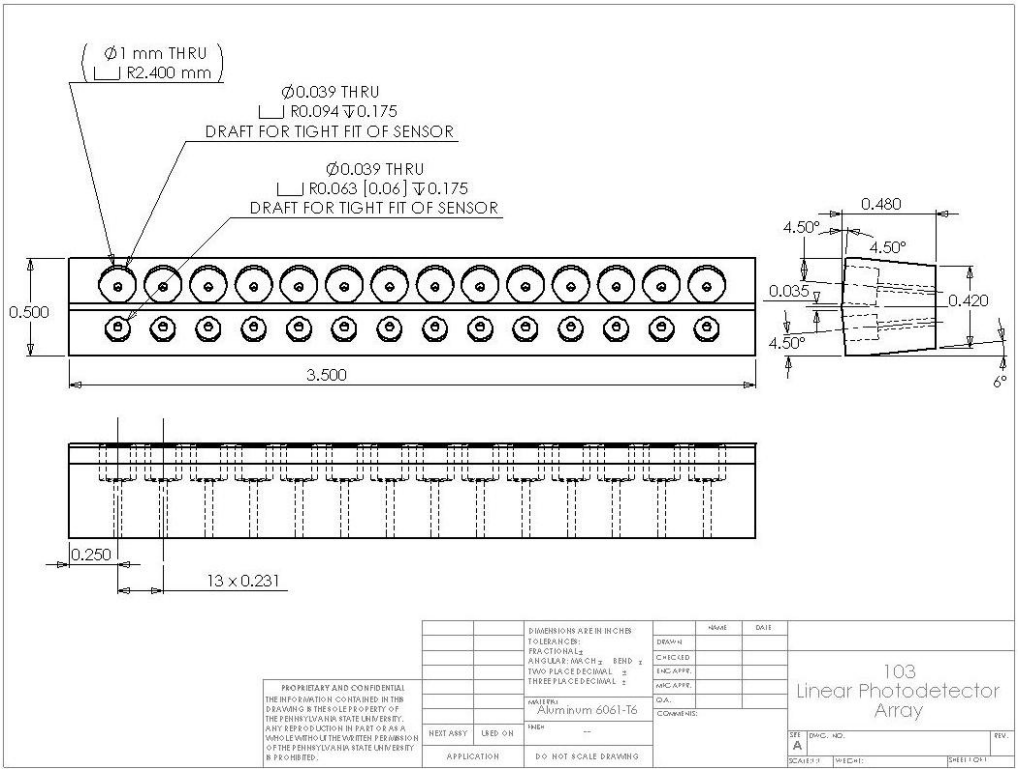
Ø1 mm THRU
⌴ R2.400 mm
Ø0.039 THRU
⌴ R0.094 ↧0.175
DRAFT FOR TIGHT FIT OF SENSOR
Ø0.039 THRU
⌴ R0.063 [0.06] ↧0.175
DRAFT FOR TIGHT FIT OF SENSOR
0.500
3.500
0.480
4.50°
4.50°
0.035
0.420
4.50°
6°
0.250
13 x 0.231
PROPRIETARY AND CONFIDENTIAL
THE INFORMATION CONTAINED IN THIS DRAWING IS THE SOLE PROPERTY OF THE PENNSYLVANIA STATE UNIVERSITY. ANY REPRODUCTION IN PART OR AS A WHOLE WITHOUT THE WRITTEN PERMISSION OF THE PENNSYLVANIA STATE UNIVERSITY IS PROHIBITED.
DIMENSIONS ARE IN INCHES
TOLERANCES:
FRACTIONAL ±
ANGULAR: MACH ± BEND ±
TWO PLACE DECIMAL ±
THREE PLACE DECIMAL ±
MATERIAL Aluminum 6061-T6
FINISH --
NEXT ASSY
USED ON
APPLICATION
DO NOT SCALE DRAWING
NAME
DATE
DRAWN
CHECKED
ENG APPR.
MFG APPR.
Q.A.
COMMENTS:
103
Linear Photodetector Array
SIZE A
DWG. NO.
REV.
SCALE: 3
WEIGHT:
SHEET 1 OF 1

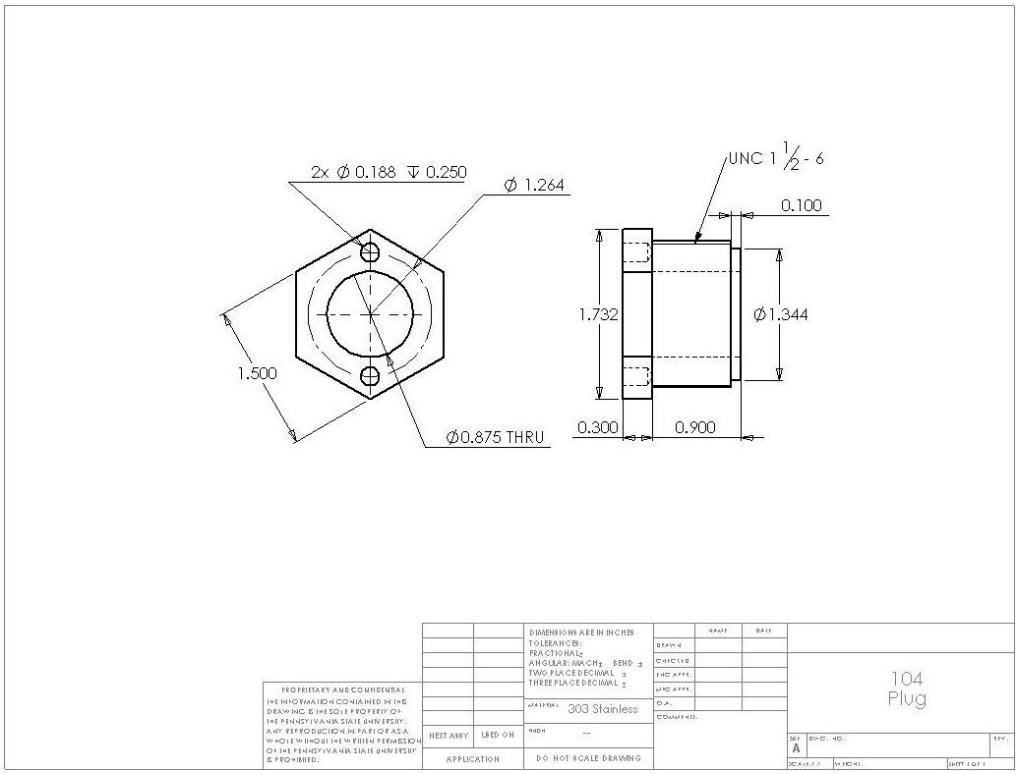
2x Ø 0.188 ↧ 0.250
Ø 1.264
UNC 1 1/2 - 6
0.100
1.732
Ø1.344
1.500
Ø0.875 THRU
0.300
0.900
PROPRIETARY AND CONFIDENTIAL
THE INFORMATION CONTAINED IN THIS DRAWING IS THE SOLE PROPERTY OF THE PENNSYLVANIA STATE UNIVERSITY. ANY REPRODUCTION IN PART OR AS A WHOLE WITHOUT THE WRITTEN PERMISSION OF THE PENNSYLVANIA STATE UNIVERSITY IS PROHIBITED.
DIMENSIONS ARE IN INCHES
TOLERANCES:
FRACTIONAL ±
ANGULAR: MACH ± BEND ±
TWO PLACE DECIMAL ±
THREE PLACE DECIMAL ±
MATERIAL 303 Stainless
FINISH --
NEXT ASSY
USED ON
APPLICATION
DO NOT SCALE DRAWING
NAME
DATE
DRAWN
CHECKED
ENG APPR.
MFG APPR.
Q.A.
COMMENTS:
104
Plug
SIZE A
DWG. NO.
REV.
SCALE: 3
WEIGHT:
SHEET 1 OF 1

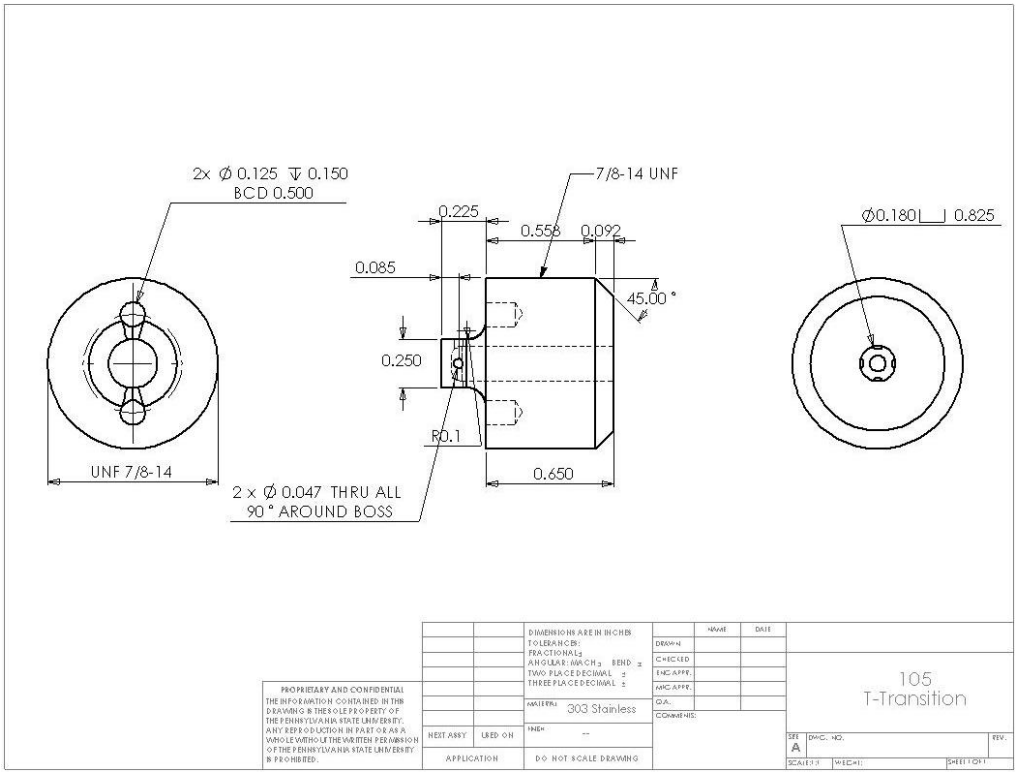
2x Ø 0.125 ↧ 0.150
BCD 0.500
7/8-14 UNF
0.225
0.558
0.092
0.085
45.00°
0.250
R0.1
0.650
Ø0.180 | 0.825
UNF 7/8-14
2 x Ø 0.047 THRU ALL
90° AROUND BOSS
PROPRIETARY AND CONFIDENTIAL
THE INFORMATION CONTAINED IN THIS DRAWING IS THE SOLE PROPERTY OF THE PENNSYLVANIA STATE UNIVERSITY. ANY REPRODUCTION IN PART OR AS A WHOLE WITHOUT THE WRITTEN PERMISSION OF THE PENNSYLVANIA STATE UNIVERSITY IS PROHIBITED.
DIMENSIONS ARE IN INCHES
TOLERANCES:
FRACTIONAL ±
ANGULAR: MACH ± BEND ±
TWO PLACE DECIMAL ±
THREE PLACE DECIMAL ±
MATERIAL 303 Stainless
FINISH --
NEXT ASSY
USED ON
APPLICATION
DO NOT SCALE DRAWING
NAME
DATE
DRAWN
CHECKED
ENG APPR.
MFG APPR.
Q.A.
COMMENTS:
105
T-Transition
SIZE A
DWG. NO.
REV.
SCALE: 1:1
WEIGHT:
SHEET 1 OF 1

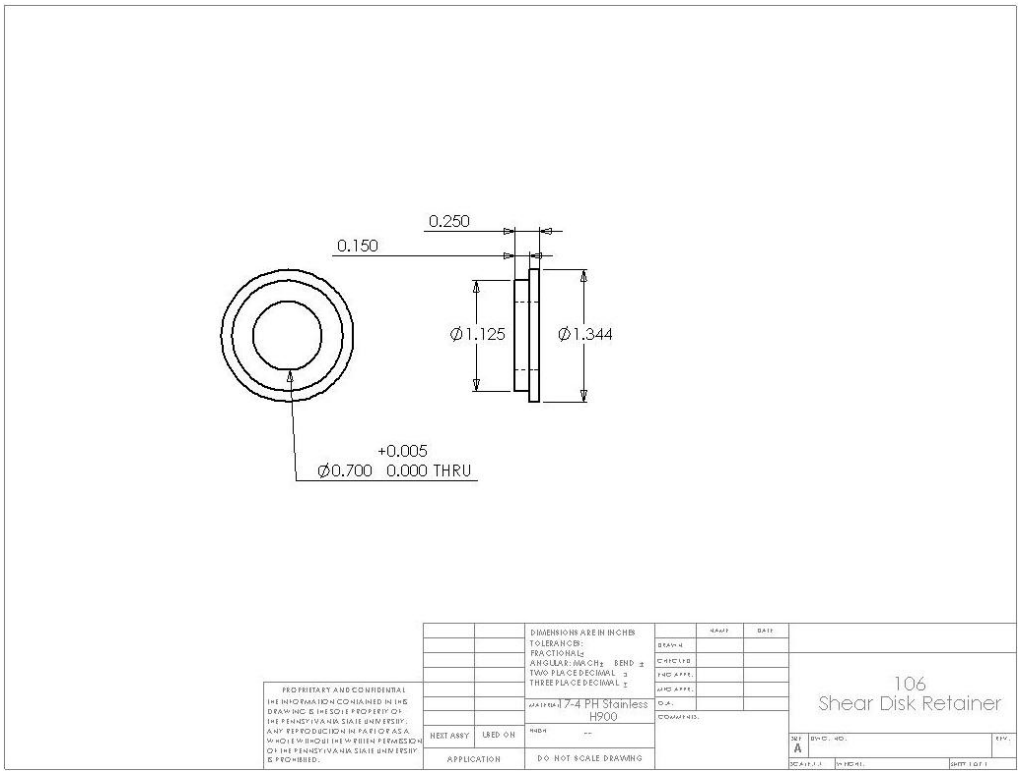
0.250
0.150
Ø1.125
Ø1.344
+0.005
Ø0.700 0.000 THRU
PROPRIETARY AND CONFIDENTIAL
THE INFORMATION CONTAINED IN THIS DRAWING IS THE SOLE PROPERTY OF THE PENNSYLVANIA STATE UNIVERSITY. ANY REPRODUCTION IN PART OR AS A WHOLE WITHOUT THE WRITTEN PERMISSION OF THE PENNSYLVANIA STATE UNIVERSITY IS PROHIBITED.
DIMENSIONS ARE IN INCHES
TOLERANCES:
FRACTIONAL ±
ANGULAR: MACH ± BEND ±
TWO PLACE DECIMAL ±
THREE PLACE DECIMAL ±
MATERIAL 17-4 PH Stainless H900
FINISH --
NEXT ASSY
USED ON
APPLICATION
DO NOT SCALE DRAWING
NAME
DATE
DRAWN
CHECKED
ENG APPR.
MFG APPR.
Q.A.
COMMENTS:
106
Shear Disk Retainer
SIZE A
DWG. NO.
REV.
SCALE: 1:1
WEIGHT:
SHEET 1 OF 1

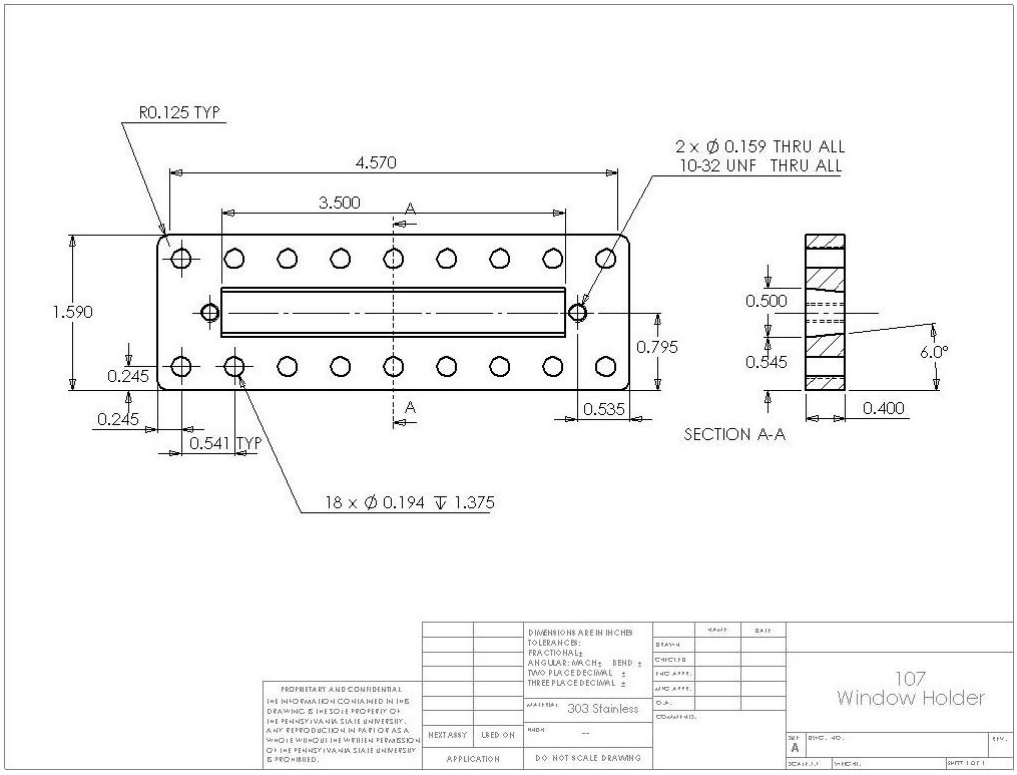
R0.125 TYP
4.570
3.500
A
2 x Ø 0.159 THRU ALL
10-32 UNF THRU ALL
1.590
0.245
0.245
0.541 TYP
0.795
0.535
18 x Ø 0.194 ↧ 1.375
0.500
0.545
6.0°
0.400
SECTION A-A
DIMENSIONS ARE IN INCHES
TOLERANCES:
FRACTIONAL ±
ANGULAR: MACH ± BEND ±
TWO PLACE DECIMAL ±
THREE PLACE DECIMAL ±
MATERIAL 303 Stainless
NEXT ASSY
USED ON
APPLICATION
DO NOT SCALE DRAWING
PROPRIETARY AND CONFIDENTIAL
THE INFORMATION CONTAINED IN THIS DRAWING IS THE SOLE PROPERTY OF THE PENNSYLVANIA STATE UNIVERSITY. ANY REPRODUCTION IN PART OR AS A WHOLE WITHOUT THE WRITTEN PERMISSION OF THE PENNSYLVANIA STATE UNIVERSITY IS PROHIBITED.
DRAWN
CHECKED
ENG APPR.
MFG APPR.
Q.A.
COMMENTS:
107
Window Holder
SIZE A
DWG. NO.
REV.
SCALE:
WEIGHT:
SHEET 1 OF 1

Appendix B

Finite Element Analysis for Chamber Strength

(SolidWorks 2009 SP4.0)

Figure 39: FEA results for head end of chamber with internal pressure. Designed to 20,000 psi with a factor of safety of 4. Maximum stress is at the pressure transducer port.

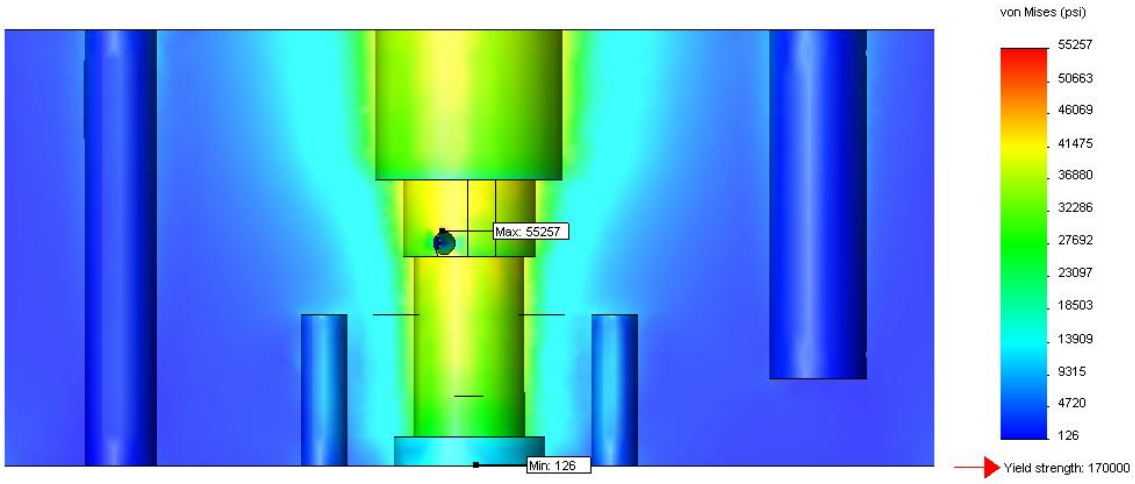

Figure 40: FEA results for axial chamber with internal pressure. Designed to 20,000 psi with a factor of safety of 4. Maximum stress is at the window interface.

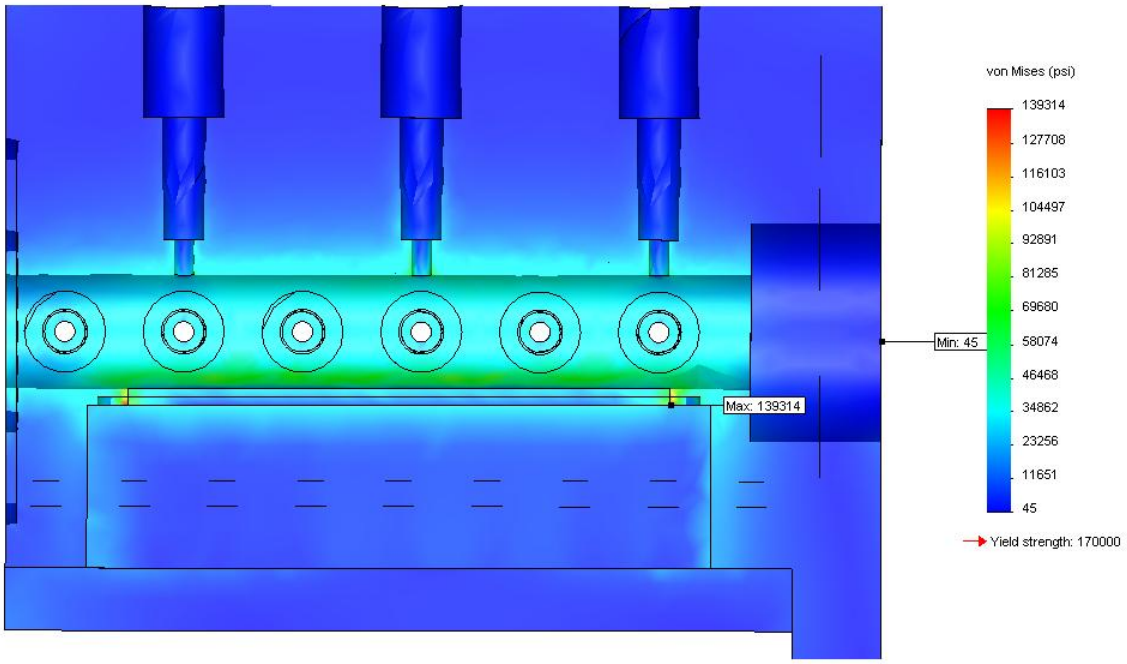

Figure 41: FEA results for radial chamber with internal pressure. Designed to 15,000 psi with a factor of safety of 4. Maximum stress is at the chamber wall.

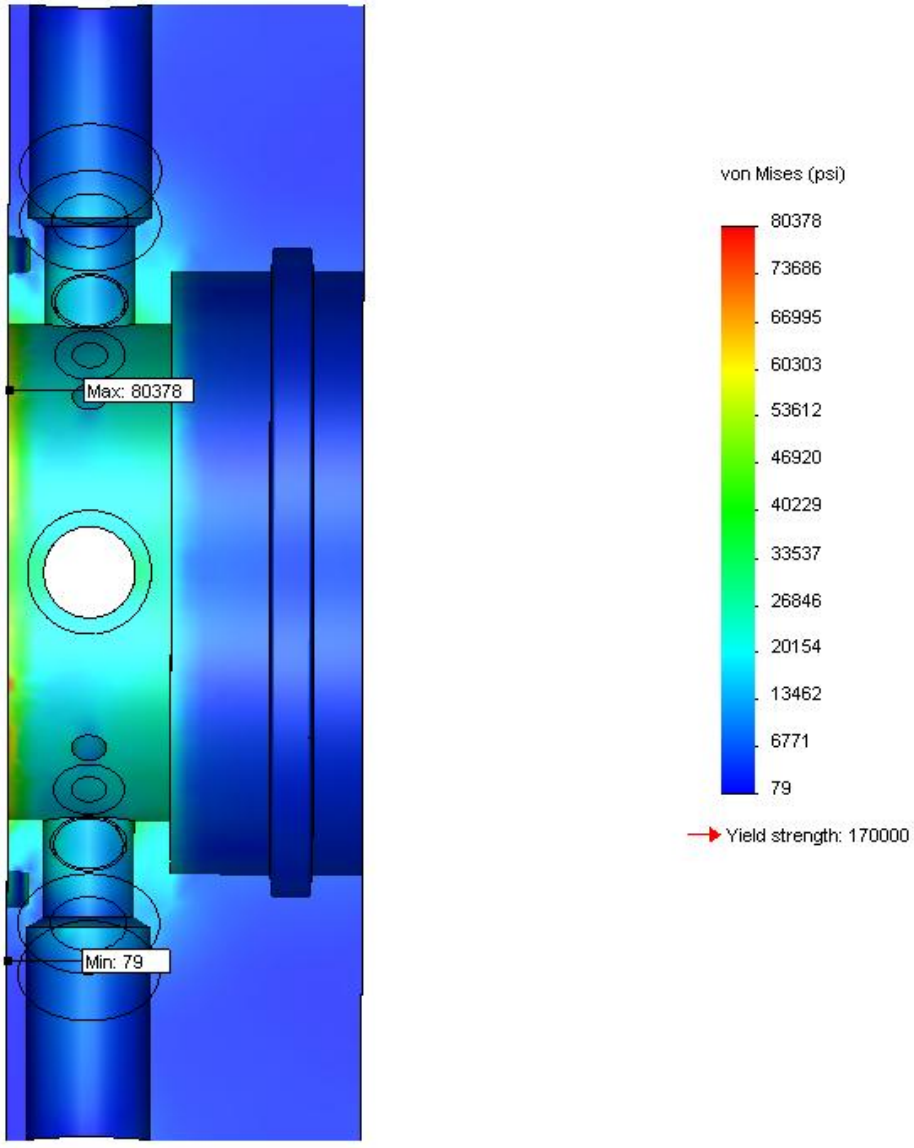

Appendix C

Circuit Diagrams

Photodetector Measurement Circuit

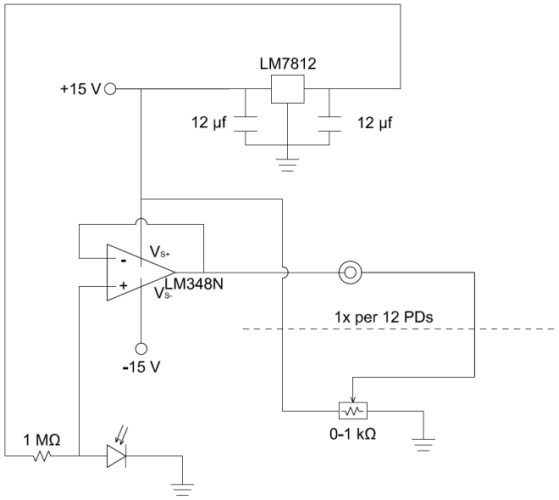

Impact Hammer

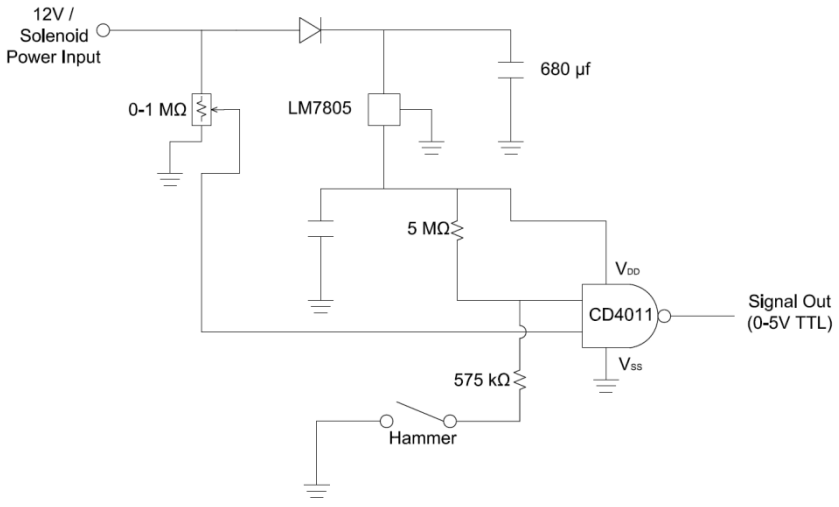

Appendix D

Properties of Ignition Train Elements

Primer

Make	Federal No. 150 large pistol primer
Type	Percussion primer
Dimensions	Height: 0.121”
	Diameter: 0.210”
Weight of charge	35mg

Black Powder (MIL-A-2250)

Chemical Composition	Potassium Nitrate	74.0% ± 1.0
	Sulfur	15.6% ± 1.0
	Charcoal	10.4% ± 1.0
Dimensions	Length: 0.228”	
	Outside Diameter: 0.202” Central Perforation Diameter: 0.047”	
Specific Gravity	1.70 ± 0.05	

Granular Propellant Physical Characteristics (M48 Ball Propellant)

Description	Value
Initial bed porosity	0.407
Initial radius of the solid propellant grain	0.0545 cm
Molecular weight of the solid propellant gas	56 g/gmole
Density of propellant	1.55 g/cm^3
Ablation temperature of the solid propellant	525 K
Ignition temperature of the solid propellant	600 K
Density of liquid products of combustion from flash tube	8.45 gm/cc
Specific heat of liquid products of combustion from flash tube	0.031 cal/gm-K
Thermal conductivity of liquid products of combustion from flash tube	0.000205 cal/cm-s-K
Thermal conductivity of M48 ball propellant	0.0005998 cal/cm-s-K
Specific heat of M48 ball propellant	0.35 cal/gm-K
Thermal diffusivity of M48 ball propellant	0.0011045 cm^2/s
Adiabatic flame temperature of BP	1930 K
Emissivity of the propellant	1
Adiabatic flame temperature of solid propellant (K)	2831

Appendix E

CEA Analysis of Black Powder Combustion Products

Combustion (Enthalpy and Pressure) Analysis

Input

```
problem
        hp
        p,atm= 150, 200, 250, t,k=3800

react
        name=K1NO3      K 1 N 1 O 3                          h,kj/mol=-494.63
        t,k=298.15      wt%=74
        name=Sulfur S 1                                      h,kj/mol=0
        t,k=298.15      wt%=10.4
        name=charcoal      C 10 CA .009 H 6.696 O 2.2117     h,kj/mol=206.69
        t,k=298.15      wt%=15.6
end

output  siunits
        short
        massf
        transport
```

Tabulated Output

Table 2: CEA output for constant pressure combustion of black powder (mass fractions below 1% omitted)

Species	*Mass Fraction*		
	Pressure = 1500 psi	Pressure = 2250 psi	Pressure = 3750 psi
CO	0.18957	0.18606	0.18278
CO_2	0.22791	0.21935	0.21248
H_2	0.01514	0.01572	0.01613
H_2O	0.10151	0.10515	0.10770
KOH	0.06687	0.05873	0.05266

N_2	0.18238	0.18445	0.18617
S_2	0.01058	0.01331	0.01584
$K_2CO_3(l)$	0.05698	0.07382	0.08787
$K_2S(l)$	0.05394	0.04848	0.04338
$K_2SO_4(l)$	0.03143	0.02720	0.02369
Temperature (K)	2293	2323	2345
Average Molecular Weight of Product Species	49.839	50.406	50.876
Ratio of Specific Heat	1.0789	1.0714	1.0653

Combustion (Internal Energy and Volume) Analysis

Input

```
problem
        uv   rho,g/cc=0.265, t,k=3800

react
        name=KNO3     K 1 N 1 O 3              h,kj/mol=-494.63        t,k=298.15     wt%=74
        name=Sulfur S 1                                               h,kj/mol=0
        t,k=298.15     wt%=10.4
        name=charcoal     C 10 CA .009 H 6.696 O 2.2117        h,kj/mol=206.69
        t,k=298.15     wt%=15.6
end
```

Tabulated Output

Table 3: CEA output for constant volume combustion of black powder (mass fractions below 1% omitted)

Species	*Mass Fraction Specific Volume = 0.265 g/cc*
CO	0.17467
CO_2	0.16802
H_2	0.01492
H_2O	0.09194

H_2S	0.01665
KOH	0.03465
N_2	0.19037
S_2	0.05073
S_2O	0.05073
KOH(*l*)	0.04446
K_2CO_3(*l*)	0.03414
Temperature (K)	2577
Average Molecular Weight of Product Species	52.033
Ratio of Specific Heat	1.0451
Pressure (bar)	881.34

Appendix F

Important Chamber Dimensions

Radial Chamber

Item	Location/Size (inches)	Note
Axial flashtube		
Length	1.855	From primer to end of vent-hole
Axial vent diameter	0.055, 0.0595, 0.065, 0.073	Four separate parts
Radial flashtube		
Length	2.385	From primer cup to vent holes
Diameter	2 x 0.065	Offset 180°
PT 1	0.956	From primer
Main chamber		
PT 2-5	0.288	From start of bed, Centered in test chamber
Volume	1.3830	in^3
Length	0.575	
Chamber	1.750	
Photodetector offset	0.217	Offset in both x and y from center to form a grid

Axial Chamber

Item	Location/Size (inches)	Note
Length of radial flashtube	2.600	From primer to center of vent-holes
Vent diameter	4 x 0.040	Axi-symmetric
Length of chamber	4.575	
Diameter of chamber	0.700	
Length of window	0.330	
Start of window	0.877	Measured from start of chamber, matches radial vent-hole location
PT 2-3	0.365	"
PT 4-6	1.094	"
PT 7-8	1.823	"
PT 9-11	2.552	"
PT 12-13	3.281	"
PT 14-16	4.011	"

PD 1	0.915	"
PD 2	1.146	"
PD 3	1.377	"
PD 4	1.607	"
PD 5	1.838	"
PD 6	2.069	"
PD 7	2.300	"
PD 8	2.531	"
PD 9	2.761	"
PD 10	2.992	"
PD 11	3.223	"
PD 12	3.454	"
PD 13	3.685	"
PD 14	3.915	"
Shear Disk Diameter	1.250	1.25 nominal, can range from 1 1/8 - 1.344

Appendix G

Inert Bed Firing Tests

Table 4: Test matrix and derived parameters

Test No.	Orifice Diameter (inches)	Inert Particle Diameter (inches)	BP Weight (grams)	Peak Pressure (psia - 5 point average)	Depth of Penetration (inches)	Mass Flow Rate (kg/s)	Froude Number $U_o^2 d_p/(g d_o^2)$	Reynolds Number $\dot{m}/(\mu d_o)$
1	0.065	0.0551	0.1811	2353.48	1.079	1.095E+05	8.352E+13	1.363E+08
2	0.065	0.0551	0.1827	2198.5	1.275	1.023E+05	8.352E+13	1.273E+08
3	0.065	0.0551	0.0858	2238.42	1.220	1.041E+05	8.352E+13	1.297E+08
4	0.065	0.0551	0.0884	1959.8	1.075	9.115E+04	8.352E+13	1.135E+08
5	0.073	0.0551	0.1827	2390.64	0.695	1.402E+05	8.352E+13	1.555E+08
6	0.073	0.0551	0.1849	2724.32	0.696	1.598E+05	8.352E+13	1.772E+08
7	0.073	0.0551	0.0855	2157.58	0.957	1.266E+05	8.352E+13	1.404E+08
8	0.073	0.0551	0.0884	2195.9	0.655	1.288E+05	8.352E+13	1.429E+08
9	0.073	0.0551	0.184	2892.74	1.159	1.697E+05	8.352E+13	1.882E+08
10	0.065	0.0551	0.1842	2538.08	0.969	1.180E+05	8.352E+13	1.470E+08
11	0.065	0.0551	0.0864	2613.4	0.808	1.216E+05	8.352E+13	1.514E+08
12	0.073	0.0551	0.087	2771.14	1.116	1.626E+05	8.352E+13	1.803E+08
13	0.065	0.0669	0.184	2696.18	0.825	1.254E+05	5.665E+13	1.562E+08
14	0.065	0.0669	0.1801	2699.66	0.829	1.256E+05	5.665E+13	1.564E+08
15	0.073	0.0669	0.1822	1634.46	0.807	9.588E+04	5.665E+13	1.063E+08
16	0.073	0.0669	0.1836	2754.16	0.969	1.616E+05	5.665E+13	1.792E+08
17	0.065	0.0669	0.1816	2672.9	0.916	1.243E+05	5.665E+13	1.548E+08
18	0.073	0.0669	0.1835	2104.72	1.070	1.235E+05	5.665E+13	1.369E+08
19	0.0595	0.0551	0.1838	2474.98	0.885	9.646E+04	8.352E+13	1.312E+08
20	0.055	0.0551	0.18	2865.18	1.269	9.541E+04	8.352E+13	1.404E+08
21	0.055	0.0551	0.1828	1989.12	1.115	6.624E+04	8.352E+13	9.749E+07
22	0.055	0.0551	0.1813	2767.36	0.979	9.215E+04	8.352E+13	1.356E+08
23	0.055	0.0669	0.1817	3039.6	0.913	1.012E+05	5.665E+13	1.490E+08
24	0.055	0.0669	0.1834	2912.68	0.732	9.699E+04	5.665E+13	1.428E+08

Figure 42: Summary of condensed phase deposition onto inert bed

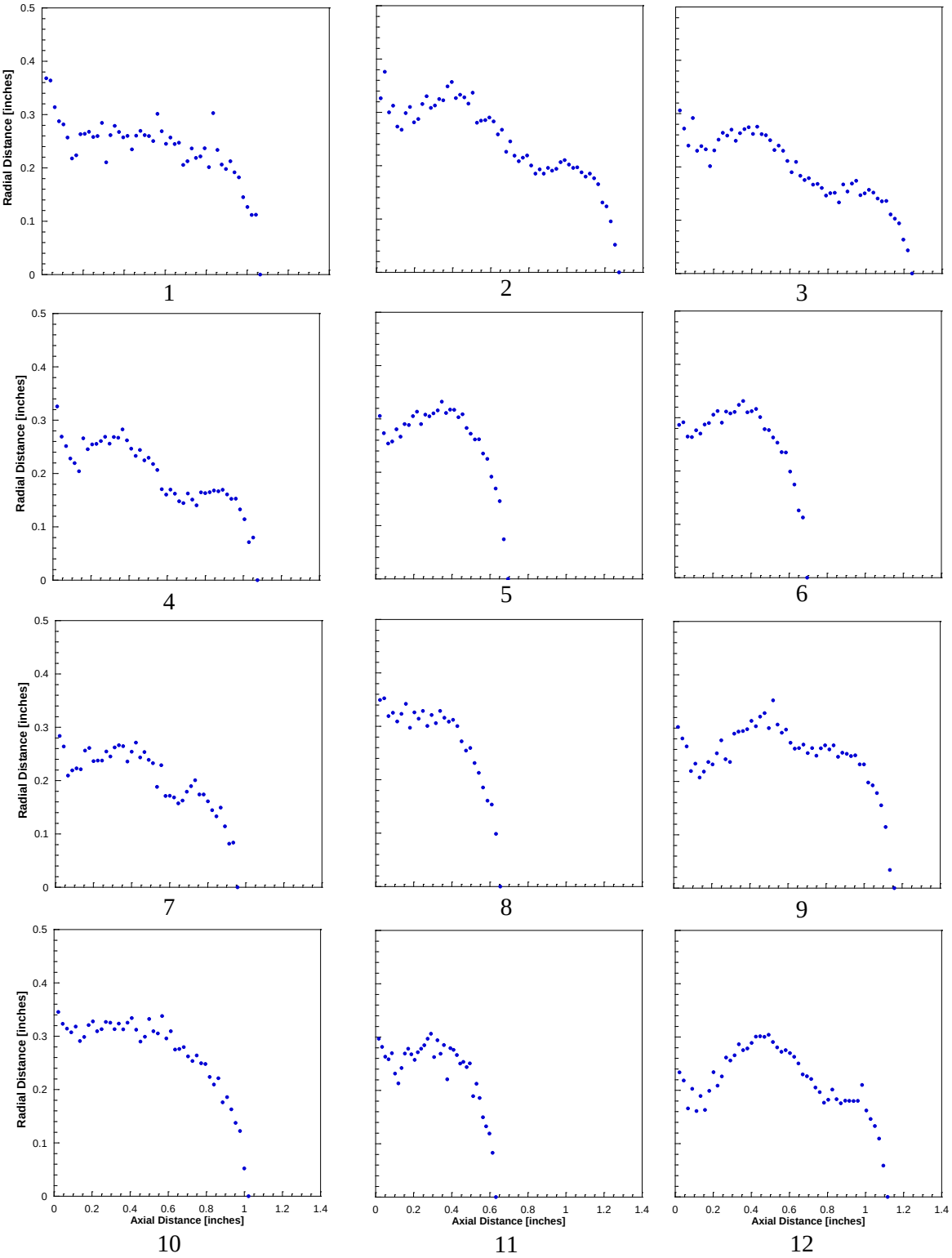

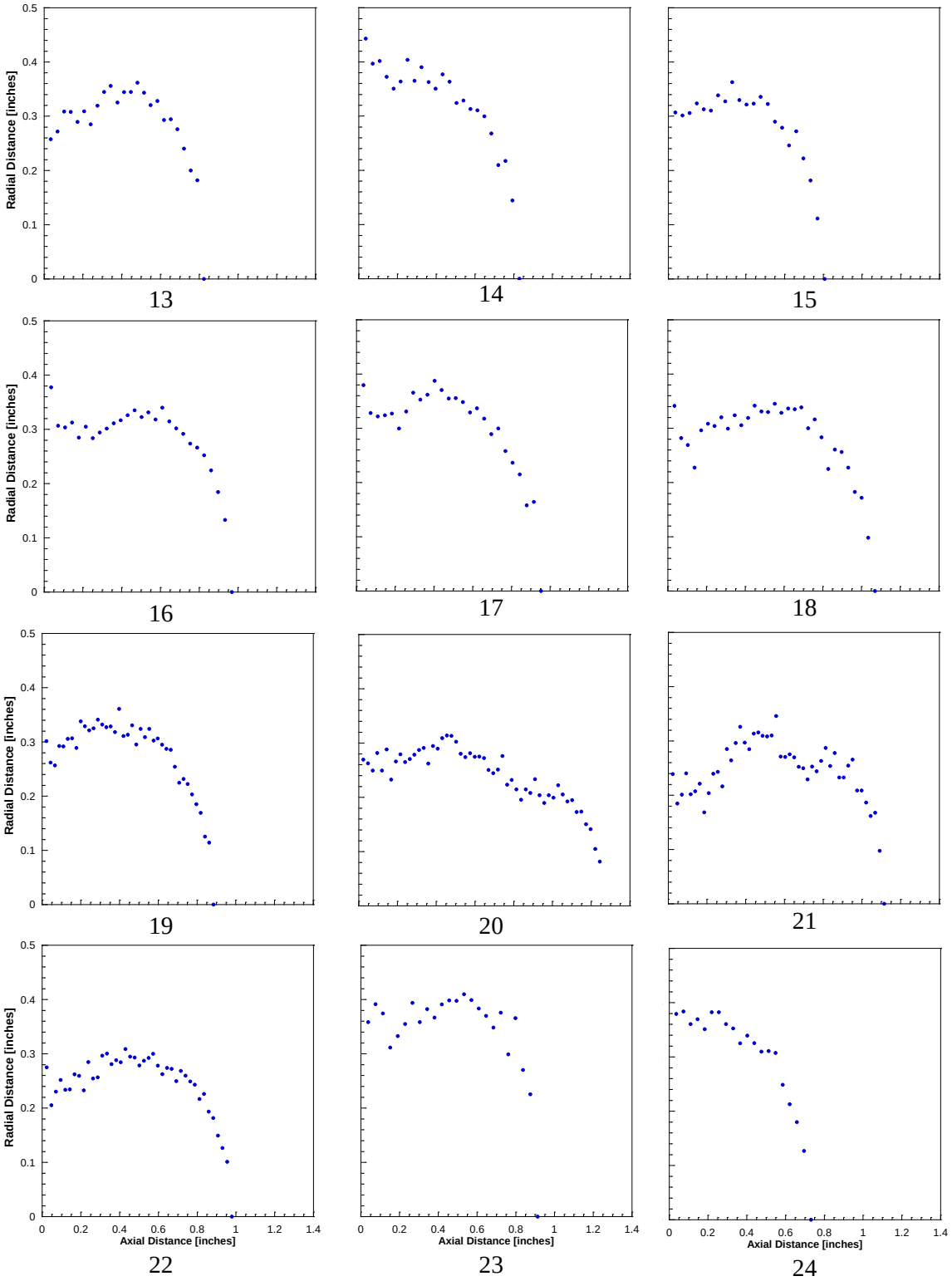
Radial Distance [inches]
Axial Distance [inches]
13
14
15
16
17
18
19
20
21
22
23
24

Appendix H

Standard Operating Procedure

STANDARD OPERATING PROCEDURE

IGNITION AND FLAME SPREADING PROCESSES IN GRANULAR PROPELLANT BEDS

High Pressure Combustion Laboratory (HPCL)
Department of Mechanical and Nuclear Engineering
The Pennsylvania State University

Approved by:	Kenneth K. Kuo Director of HPCL	Date:
Written by:	Alexander Colletti Research Assistant	Date:
Reviewed by:	Eric Boyer Safety Officer	Date:

THE PENNSYLVANIA STATE UNIVERSITY
HIGH PRESSURE COMBUSTION LABORATORY
UNIVERSITY PARK, PA 16801

STANDARD OPERATING PROCEDURE

VERSION: 1.1 4 JANUARY 2010

SAFETY

I. Purpose

To establish safe operating procedures associated with laboratory measurements of ignition and flame spreading processes of granular propellant beds used in the firing of mortar systems.

II. Scope

This SOP applies to operations associated with laboratory testing of granular propellant combustion in Rooms 107 and 109 at the High Pressure Combustion Laboratory (Bldg 430). Operations that are not adequately covered by this SOP will be addressed in a separate SOP or a supplement to this SOP.

III. Applicability

This SOP applies to all Penn State, HPCL, and visiting personnel and all other personnel assigned to support the operation of the ARO experiment.

IV. Responsibility

A. The Director of the High Pressure Combustion Laboratory and Distinguished Professor of Mechanical Engineering, Dr. Kenneth K. Kuo, is responsible for the overall enforcement of this SOP. Dr. Kuo is further responsible that only trained personnel are assigned to these operations and that all personnel are informed of all of the hazards associated with this experimental procedure.

B. The Experimentalist/Researcher/Graduate Student (E/R/GS) is responsible for application and enforcement of this SOP and overall on-site supervision of the experiments, to include taking necessary actions to protect all personnel, equipment, and facilities from any blast, fragmentation, or fire resulting from an experiment under his (or her) control. The E/R/GS is responsible that all personnel assigned to the testing programs have been adequately trained. Also, prior to any operation, they have been thoroughly briefed on duties, responsibilities, and hazards that may be involved.

V. Personnel Limits

A. Personnel will be limited to the minimum required for safe and efficient operation of each experiment.

B. A minimum of two trained persons must be present for any hazardous operation.

C. Observing personnel will be limited to those having an official interest in the experiment.

VI. Hazardous Material Limits

Hazardous material at least at the test site and fuel processing site will be limited to the amount necessary for safe and efficient operation of the program. All material not involved in the current test will be adequately protected and located so that it is not exposed to any personnel.

VII. General Safety Requirements

A. Experiments involving any live primer or propellant will be conducted remotely in the test cell (Room 109).
B. All test preparations will be conducted in Room 107 and 109. Heat and other sources of ignition will be kept away from the test jig or energetic components.

VIII. Personal Protective Equipment Requirements

A. Safety glasses or face shield will be worn for all eye hazard operations.

IX. Sequence of Operations

A. Description of System

A test rig has been developed to characterize igniter jet penetration into an inert bed and flame spreading in various granular propellants. By using a cylindrical chamber with a low length to diameter ratio, various instruments can be used to measure properties such as pressure-time traces, gas evolution, flame spreading, etc. The test rig is modular and can also accommodate a test section with a high length–to-diameter to examine axial flame spreading. In order to safely prepare and fire a test, this SOP has been developed. For any given test, either the radial or axial test section can be run. The rough outline of the steps and approximate time frames (after initial setup) for each procedure are as follows:

1. Instrumentation, Test Rig Preparation, and Checkout
2. Primer Preparation and Loading
3. Radial Test Section Preparation and Propellant Loading
4. Axial Test Section Preparation and Propellant Loading
5. Instrumentation, Control Preparation, and System Checkout
6. Firing
7. Turnaround time
8. Cleanup and Disassembly

Because of the energy contained in the system, tests are fired remotely in a reinforced test cell. Numerous physical and procedural safeties have been incorporated into the system.

SAFETY: *Utilize the necessary safety gear for each section of the procedure. To conduct any part of this procedure, protective eyewear, a lab coat, long pants, and shoes which cover the entire foot are REQUIRED. Consult the HPCL Safety Manual as frequently as needed. However, each section may have specific safety precautions, which will be noted at the beginning of that section.*

The propellant is obtained from a system classified as a HD 1.4 low explosive and must be stored and handled in accordance with DOD, ATF, and any other applicable rules and regulations.

1. INSTRUMENTATION, TEST RIG PREPARATION, AND CHECKOUT

The following procedures outline the steps required to successfully implement pressure transducers and photodetectors/photodiodes. The pressure transducers used are a PCB model (111-A23) each factory calibrated. Because of the event length and transducer characteristics, tests using this system require many channels of high-frequency (100 kHz) data acquisition.

Materials Required:
1. PCB pressure transducers and wires
2. RTV
3. Radial test data sheet
4. Nicolet Vision data acquisition system
5. Nicolet Multi-Pro data acquisition system
6. Radial or axial test chamber

1.1. Preparation of PCB pressure transducers

1.1.1. The PCB pressure transducers will be used without their pipe thread adapter. However, this is the part of the sensor that has the serial number data on it. It has been copied to the straight thread adapter, but care should be taken to make sure that each PCB's serial number is accounted for. Remove the pressure transducer from this adapter.

1.1.2. Apply a coat of RTV to each end of the PCB pressure transducers to protect the sensor from the intense heat it will experience (*note: Allow 24 hours for the RTV to fully cure).*

1.1.3. Check the condition of the copper sealing rings and replace if they show damage or wear.

1.1.4. Attach PCB pressure transducers to the pressure signal wire and check for continuity by turning on the PCB display box and seeing if the PCB transducer signal indicator goes to "green".

1.1.5. Repeat procedure for each PCB pressure transducer until the transducers checkout (*note: if a bad signal occurs either retry screwing the wires on or replace the PCB wires with new ones).*

1.1.6. Remove the PCB wires from the PCB transducers for now.

1.2. Preparation of infrared/visible light photodetectors (IR-PD/VL-PD)

1.2.1. Connect short barrel connectors directly to the photodetector panel.

1.2.2. Connect one line of the panel to the Nicolet Vision and run program "ARO Radial".

1.2.3. Check each IR-PD and VL-PD and ensure that it shows a constant voltage of around 0-5 mV when exposed to just room light.

1.2.4. These can be quickly tested to ensure response by holding the flame of a lighter near the sensor checking for a varying response on the DAQ. For this signal the response should be on the order of 5-10 mV for either sensor.

1.2.5. Remove the photodetectors from the panel and set aside.

1.3. Diagnostic assembly

1.3.1. The pressure ports on the chamber need to be filled with RTV to allow passage of the pressure data to the PCB. On the head end fill the pressure port with RTV past the first step in the hole. Do *not* fill the smaller hole in the black powder retainer.

1.3.2. There are five pressure ports on the radial chamber and 15 on the axial chamber. Each position is numbered and corresponds to a position on the data sheet.

1.3.3. Hand-tighten each PCB into a pressure port ensuring that the copper sealing rings will mount flush. It is not necessary to use any thread sealant for the pressure transducers.

1.3.4. Fill all the holes with RTV past the first step in the hole.

1.3.5. Tighten down the sensors with an even torque wrench to 25-35 in-lbs.

1.3.6. For any position where pressure information will not be measured install a plug with a copper sealing ring to fill the position.

1.3.7. Installation of the sensors will extrude RTV into the main chamber sections. Remove this before running the experiment.

1.3.8. There are 34 photodetector ports on the radial chamber. They cannot all be run at the same time due to limitation on the DAQ systems. A there are maximum of 33 sensors which can be run at the same time to be split among the photodetectors and the PCBs. On the axial chamber there are 28 photodetector ports split evenly between IR-PD's and VL-PD's

1.3.9. Place each photodetector into the desired position on the photodetector array.

1.3.9.1. On the radial chamber: the IR-PDs should fit as a loose press fit. The VL-PDs, however, require a sleeve to fit. This vinyl sleeve is first placed into the array then the sensor is placed inside of that assembly.

1.3.9.2. On the axial chamber: the IR-PDs and the VL-PD's should fit as a loose press fit. See Figure 43*. If the sensors begin to fit loosely the side of the hole can be staked with a center punch.*

1.3.10. Indicate on the test data sheet the location of the photodetectors to be used on that test.

1.3.11. Bolt the two photodetector retainers over the sensors to keep them in place.

1.3.11.1. For the radial chamber: bolt the retainer as shown in Figure 44*. If the proper allen wrench cannot be located a T10 torx driver has worked well.*

1.3.11.2. For the axial chamber: this step is unnecessary. See 0 *if the detectors are not being well retained.*

1.3.13. Put the assembly aside for later installation.

Figure 43: IR/VL Photodetectors installed on axial chamber

Figure 44: IR Photodetectors installed with retainer on radial chamber

1.4. DAQ set-up

1.4.1. The radial chamber requires the use of two DAQ systems: the Nicolet Vision and the Nicolet Multi-Pro. Boot them both up.

1.4.2. Open the Windows Nicolet data acquisition application on the Multi-Pro mobile DAQ unit.

1.4.3. Select and load the program labeled "ARO".

1.4.4. Each time the program is loaded the DAQ boards need to be reselected. This can be avoided by leaving the program open. Start by turning on the DAQ.

1.4.5. Within the program go to: Control:Select Recorder:Yes:Add all. Choose Use: 4 Channels 5 times. If this is not the first time running deselect the Reset Recorder checkbox. It is selected by default.

1.4.6. Still within the program, click on the configure channel button. Set the Input Span, Mid Scale, Coupling mode DC, + Input. For channels with a PT (or trigger signal), set the Input Span to 6V and Mid Scale to 3. For channels with an IR-PD or a VL-PD, set the Span to 3 Volts and Mid Scale to 1.5V. Choose these checkboxes on the right and choose Copy to All Recorders for the settings that will be the same for all sensors. This does not need to be done if the Reset Recorder checkbox is deselected in the previous step.

1.4.7. Attach BNC cables as indicated on the datasheet.

1.4.8. Hit "Record" for a trial run to see if the signals are read (*note: signals should be near zero in value for the PCBs and 0-5mV for the IR-PDs and VL-PDs*).

1.4.9. Hit "Stop".

1.4.10. Open the "Acquisition" tab and label the upcoming test firing.

1.4.11. Press "Esc" to exit the setup.

1.4.12. Load the program labeled "ARO" on the Nicolet Vision.

1.4.13. Attach BNC cables as indicated on the datasheet.

1.4.14. The trigger signal is located on the panel output label auxiliary. A BNC tee should be placed on that output of the control panel so that it can be connected to channel 1 on both systems as a simultaneous trigger.

1.4.15. Hit “Record” (this time a physical button) for a trial run to see if the signals are read.

1.4.16. Allow the programs to idle. They will wait for the trigger signal to begin recording.

2. PRIMER PREPARATION AND LOADING

This system uses a .45 ACP cartridge to hold the primer and to seal the chamber. For each test, the cartridge must be cleaned, sized, and re-primed. *(Note: even new cartridges should go through all steps including sizing to ensure correct and consistent dimensions.)*

Materials Required:
1. Lab coat and protective glasses
2. .45 ACP cartridge (unloaded brass shell only)
3. Primer (e.g. Federal 150)
4. Priming tool
5. Hand press and carbide sizing/de-priming die

2.1. Igniter Primer Preparation

2.1.1. Acquire a used .45 ACP cartridge and large pistol primer from the day box.

2.1.2. Follow the Lee Hand Press guide steps 1-6 to de-prime a used cartridge. Even if a cartridge is de-primed used the tool to bring it back to proper sizing tolerances. *(Note: no lubrication is necessary as specified by the guide because the sizing die is carbide.)*

2.1.3. Use the primer pocket tool to clean the primer pocket.

2.1.4. To insert a new primer follow the RCBS Universal Hand Priming Tool guide.

3. RADIAL TEST SECTION PREPARATION AND PROPELLANT LOADING (FOLLOW *EITHER* 3 OR 4)

The following procedures outline the steps required to assemble and load the radial chamber. The chamber first needs to be partially assembled. The granular propellant is then added and finally the chamber assembly is completed.

Materials Required:
1. Protective glasses
2. .45 ACP cartridge (cleaned, sized, primed)
3. Black powder pellet
4. Granular propellant (e.g. M48 ball propellant)
5. Radial test chamber

3.1 Assemble head end

3.1.1. Place one black powder pellet into the end of the black powder (BP) retainer.

3.1.2. To ensure that the black powder pellet will not move before the firing apply a small circular bead of liquid nitrocellulose (in a container marked liquid cellular nitrate lacquer). Place several wraps of Teflon tape directly below the shoulder ensuring the pressure port remains clear. See Figure 45.

Figure 45: Installed black powder pellet with lacquer

3.1.3. Install the BP retainer into the head end cap using the 1/8" diameter steel pin for alignment. See Figure 46.

3.1.4. Place a -017 O-ring over the end of the BP retainer and a -010 O-ring on the flashtube section. The latter should be covered lightly with halocarbon grease. Tighten down the flashtube section with a spanner wrench. The -017 o-ring is non-reusable and must be replaced every test. See Figure 47.

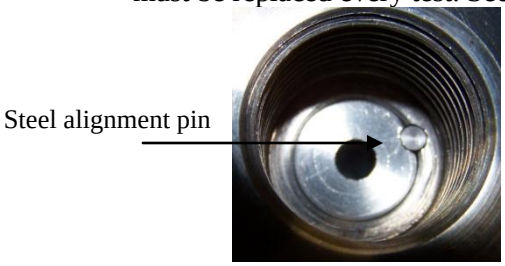

Figure 46: Installed black powder retainer

Figure 47: Installed flashtube section

3.2. Assemble test jig

3.2.1. Obtain the radial chamber test section.

3.2.2. Place head flat onto table with the primer end down. Place the radial chamber on top of it aligning the outer bolt circles.

3.2.3. Trim a sheet of paper to use to retain the ball propellant and place it inside the chamber.

3.2.4. Fill the inside of the chamber to the step for the window with ball propellant for that particular test. See Figure 48.

3.2.5. Place the sacrificial window and the steel annulus that goes around it into the chamber.

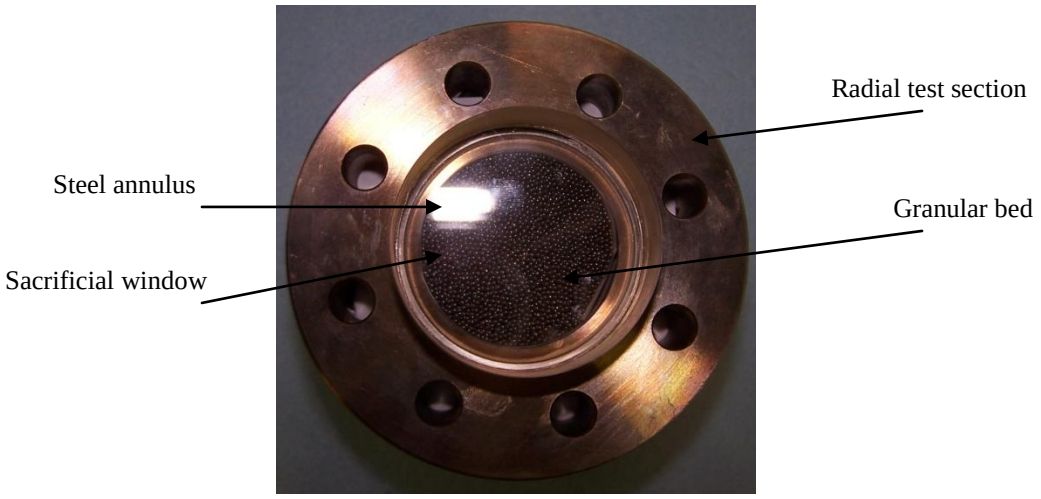

Figure 48: Radial chamber with ball propellant and sacrificial window in place.

3.2.6. Install -138 O-ring into the piston seal lightly lubricated with halocarbon grease.

3.2.7. Place the first quartz window into the chamber. Ensure that it is seated completed in the opening. Push it into place with a soft, clean rag. See Figure 49.

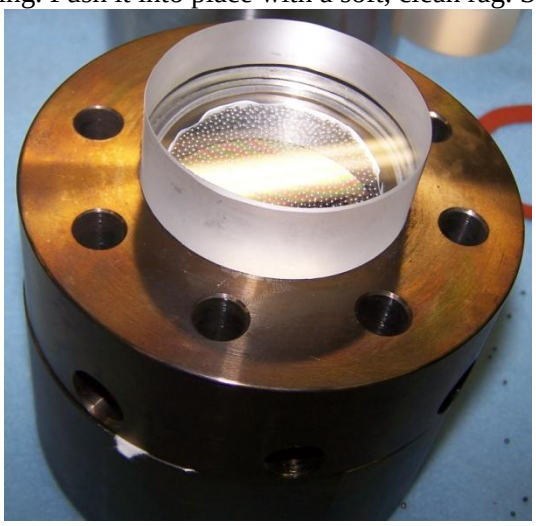

Figure 49: Radial chamber with quartz window installed

3.2.8. Place a thin film of mineral oil over the top surface of the quartz window.

3.2.9. Place the second quartz window on top with an orange rubber gasket on top.

3.2.10. Carefully place the window holder end of the second quartz window and align the bolt holes. See Figure 50.

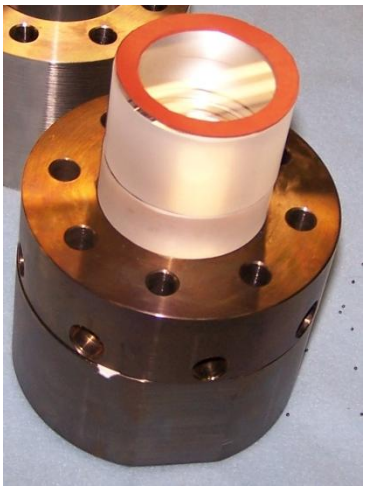

Figure 50: Positioning quartz windows and gaskets in radial chamber.

3.2.11. Hand-tighten 3/8”-16 bolts that connect the parts.

3.2.12. Place the assembly into the vice via the flats on the head end cap.

3.2.13. Fully hand torque the connecting bolts in a star pattern.

3.2.14. Connect this assembly to the L-bracket with 4, 3/16”-16 bolts

3.2.15. Place the cartridge over the end of the BP retainer.

3.2.16. On the other side of the head end cap, install the cartridge retainer with 2, 1/8”-diameter steel pins for alignment. Bring flush with 6 ¼”-20 socket head bolts. (See Figure 51.)

Figure 51: Installed cartridge retainer

4. AXIAL TEST SECTION PREPARATION AND PROPELLANT LOADING (FOLLOW *EITHER* 3. OR 4)

4.1 Assemble head end

4.1.1. Follow all steps listed in 3.1.

4.2. Assemble test jig

4.2.1. Obtain axial test section.

4.2.2. Place the sacrificial window into the long slot.

4.2.3. Into the recessed o-ring groove place a custom-cut 1/16” O-ring. (Note: stock O-rings cannot be used here because they do not come in a long enough length.) See Figure 52.

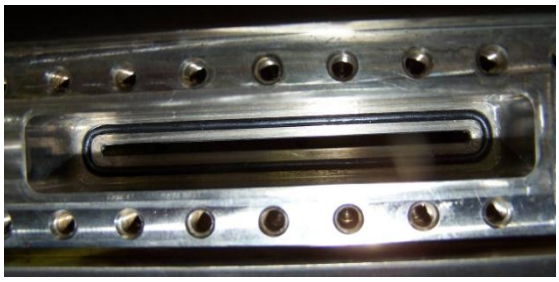

Figure 52: Axial chamber with installed o-ring

4.2.4. Place a quartz window into the hole and wet the top surface with mineral oil.

4.2.5. The window holder is installed over the window and bolted down with 18, 10-32 x ¾" bolts.

4.2.6. The tapered photodetector holder, from 0, fits into the gap in the window holder and is bolted down with 2, 10-32 x 3/8" button head bolts. See Figure 53.

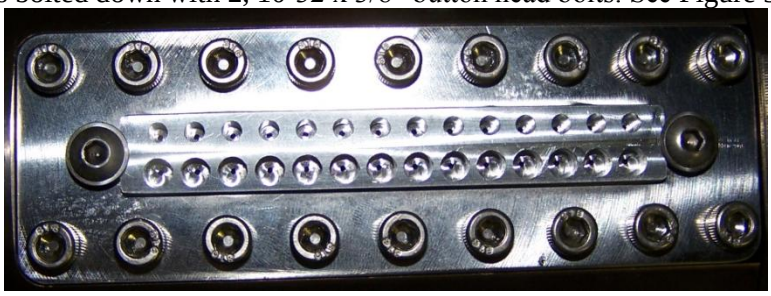

Figure 53: Axial test section with installed photodetector array

4.2.7. Lubricate -138 and -120 o-rings lightly with halocarbon grease. Install these onto the face of the axial chamber.

4.2.8. Place the head end flat onto table with the primer end down. Carefully place the axial chamber on top of it aligning the outer bolt circles. Align the test section so that window port will be facing up.

4.2.9. Attach the axial chamber to the head end with the 6 long 3/8"-16 bolts. To ensure that the o-rings seal properly the bolts must be tightened down with significant force. Tighten the bolts in an alternating pattern.

4.2.10. Fill the chamber with ball propellant.

4.2.11. Place the shear disk, of appropriate thickness for the test, followed by the shear disk retainer into the opening.

4.2.12. Install the threaded end cap tightly with the spanner wrench.

4.2.13. Connect this assembly to the L-bracket with 4, 3/16"-16 bolts

4.2.14. Place the cartridge over the end of the BP retainer.

4.2.15. On the other side of the head end cap, install the cartridge retainer with 2, 1/8"-diameter steel pins for alignment. Bring flush with 6 ¼"-20 socket head bolts.

5. INSTRUMENTATION, CONTROL PREPARATION, AND SYSTEM CHECKOUT

The following procedures outline the steps required to successfully instrument and checkout areas of the test firing and data acquisition before a firing:

Materials Required:

1. Lab coat, protective gloves, and protective glasses
2. Nicolet data acquisition systems

3. Allen wrench set
4. PCB wires
5. Flash tube holder block
6. Firing Pin

5.1 Pendulum and Solenoid Checkout

5.1.1. Inside the chamber connect the cable to the hammer impact detector box located below the test deck.

5.1.2. Lift the pendulum to the height where the retractable rod can be extended and the pendulum can rest on the edge of the rod.

5.1.3. Exit the test chamber.

5.1.4. Connect a BNC cable from auxiliary to the DAQ and set the DAQ to record.

5.1.5. Turn on the control panel to the mortar system (Figure 54).

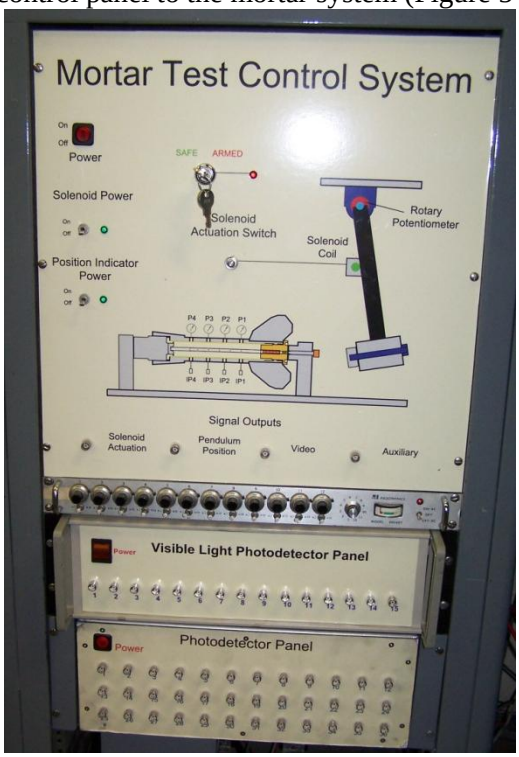

Figure 54: Control panel and photodetector panels

5.1.6. Activate the switch to the solenoid valve.

5.1.7. Insert the key and switch to "ARMED".

5.1.8. Lift the trigger and listen for the pendulum to fall and strike the firing block.

5.1.9. Turn the safety key back to "SAFE".

5.1.10. If the pendulum fell, continue to the next step. If the pendulum did not fall, check the continuity of the wires and power in the battery and repeat the procedure (*note: may need to replace the wires*).

5.1.11. Check that a clean signal showed up on the DAQ when the hammer impacted. It should rise from 0 to 5 V very rapidly.

5.1.12. Turn off the control panel.

5.2. Installation

5.2.1. Open the garage bay door.

5.2.2. Place the chamber on the deck of the test rig so that it is against the firing pin block.

5.2.3. Secure the assembly to the deck by screwing in bolts from beneath the deck to the head end support.

5.2.4. Tighten the screws beneath the deck to secure the test rig.

5.2.5. For the axial chamber: place the end support under the shear disk end of the chamber. There are 3 bolts that connect it to the test deck, push it as close to the primer end of the chamber as possible.

5.2.6. Attach the PCB wires to the PCBs and check continuity from the control panel (*note: if bad signal either retry screwing the wires on or replace the PCB wires with new ones).*

5.2.7. Attach the photodetectors and wires and check continuity by checking the DAQ signal.

5.2.8. For the radial test section:

5.2.8.1. Attach the aluminum ring clamps surrounding the test section

5.2.8.2. Secure the stainless steel wire mesh over the clamps with a hose clamp while carefully routing the pressure transducer wires through the slits in the wire mesh.

5.2.9. Place the firing pin through the hole in the firing pin block so that it just touches the second section of the firing pin. .

5.2.10. Make sure that all HPCL personnel are clear from the testing area and verify that the outside gates are locked. Open the garage door if running with any granular propellant. If the test is only running with the primer and black powder turn on the overhead fan.

5.2.11. Raise the pendulum and secure it on the extended rod of the solenoid valve (see Figure 55 and Figure 56 for view of final assembly). This step should only be executed immediately before running the test.

5.2.12. Exit the chamber and close the door.

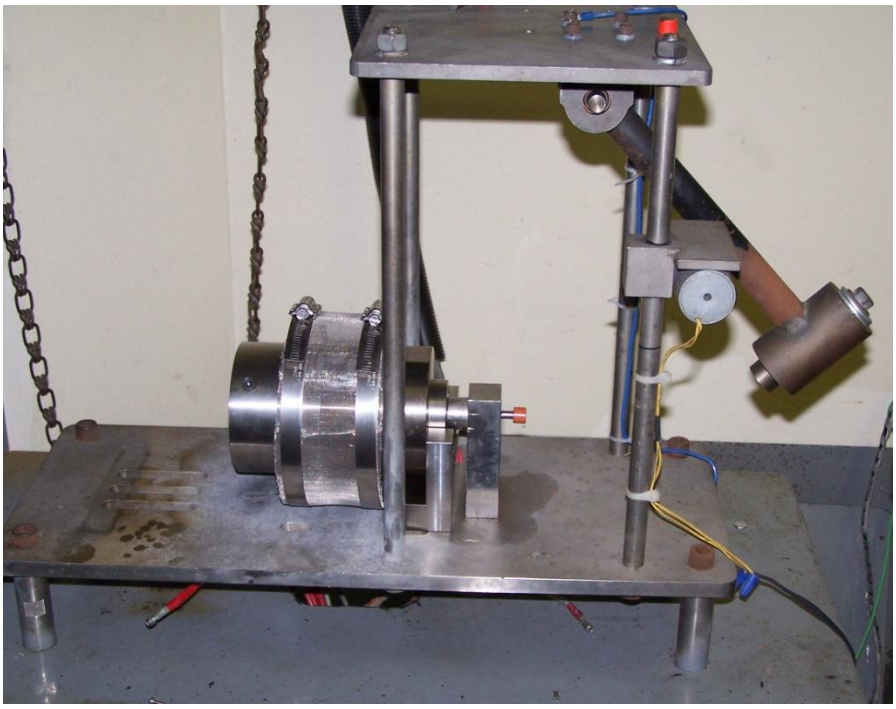

Figure 55: Photograph of the assembly with the radial test section in place before a firing.

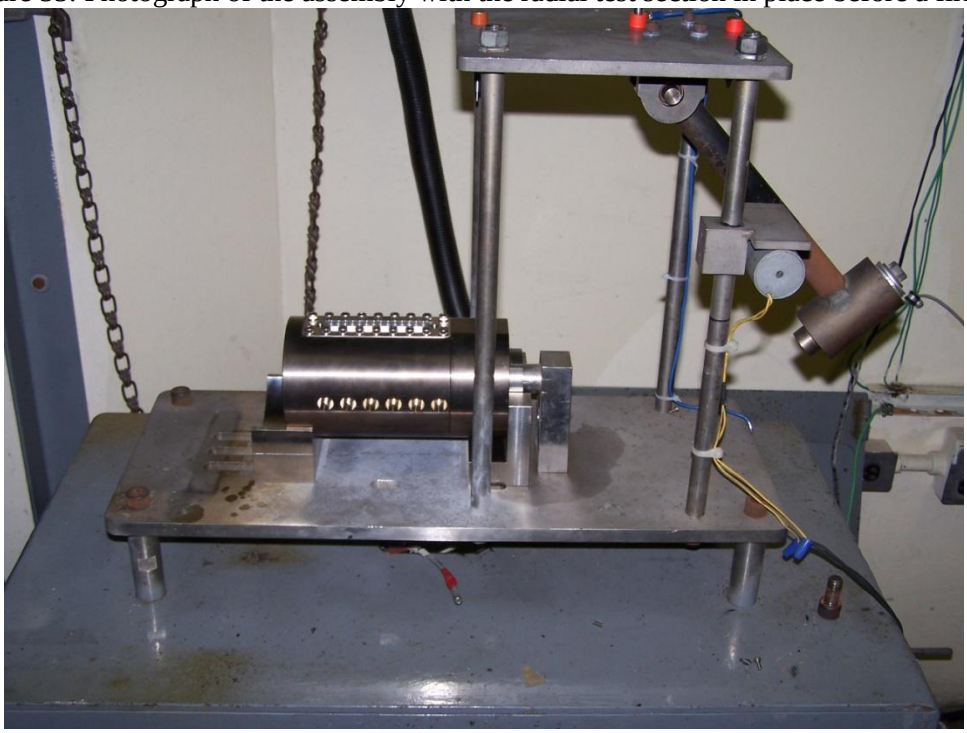

Figure 56: Photograph of the assembly with the axial test section in place before a firing.

6. TEST RIG FIRING PROCEDURE

SAFETY: *Be sure to wear hearing equipment during a test firing, tests can be very loud.*

The following procedures outline the steps required to successfully complete a firing:

Materials Required:
1. Ear protection
2. Control panel
3. Nicolet data acquisition systems
4. TVs and VCRs
5. Intercom microphone

6.1 Pre-test Preparation

6.1.1. Re-verify that the PCB transducers and photodetectors and their signal wires all have continuity and correct signal levels.

6.1.2. If a video camera will be used, verify that the field of view captures the desired area.

6.2. Control Panel Operation

6.2.1. Turn on the Mortar Test Control System control panel power switch (see Figure 57 for control panel details).

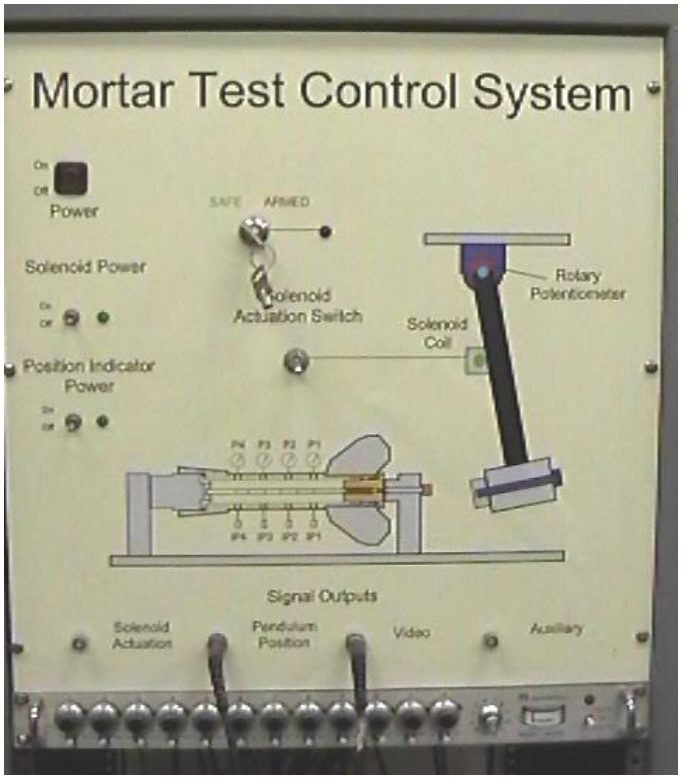

Figure 57: Photograph of the Mortar Test Control System for testing

6.2.2. Turn on the solenoid power switch.
6.2.3. Turn on the position indicator power switch.
6.2.4. Check continuity on the transducers again.
6.2.5. Check video and data acquisition systems again.

6.3. Radial test Rig firing

6.3.1. Make an announcement over the loud speaker *"May I have your attention please, we are conducting an ARO firing in room 109. Please stay away from Room 109 and the fenced-in area. Thank you."*
6.3.2. Press record on the video recording systems and start the stopwatch.
6.3.3. Insert the safety key and turn to "ARMED".
6.3.4. Press the "Solenoid Actuation Switch" up (for firing).
6.3.5. If there are any problems with the firing, turn off control panel and wait either 15 minutes for primer firings or 30 minutes for tests with granular propellant before entering test chamber.
6.3.6. Stop the video recording systems.

6.4. Post-firing

6.4.1. Turn the safety key back to "SAFE" and turn off all the power switches on the control panel.
6.4.2. Wait until the smoke has cleared the test cell.
6.4.3. Remove the firing pin from the firing pin block.
6.4.4. Disassemble the PCB wires from flash tube and remove the test set-up from the test rig (refer to Section 7 for chamber disassembly).
6.4.5. Remove the entire photodetector assembly.
6.4.6. Clean necessary parts of leftover ball propellant particles and black powder.

7. CHAMBER DISASSEMBLY

The following procedures outline the steps required to disassemble the flash tube test rig to prepare for another test firing or to stop firing. This step-by-step process takes around 20 minutes to complete:

Materials Required:
1. Lab coat and protective glasses
2. Allen wrench set
3. Brush or broom
4. Dust pan

7.1 Place the assembly into a vice on the flats on the head end.
7.2 Remove the head end mount.
7.3 For the radial chamber: Remove the aluminum clamps that are holding the wire mesh being careful to keep the unburnt ball propellant contained.
7.4 Remove all the 3/8" bolts that hold the assembly together.
7.5 Remove the window holder being careful to ensure that the quartz window does not fall out of the test jig.

7.6 Remove the second window from the chamber. It will require more force because of the piston seal. Be careful of glass shards from the sacrificial window.

7.7. Carefully remove the remaining debris from the main test section taking photographs as necessary.

7.8. After removing the test section disassemble the head end.

7.9. Clean the test rig and test stand of leftover ball propellant particles.

8. TROUBLESHOOTING

The following procedures outline the steps required in some troubleshooting areas of the flash tube test firing procedure.

8.1. Firing malfunction

The E / R / GS will perform the following steps if the radial chamber fails to initiate:

8.1.1. Interrupt or de-energize all powered instrumentation lines to the test chamber.
8.1.2. Turn off the solenoid power.
8.1.3. Observe the system using the remote camera for any signs of smoke or fire.
8.1.4. If no signs of ignition are seen, wait for 30 minutes before entering the test cell.
8.1.5. Diagnose the problems.

9. POSTING REQUIREMENTS

A copy of this SOP, and any other related SOPs, will be prominently displayed at the site of this experimental operation. (Test Cell Room 109, HPCL, Bldg 430).